# MILLENNIAL-SCALE VARIABILITY IN LATE PLEISTOCENE ICE-RAFTING TO THE SOUTH ATLANTIC OCEAN

By

SHARON L. KANFOUSH

A DISSERTATION PRESENTED TO THE GRADUATE SCHOOL
OF THE UNIVERSITY OF FLORIDA IN
PARTIAL FULFILLMENT OF THE REQUIREMENTS
FOR THE DEGREE OF DOCTOR OF PHILOSOPHY

UNIVERSITY OF FLORIDA

2002

ACKNOWLEDGMENTS

I wish to thank several people for their help in this project, without whom it would not have been possible. First, I am grateful to Dr. David Hodell for generously sharing his knowledge of the subject matter and for teaching me a rigorous, hence fruitful, approach to science. I am also grateful to Dr. Paul Ciesielski and Dr. Jim Channell for serving on my committee and providing insightful feedback. I thank Dr. Claire Schelske and Dr. Joann Mossa for serving on my committee and providing support and encouragement. I am grateful to Dr. Mike Perfit and Dr. Paul Mueller for the many teaching assignments that provided invaluable experience as well as financial support. I am very thankful to my parents for the support they have given me throughout my life and especially in academic endeavors. I am especially thankful to Dan for everything.

I am indebted to numerous friends and colleagues who facilitated fieldwork in the South Atlantic and willingly shared samples and data as well as their expertise. Feedback from Dr. Christopher Charles regarding my interpretations of my data proved invaluable. I thank Dr. Dietz Warnke for sharing insight garnered from his vast experience in IRD analyses and interpretation. I thank Dr. Joseph Stoner for the many interesting discussions out of which grew many new research ideas. I thank Kathy Venz Curtis, Dr. Ellen Martin and Dr. Jaye Cable for providing such inspirational role models for women in science and for their encouragement and support throughout this project. The following individuals provided assistance as well as good company in the laboratory: Mike Rosenmeier, Dr. Jason Curtis, Rhonda Cabanilla, Gianna Brown and Kendall Fountain. Samples for this study were provided by the Ocean Drilling Program on Leg 177 and the preceding site survey cruise with sponsorship from NSF. This research was supported by U.S. Science Support Program grant F000849 to David Hodell and me; and NSF grant OCE-9907036 to David Hodell and Christopher Charles.

TABLE OF CONTENTS

Page

ACKNOWLEDGMENTS ..... ii

ABSTRACT ..... v

CHAPTER

1 INTRODUCTION ..... 1

Statement of Objectives ..... 1
Millennial Climate Variability ..... 1
Antarctic Ice Sheet ..... 2
Previous Work ..... 6
Ice-Rafted Debris ..... 6
IRD as an Indicator of Ice-Sheet Change ..... 7
South Atlantic IRD ..... 10
Study Area ..... 11

2 THE LAST GLACIAL-INTERGLACIAL CYCLE ..... 15

Introduction ..... 15
Materials and Methods ..... 17
Results ..... 23
Last Glacial Period (Marine Isotope Stages 2-4) ..... 23
Termination I ..... 29
Holocene (Marine Isotope Stage 1) ..... 31
Discussion ..... 34
Interpretation of South Atlantic IRD ..... 34
Relationship to NADW Flux ..... 44
Interhemispheric Linkage ..... 46
Conclusions ..... 47

3 RELATIONSHIP TO ENVIRONMENTAL AND CLIMATIC PROXIES ..... 49

Introduction ..... 49
Materials and Methods ..... 50
Results ..... 51
Planktic Oxygen Isotopes ..... 51
Benthic Oxygen Isotopes ..... 53
Benthic Carbon Isotopes ..... 54

Discussion . . . . . 54
Marine-Ice Correlations Using Stable Isotope Records . . . . . 54
Testing Marine-Ice Correlations Using Paleointensity . . . . . 66
Interhemispheric Relationships . . . . . 72
Conclusions . . . . . 79

4 THE LAST FOUR CLIMATIC CYCLES . . . . . 81

Introduction . . . . . 81
Materials and Methods . . . . . 82
Results . . . . . 85
Glacial Periods . . . . . 88
Interglacial Periods . . . . . 90
Glacial Terminations . . . . . 94
Discussion . . . . . 95
Whole-Core Physical Properties as Proxies of IRD . . . . . 95
Glacial-to-Interglacial Variability . . . . . 99
Suborbital Variability . . . . . 101
Marine-Ice Correlation . . . . . 104
Conclusions . . . . . 109

5 SYNTHESIS . . . . . 112

Synthesis of Late Pleistocene Ice-Rafting and AIS Dynamics . . . . . 112
Future Work . . . . . 114
Interpretation of IRD Layers . . . . . 114
Identification of Source Areas . . . . . 116
Potential Causes of Increased Ice Discharge . . . . . 118

REFERENCES . . . . . 120

BIOGRAPHICAL SKETCH . . . . . 139

Abstract of Dissertation Presented to the Graduate School
of the University of Florida in Partial Fulfillment of the Requirements for the Degree of Doctor of Philosophy

MILLENNIAL-SCALE VARIABILITY IN LATE PLEISTOCENE ICE-RAFTING TO THE SOUTH ATLANTIC OCEAN

By

Sharon L. Kanfoush

August 2002

Chairman: David A. Hodell
Major Department: Geological Sciences

Variability of ice discharge to the South Atlantic Ocean has been reconstructed on the basis of ice-rafted debris (IRD) concentration within marine sediments at three sites along a transect from 41° to 53°S, spanning the Polar Frontal Zone (PFZ). Discrete IRD layers recur on millennial timescales during the last glaciation (marine isotope stages (MIS) 2-4). Peaks in IRD are synchronous north and south of the PFZ. Therefore, such layers are not the result of temperature-controlled shifts in the locus of iceberg melting. Rather their synchroneity implies that the IRD layers represent increases in Antarctic ice discharge.

Downcore phase relationships and marine-ice core correlations suggest that millennial South Atlantic (SA) IRD events occur on the cooling limb after millennial-scale warming events on Antarctica. SA IRD events coincide with near-peak warmth of interstadial events recorded in Greenland ice, indicating an anti-phase relationship compared to Antarctic ice. Comparison of SA events with sea-level records suggests existence of sea-level linkage whereby melting of Greenland ice associated with enhanced North Atlantic Deep Water (NADW) formation and interstadial-warmth elevated sea level and "un-pinned" Weddell Sea ice shelves.

The millennial-scale pulses in IRD delivery to the South Atlantic that marked the last glaciation are characteristic of the last four glacial periods (MIS 2-4, MIS 6, MIS 8 and MIS 10) at Site 1094 (53°S). Suborbital variability in ice rafting also characterizes each of the last five interglacial periods (the Holocene, MIS 5, MIS 7, MIS 9 and MIS 11). An early hypsithermal period, characterized by low IRD and high foraminiferal abundance, is followed by a reversal of these conditions interpreted as a neoglaciation. Millennial IRD variability between glacial and interglacial periods is fundamentally different with respect to character (magnitude and recurrence interval) as well as cause. Whereas millennial IRD events of glacial periods are interpreted to represent times of increased Antarctic ice discharge, IRD deposition during interglacial periods is instead a manifestation of changes in iceberg and sea ice survivability controlled by fluctuations in sea-surface temperature resulting from north-south migration of the PFZ and winter sea-ice margin.

# CHAPTER I
# INTRODUCTION

## Statement of Objectives

### Millennial Climate Variability

The discovery of rapid (1000-, 1450-, and 3000-year) climatic oscillations in the Greenland ice cores, the so-called "Dansgaard-Oeschger" (D-O) Events (Johnsen et al., 1992; Dansgaard et al., 1993; Grootes et al., 1993), marked one of the most important recent findings in climate research. The recognition and correlation of Heinrich and higher-frequency ice-rafting events in the North Atlantic provided evidence for millennial-scale, quasi-periodic (~7000 to 10000-year, 2000 to 3000-year and 1450-year) instability of the Laurentide Ice Sheet during the last glacial period (Heinrich, 1988; Andrews and Tedesco, 1992; Bond et al., 1992; Broecker, 1994; Fronval et al., 1995). Their subsequent association with the D-O cycles spurred an ardent search for evidence of similar high-frequency cyclicities in other climatic records from around the globe (Bond et al., 1993; Bond and Lotti, 1995).

Since these initial findings more than a decade ago, evidence of millennial variability has been found in numerous ice-core, marine and terrestrial records from both the northern and southern hemispheres at periodicities similar to those of the D-O events (Porter and An, 1995; Behl and Kennett, 1996; Charles et al., 1996; Blunier et al., 1998; Schulz et al., 1998) and to those of the Heinrich events (Grimm et al., 1993; Keigwin and Lehman, 1994; Lowell et al., 1995) revealing their global signature (see Leuschner and Sirocko, 2000 for a review). In addition to the vast spatial scale of the inferred climate changes, which is too large to be explained by local oceanographic or meteorological changes, the apparent magnitude of change in many records is alarmingly large and the rate of change occurs extremely rapidly, on the order of

centennial and perhaps even decadal scales (Bond et al., 1997, 2001; Broecker, 1997; Taylor et al., 1997; Thompson et al., 1997, 1998; Adkins et al., 1998; Sachs and Lehman, 1999; Severinghaus and Brook, 1999; Peterson et al., 2000; Hendy et al., 2002).

The trigger of these seemingly global climate oscillations remains unknown and the subject of intense interest and speculation. One hypothesis is that changes in the strength of thermohaline circulation, changes in the rate of formation of North Atlantic Deep Water (NADW), affected the delivery of heat to high latitude regions of both hemispheres (Broecker and Denton, 1989). Alternatively, instabilities inherent to large ice sheets impact local oceanography and/or meteorology and subsequently propagate globally (MacAyeal, 1993). Yet another potential mechanism is that changes in surface ocean circulation may lead to increases or decreases in tropical sea surface temperatures and increase or decrease, respectively, water vapor flux to the overlying atmosphere (Broecker, 1995; Webb et al., 1997) thus initiating climatic impacts that are then propagated globally by such means as redirecting jet streams in either hemisphere (Cane, 1998).

Southern hemisphere climate records capturing millennial variability include both marine sediment records and terrestrial climate archives. Analysis of South Atlantic core RC11-83 revealed oscillations in benthic carbon isotopes that bore a striking resemblance to D-O events recorded in Greenland ice (Charles et al., 1996). Glacial advances in alpine glaciers of Chile and New Zealand were shown to be coeval with pulses in ice-rafting within the North Atlantic Ocean (Lowell et al., 1995). The global nature of millennial variability and, specifically, its presence within southern hemisphere records raised the question of how, or if, similar variability was manifested in the dynamics of the Antarctic Ice Sheet (AIS).

**Antarctic Ice Sheet**

The Antarctic Ice Sheet comprises two morphologically and behaviorally distinct ice-sheets: the thicker, land-based East Antarctic Ice Sheet (EAIS) and the thinner, marine-based West Antarctic Ice Sheet (WAIS) (Figure 1-1). Presently grounded well over a kilometer below

sea level, the WAIS is potentially susceptible to small perturbations in sea level (Hollin, 1962; Denton and Hughes, 1983; Denton et al., 1986; Anderson and Thomas, 1991). This inherent instability was also a characteristic of the Laurentide Ice Sheet during the last glaciation, which was partially grounded below sea level in the Hudson Bay region (Andrews and Tedesco, 1992; Marshall et al., 2000). Under full glacial conditions, the WAIS was about two-thirds larger than the present-day WAIS, sea level was ~120 m lower, and grounded ice shelves in marginal seas around Antarctica were more extensive (Denton and Hughes, 1983; Bindschadler et al., 1998). Consequently, analogy with the LIS suggests that the Pleistocene history of the WAIS also includes millennial-scale episodes of instability and surging. Similarly, analogy with the North Atlantic implies that marine sediments from offshore Antarctica should record such episodes of ice-sheet instability as layers enriched in ice-rafted detritus (IRD).

Late Pleistocene history of the AIS has important implications to modern society. Of the modern world total of frozen fresh water, more than 90% lies in Antarctica (Meier, 1983). The WAIS alone presently contains enough ice to elevate global sea level by ~5 to 6 m if it were to suffer complete collapse (IPCC, 1996). Anthropogenic global warming during the twentieth century is estimated to be about 0.6±0.2ºC and increased heat content has been detected in the atmosphere, the world ocean and the cryosphere (IPCC, 1996; Levitus et al., 2001). In response to increasing temperature, mountain glaciers around the world are reported to have already suffered dramatic recession and are contributing to global sea-level rise at an estimated rate of about 0.4±0.2 mm/yr (Meier, 1984, 1993; Dowdeswell et al., 1997; Dyurgerov and Meier, 2000; Irion, 2001). A negative mass balance has also been reported for some modern polar ice caps. Whether the result of melting or increased basal creep, rapid thinning has been detected in southern Greenland (Davis et al., 1998; Krabill et al., 1999). Likewise, numerous pronounced changes occurred recently in the Antarctic region, capturing public as well as scientific attention. Recent changes in the AIS include large calving events, particularly from the Ronne-Filchner and Ross ice shelves and the smaller ice shelves of the Antarctic Peninsula (Rott et al., 1996; Frezzotti

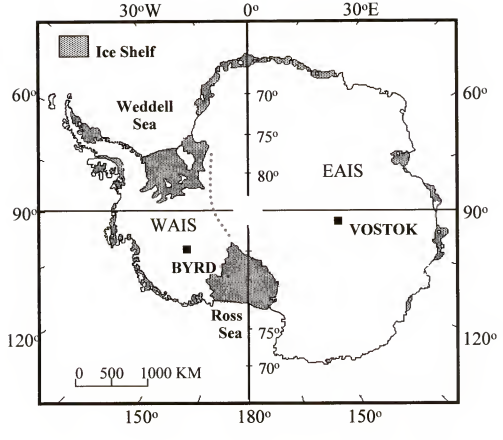


Figure 1-1. Map of the Antarctic Ice Sheet showing the localities and features mentioned in the text. The Transantarctic Mountains (approximated by the dotted line) separate the East Antarctic Ice Sheet (EAIS) from the West Antarctic Ice Sheet (WAIS). Numerous ice shelves are shown (stippled pattern), the largest of which are the Filchner-Ronne Ice Shelf of the Weddell Sea region within the South Atlantic sector of the Southern Ocean and the Ross Ice Shelf of the Ross Sea region within the Pacific sector. The locations are indicated of the Vostok Ice Core of East Antarctica and the Byrd Ice Core of West Antarctica.

et al., 1998; Lazzara et al., 1999; Krajick, 2001). In addition, rapid glacier recession has been reported (Skvarca, 1993; Ferrigno et al., 1998; Rignot, 1998) as well as increased ice flow velocities and thinning (Bindschadler et al. 1994). The recent appearance of pronounced crevasses in ice shelves likely serves as a prelude to future calving events (Shepherd et al., 2001). Although more common in the marine-based WAIS, similar dramatic changes have also characterized the land-based and presumably more stable EAIS (Wendler et al., 1996; Frezzotti et al., 1998).

Some researchers attributed the recent changes in the AIS to the anthropogenic rise in atmospheric and sea-surface temperatures (Mercer, 1978; Doake and Vaughn, 1991; Vaughn and Doake, 1996). Within the geologic record, analogues to anthropogenic global warming may be found in marine isotopic stages (MIS) 11, 9 and substage 5e, for which some paleoclimatic proxy records suggest atmospheric and sea-surface temperatures (SST) warmer than present (Burckle, 1993; Howard, 1997; Petit et al., 1999). Evidence for potential late Pleistocene WAIS collapse during MIS 11 and 5e exists in the form of coral terraces, indicating higher than present sea level; and diatom and Beryllium-10 evidence suggesting the existence of an open marine environment beneath the modern Ross Ice Shelf (Mercer, 1978; Neuman and Hearty, 1996; Scherer et al., 1998).

In contrast, others argue that modest increases in atmospheric temperature will lead to increased snow, and ice, accumulation thus resulting in enlargement of the AIS and grounding-line advance (Huybrechts, 1990). Some coastal sites, for example, experienced increases in accumulation over nearly a century of increased global temperatures (Domack et al., 1991; Thomas, 1991). Still others maintain that recent grounding-line retreat occurring in portions of the AIS is not a consequence of global warming, but instead simply the ongoing recession triggered in the early Holocene, and that such recession would likely continue even in the absence of external forcing (Conway et al., 1999).

Not surprisingly, much interest and speculation exist about what factors control the stability of the AIS and how it will respond to future anthropogenic greenhouse warming (Alley and Whillans, 1991; MacAyeal, 1992; Bindschadler, 1998; Oppenheimer, 1998). Central to answering these questions is reconstruction of how stable the Antarctic Ice Sheet has been in the past, and under what climatic conditions it has behaved in an unstable manner. Examination of deep-sea sedimentary records is one powerful means by which this can be ascertained.

## Previous Work

### Ice-Rafted Debris

The primary method used in this study for reconstruction of late Pleistocene AIS stability is examination of past changes in the concentration of ice-rafted debris in the deep-sea sedimentary record. The pelagic environment, the open ocean, is far removed from land and characterized by water depths on the order of a few kilometers. As a result, pelagic sequences (or deep-sea sediments) typically are derived from the accumulation of fine- to medium-grained carbonate or siliceous tests of microorganisms that live in the overlying water mass. Additionally, varying amounts of fine-grained eolian dust derived from terrestrial sources may be found among the sediments accumulated in a pelagic setting. Examination of pelagic sequences of high latitudes, however, often reveals the inclusion of minor amounts of continentally-derived coarse-grained, sand- to gravel-sized, rock or mineral fragments. Such sediments are too large to be transported by eolian processes and the tremendous distance from land to the site of deposition, in combination with their coarse size, precludes current transport. Thus, rafting by ice is the only remaining mechanism by which such particles can be delivered to the deep-sea (Murray and Renard, 1884; Philippi, 1910).

Sedimentary particles transported by ice to the site of deposition, termed ice-rafted debris (IRD), can range in size from fine silts to large boulders and are poorly sorted. Ice-rafted particles are, depending on the source materials, typically angular and mineralogically immature (Conolly and Ewing, 1965a, b). The ice can originate from glaciers or ice shelves or may be sea ice. The

motion of ice comprising continental glaciers, such as the Antarctic Ice Sheet, downward and outward from a central zone of accumulation, results in erosion of some of the underlying rock and sediment which then becomes incorporated within the basal ice (Iverson, 1993; Fitzsimons et al., 1999). Upon reaching the coast, glaciers calve off icebergs laden with ice-borne sediments or they may merge into ice shelves that then generate icebergs laden with sediment where they reach the coastline. Consequently, icebergs typically transport debris eroded from land. They may, however, also incorporate minor amounts of marine sediments if they become grounded. Furthermore, glaciers can store many layers of volcanic ash derived from atmospheric fallout that is then released by calving and melting (Lackschewitz and Wallrabe-Adams, 1997; Wilch et al. 1999).

In addition to icebergs, sea ice, originating from the freezing of seawater, can also be an agent of IRD transport to the deep-sea (Ruddiman and Glover, 1972). Atmospheric fallout can deposit volcanic ash on sea ice, which then acts as a conveyor of this material to the deep-sea during its seasonal advance and retreat (Smith et al., 1983). Alternatively, although of lesser importance, coastal sea ice may freeze-in nearshore sediment and thus transport continentally-derived lithics to the deep-sea (Ruddiman and Glover, 1972; Lizitsin, 1978; Reimnitz et al., 1998). Sea ice may also contain minor amounts of continentally-derived material deposited on the ice by strong offshore winds (Kindle, 1924).

**IRD as an Indicator of Ice-Sheet Change**

Philippi (1910) was among the first researchers to invoke IRD evidence for glacial expansion. He interpreted the increased northward extent of ice-rafted debris in the Antarctic as evidence of expansion of the Antarctic Ice Sheet during the Pleistocene. Similarly, in the North Atlantic, zones of increased IRD within deep-sea sediments were shown to be accompanied by colder water foraminifera and were interpreted as a record of part of the last glaciation (Bramlette and Bradley, 1941). Also using North Atlantic cores, Conolly and Ewing (1965a) correlated zones of high IRD with the cold-water foraminiferal assemblages of Ericson and others (1961).

Conolly and Ewing (1965b, 1970) then shifted their focus to the Antarctic and the North Pacific, respectively, where they used IRD to delineate glacial stages. In a later study of the North Pacific, Kent and others (1971) detected eleven intervals of increased IRD during the last 1.2 million years. In a detailed investigation of the spatial distribution of IRD deposition in the North Atlantic during the last 125,000 years, Ruddiman (1977) demonstrated that the IRD flux is positively correlated with Northern Hemisphere ice-sheet size and that the main axis of IRD deposition shifted throughout the glacial changes.

In addition to its utility in delineating such glacial-interglacial changes, identification and quantification of discrete layers of IRD in sediments from the North Atlantic Ocean contributed much to our understanding of the shorter-term (millennial-scale) dynamics of the Laurentide Ice Sheet during the last glaciation and to our recognition and understanding of millennial-scale climate variability (Heinrich, 1988; Andrews and Tedesco, 1992; Bond et al., 1992; Broecker, 1994; Fronval et al., 1995). Heinrich layers within the North Atlantic were shown to be enriched in detrital carbonate and to be depleted in planktic foraminifera in relation to ambient sediments (Heinrich, 1988). Later studies showed that such events are also characterized by very high sedimentation rates in relation to ambient rates and are accompanied by low planktic oxygen isotopic anomalies (Dowdeswell et al, 1995: Cortijo et al., 1997; Veiga-Pires and Hillaire-Marcel, 1999). From these factors, in combination with the observation that such layers thin substantially from the Labrador Sea toward the eastern North Atlantic, it was concluded that these layers were the result of repeated millennial-scale glacial surging and dramatically increased ice discharge from the Laurentide Ice Sheet in the Hudson Straits region (Bond et al., 1992; Broecker, 1994). The Heinrich layers were shown to be correlative with the most intense cold phases culminating in bundles of progressively colder D-O events, and that each Heinrich event was immediately followed by rapid and pronounced warming that marked the start of a new bundle of D-O events (Bond et al., 1993; Bond and Lotti, 1995). Thus, the ice discharges and inferred instability of the Laurentide ice sheet have a clear association with regional climate, yet whether they are the result

or the cause of these rapid climate oscillations remains debated (MacAyeal, 1993; Denton and Hendy, 1994).

In summary, I applied the principles of the IRD method to distal marine sediments to reconstruct the late Pleistocene history of the stability of the Antarctic ice sheet. The application of this method is important for several reasons. First, IRD (particularly non-ash lithics) in remote South Atlantic sediments can only be derived from glacial activity on the Antarctic continent or nearby glaciated islands. This contrasts with late Pleistocene oxygen isotopic records from the South Atlantic that, while capable of recording influx of meltwater or icebergs from Antarctica, are potentially a combined signal, being a function of the temperature of growth and/or the $\delta^{18}O$ of seawater, which is in turn a function of continental ice volume and salinity (Emiliani, 1955; Craig, 1965; Shackleton, 1974). Ice-rafted debris within distal sediments, such as described here, also contrasts with lithics within proximal sediments that can be delivered to the site by a variety of nonglacial as well as glacial processes. Second, the IRD records presented in this dissertation will increase knowledge of past ice sheet dynamics and climate in a region with few existing records and at a resolution and length surpassing any known previous records. The record presented here has a length equal to and resolution surpassing that of the Vostok ice core (previously the longest and most continuous record of Antarctic climate variability), which extends through the last 420 kyr and captures variability on millennial time-scales (Petit et al., 1999). Third, in providing analysis of IRD data on the same core material as whole-core physical properties measurements, this study should contribute to an understanding of the degree to which ice-rafted components contribute to such signals and potentially to the identification of a more rapid, less labor-intensive physical-properties proxy of IRD. This would ultimately facilitate analysis of a greater density and spatial distribution of cores and, thus, a greater understanding of the history of and the controls on ice-rafting in the Southern Ocean.

**South Atlantic IRD**

Many studies of IRD in circum-Antarctic sediments focused on ascertaining the time of initial glaciation of Antarctica (Margolis and Kennett, 1971; Watkins et al., 1974). In addition to the coarse grain size of the debris, Margolis and Kennett (1971) analyzed surface textures of quartz grains that yielded direct evidence that their mode of transport was via ice. In contrast to the North Atlantic, however, high-resolution Pleistocene records of IRD from the Southern Ocean are sparse and, until recently, have focused primarily on longer-term glacial-interglacial timescales (Philippi, 1912; Conolly and Ewing, 1965b; Keany et al., 1976; Cooke and Hays, 1982). Cooke (1978) reported that accumulation rates of IRD at the Last Glacial Maximum (LGM) are greatest in the Atlantic sector of the Southern Ocean and gradually diminish eastward. In addition, IRD accumulation diminishes abruptly north of 46°S. These spatial patterns suggest that IRD, consisting predominantly of volcanics, originates primarily from the South Sandwich Islands and secondarily from the Antarctic Peninsula and that IRD accumulation is controlled in large part by the position of the winter sea-ice margin (Cooke, 1978).

In the southeast Indian sector of the Southern Ocean, increased fluxes of ice-rafted quartz on millennial timescales were interpreted to indicate pulse-like surges in the production and melting of icebergs between 17- and 35-ka (Labeyrie et al., 1986). Accompanied by meltwater influx, these quartz pulses imply that the Antarctic Ice Sheet exhibited periods of instability on millennial timescales during the latter part of the last glaciation and at the last glacial maximum. An alternative interpretation of Southern Ocean sedimentary layers enriched in coarse-grained lithics is that they represent latitudinal migration of the Polar Frontal Zone (PFZ), a pronounced sea-surface temperature (SST) boundary that separates cool (~0-2°C) Antarctic water from comparably warm (~2-4°C) Subantarctic water to the north, and thus temperature-controlled shifts in the position of iceberg melting and IRD fallout (Keaney et al., 1976; Smith et al., 1983; Whitworth and Nowlin, 1987). The result would be discrete layers enriched in IRD even in the face of an unchanging rate of ice discharge. The two mechanisms can explain fluctuations of IRD

in Southern Ocean sediments yet have wholly different implications for AIS dynamics. Therefore, before IRD can be used as a proxy for AIS stability, the precise meaning of such layers must be ascertained and is the first question addressed in this study.

## Study Area

The Antarctic continent is encircled by three oceanic basins: the South Atlantic-Indian, the South Indian, and the Southeast Pacific or Bellinghausen Basins, each defined by the 4000-meter isobath (Heezen and Tharp, 1972). The Antarctic continent marks the southern boundary of each basin and the surrounding shelf reaches depths of greater than 500 meters, the deepest shelf in the world. The area of study lies within the southeast Atlantic sector of the Southern Ocean (Figure 1-2). This basin was selected for a number of reasons.

First, the drift of icebergs is controlled largely by the predominant winds and currents (Vinje, 1980). The sources of most icebergs in the South Atlantic are ice shelves such as those found in the Weddell Sea region (Warnke, 1970). Melting and freezing at the base of ice shelves such as these can produce debris-rich basal ice that can move upward and become protected, as new ice is added by underplating (Eiken et al., 1994; Bombosch and Jenkins, 1995; Hulbe, 1997). Thus, if increased discharge, due to abrupt surging and/or melting, of ice in West Antarctica occurred, evidence of such change should be recorded in my sediment cores from the southeast Atlantic because they are situated downdrift of icebergs originating in the Weddell Sea region and other icebergs transported by the Weddell Gyre and the Antarctic Circumpolar Current (Figure 1-3) (Atlas of Antarctica, 1969; Drewry and Cooper, 1981; Gloersen et al., 1992).

Second, deepwater in the South Atlantic is a mixture of outflows from all ocean basins. Consequently, the sediments here record globally important variations in thermohaline circulation (Charles et al., 1996). Ice-rafting events recorded within South Atlantic sediments, accordingly, can be compared with changes in thermohaline circulation, such as NADW flux, recorded within the same sediment core. Comparison of different proxy records within the same stratigraphic

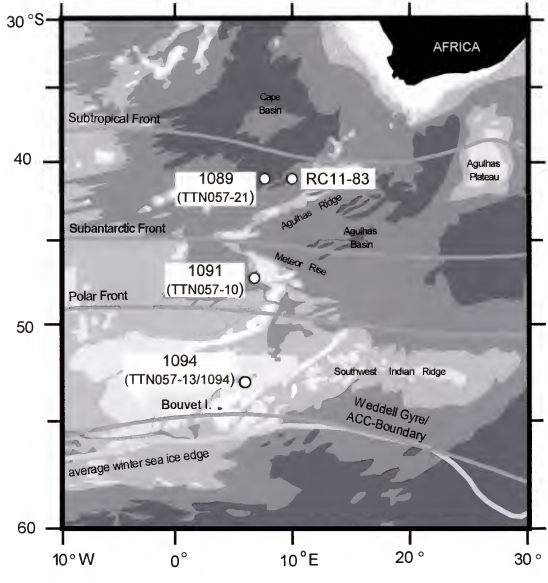


Figure 1-2. Site map of the southeast Atlantic showing the core locations discussed in this study relative to modern positions of important oceanographic boundaries and the winter sea-ice margin. Modified after Figure 1, p. 35, Shipboard Scientific Party, 1999.

record provides a means to circumvent chronological limitations that potentially hinder attempts to delineate brief (millennial) events.

Lastly, the subantarctic region is the primary source of moisture for the Antarctic continent and, therefore, a good location from which to obtain a deep-sea sedimentary analogue to existing Antarctic ice-core records (Mortyn, 2000). The co-existence of high-resolution ice core records and marine analogues will enable placement of changes in atmospheric variables within the context of changes in ocean circulation, thus facilitating comparison of ice-rafting events with changes in atmospheric variables recorded in Antarctic ice.

Strong gradients in surface water characteristics exist within the subantarctic South Atlantic region. Therefore, a single core cannot fully record and convey the whole host of processes operating over millennial-scale climate oscillations (Shipboard Scientific Party, 1999). For example, as described previously, two processes can potentially explain downcore fluctuations in the concentration of ice-rafted debris in South Atlantic sediments: either increased Antarctic ice discharge (Labeyrie et al., 1986) or migration of warm sea-surface temperatures and the associated iceberg melting line over the site (Keany et al., 1976). Consequently, to capture a range of the processes operating within this region and to distinguish between the two explanations described above for IRD fluctuations, sediments were analyzed from three sites along a north-south transect from 41°S to 53°S spanning the Polar Frontal Zone (PFZ). The northernmost site, from which piston core TTN057-21 was recovered (at ~41°S), lies within the Subantarctic Zone north of the present-day position of the PFZ in waters characterized by sea surface temperatures of ~2-4°C (Figure 1-2). Pleistocene sedimentation alternates between mud- and carbonate-rich sediments at average rates of ~17 cm/kyr (Shipboard Scientific Party, 1999). A mid-latitude site, from which piston core TTN057-10 was recovered (at ~47°S), is situated within the present-day PFZ. Diatom oozes were deposited at Pleistocene sedimentation rates of ~15 cm/kyr. From the southernmost site, Site 1094 (at ~53°S), a spliced sediment record was recovered consisting of piston core TTN057-13 and ODP drillcore material 1094. This site is

situated within the Antarctic Zone characterized by SST of ~0-2 °C. It also lies within the biogenic silica belt of the Southern Ocean south of the modern PFZ and about 2° north of the modern average limit of winter sea ice (Zwally et al., 1983; Gloerson et al., 1992). The average late Pleistocene sedimentation rate is ~30 cm/kyr, and includes diatom oozes and coarse-grained ice-rafted lithic material. Coarse lithics occur within sediments at each of the three sites but at the highest concentrations in Site 1094 (Shipboard Scientific Party, 1999).

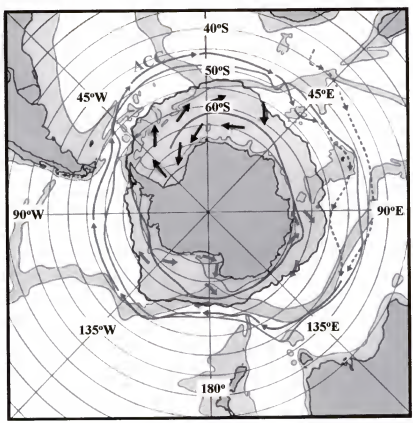


Figure 1-3. Large-scale circulation in the Southern Ocean, including the Antarctic Circumpolar Current (ACC; gray arrows) and the Weddell Gyre (black arrows) (modified after Figure 4.1.2, p. 161, Gloersen et al., 1992).

CHAPTER 2
THE LAST GLACIAL-INTERGLACIAL CYCLE

## Introduction

Despite its relevance to issues of natural and anthropogenic climate change, the behavior of the Antarctic Ice Sheet on millennial timescales has not been established. Because much of the West Antarctic Ice Sheet is grounded below sea level (similar to the Laurentide Ice Sheet during the last glaciation) and was about 2/3 larger than today under full glacial conditions, there is reason to suspect that the Pleistocene history of the WAIS may have included millennial-scale episodes of instability similar to the LIS (Denton and Hughes, 1983; Denton et al., 1986; Anderson and Thomas, 1991; Andrews and Tedesco, 1992; Bindschadler et al., 1998). If so, sediments offshore Antarctica should record such episodes as layers enriched in IRD.

Pleistocene records of IRD from the Southern Ocean have been limited to glacial-interglacial timescales, mostly because of chronological uncertainties (Conolly and Ewing, 1965; Keany et al., 1976; Cooke and Hays, 1982). General improvements to the dating and chronological resolution of deep-sea sediment cores allow me to document millennial-scale episodes of IRD delivery to the South Atlantic over the last glacial-interglacial cycle. This analysis of a transect of three cores spanning a steep sea-surface temperature gradient, the Polar Frontal Zone, will enable distinction between the two potential mechanisms for temporal IRD fluctuations; increased ice discharge from the Antarctic continent (Labeyrie et al., 1986) versus temperature-controlled variations in the position of melting of debris-laden icebergs (Keany et al., 1976).

Within the last glaciation, MIS 3 is characterized by millennial-scale fluctuations in sea level attributed to discharge of icebergs from the Laurentide Ice Sheet during Heinrich Events

(Yokoyama et al., 2001; Chappell, 2002). Alternatively, the observed millennial highstands of the last glaciation are potentially due to melting of northern hemisphere ice during prominent interstadial events and could have served as a sea-level linkage that then triggered discharge of Antarctic ice (Denton and Hughes, 1983; Kanfoush et al., 2000a). Evidence of such ice discharge should be recorded as millennial increases in IRD concentration in South Atlantic sediments of glacial age.

The glacial termination was marked by two or three brief intervals of rapid eustatic sea-level rise separated by intervals of lower rates (Fairbanks, 1989; Blanchon and Shaw, 1995). These intervals of rapid sea-level rise have been suggested to be evidence of catastrophic ice-sheet collapse (Blanchon and Shaw, 1995). Climate proxy records demonstrated that warming in the southern hemisphere preceded that of the northern hemisphere during the deglaciation (Charles et al., 1996; Blunier et al., 1998). Disintegration of the Antarctic Ice Sheet or the marine-based West Antarctic Ice Sheet has been proposed as the likely source of the earliest of the first large jumps in sea level during the last deglaciation (meltwater pulse (mwp) Ia; Fairbanks, 1989; Clark et al., 1996). Conversely, although Nakada and Lambeck (1988) reported a large (as high as 30%) Antarctic contribution to sea-level rise over the last deglaciation, they suggested that southern hemisphere deglaciation occurred synchronously with or even lagged northern hemisphere deglaciation.

Climate variability during the Holocene has potential significance in predicting how climate may change in the future (Broecker, 1998). Whereas temperature proxies ($\delta^{18}O$ and $\delta D$) in Greenland ice cores show little evidence for variability and provide an impression of Holocene climate stability (Stuiver and Grootes, 2000), other paleoclimatic evidence suggests that the Holocene was instead characterized by an early interval during which conditions were warmer than present (the so-called Hypsithermal) followed by cooling and glacial advance beginning about 5000 yrs ago marking the start of the Neoglaciation (Porter and Denton, 1967; Denton and Karlen, 1973; O'Brien et al., 1995; Keigwin, 1996; Bond et al., 1997). Southern Hemisphere

evidence of this change includes glaciological evidence, such as advance of mountain glaciers between about 5400 and 4900 calendar years before present, and marine paleoclimatic evidence (Denton and Karlen, 1973; Clapperton and Sugden, 1988; Keigwin, 1996; Porter, 2000). Despite significant spatial variability in Holocene temperature trends caused by both changes in local ice sheet elevation and climate, Antarctic ice cores provide support for an Antarctic Hypsithermal (Masson et al., 2000).

The behavior and role of the AIS during the last glacial-interglacial cycle remains a subject of debate. I quantified variations in IRD in cores from the South Atlantic sector of the Southern Ocean to study Antarctic Ice Sheet dynamics during the last climatic cycle. Questions to be addressed include the following:

- Did millennial-scale variations in IRD occur in the Southern Ocean during the last glacial, and do they represent instability of the AIS on millennial timescales?
- Was the AIS a significant contributor to sea-level rise during the last deglaciation and, if so, when?
- Is there evidence for IRD in the Holocene?

## Materials and Methods

I compared IRD fluctuations in all three cores along the north-south transect across the PFZ from ~41° to 53°S (Figure 1-2). The southernmost record (TTN057-13/1094) at 53°S is located south of the present-day PFZ and north of the average winter sea-ice limit (Zwally et al., 1983; Gloerson et al., 1992). TTN057-13-PC4 is a 14-meter piston core retrieved in February 1996 from the seafloor near Bouvet Island at 53.2°S 05.1°E in 2850 meters water depth. The core consists of muddy diatom oozes containing minor amounts of coarse-grained lithic material. The core was sampled at 3- or 5-cm intervals, corresponding to a temporal resolution of approximately 15 to 150 years. To extend the record to the base of the last glacial period, the piston core was spliced to Ocean Drilling Program (ODP) core 1094C-2 that was retrieved in January 1998 from the same site during Leg 177. For piston core TTN057-13, the weight percent

biogenic silica (%BSi) was measured using a molybdate blue spectrophotometry method (DeMaster, 1981). Analytical precision, estimated by the standard deviation (one sigma) of repeated analysis of a dissolved silica standard (n = 49) and replicated samples (n = 44), was ±1.0%. In samples where a sufficient number of specimens could be found, oxygen isotopic measurements were made of the planktic foraminifera *Neogloboquadrina pachyderma* (sinistral) from the >150μ fraction at the University of Florida using a Finnigan MAT252 mass spectrometer coupled to an automated carbonate preparation system (Kiel III) consisting of 46 single-reaction chambers. Isotopic ratios are reported in standard delta notation relative to V-PDB (Coplen, 1996). Analytical precision, estimated by the standard deviation (one sigma) of repeated analysis of NBS-19, was ±0.06 per mil.

Using the planktic foraminiferal oxygen isotopic records, the two cores were spliced at a depth of 9.7 m and depths in 1094 were adjusted upward by 3 meters. Eleven accelerator mass spectrometry (AMS) $^{14}$C-dates on monospecific samples of *N. pachyderma* (sin) from eight stratigraphic horizons provide chronological control to a depth of 9.7 meters (~38 ka) (Table 2-1). Below this level, the marine isotopic stage (MIS) 4/3 and 5/4 boundaries were assigned ages of 59 and 74 ka, respectively (Martinson et al., 1987). Intervening ages were interpolated assuming linear sedimentation rates between these dates and to the base of 1094C-2, resulting in an estimate of ~82 ka for the basal age of the spliced record. After applying an 800-year reservoir correction, all radiocarbon ages were corrected to calendar years using IntCal for dates < 12,000 years (Stuiver et al., 1998) and Bard and others (1998) for dates > 12,000 years. All dates then presented for each of the three sediment records are expressed in calendar years. Sedimentation rates for TTN057-13/1094 were lower during the last glaciation (15.5 cm/kyr on average) and gave way to higher rates during the deglaciation and Holocene (56.4 cm/kyr on average) (Figure 2-1).

Table 2-1. Chronology for the spliced TTN057-13/1094 record.

| CAMS # | Sample ID | Depth (cm) | Conventional $^{14}C$ (yr) | Error (yr) | Calibrated Age (yr) | Reference |
|---|---|---|---|---|---|---|
| 52001 | X 18-23 | 21 | 1590 | +/-80 | 720 | 45 |
| 50099 | X 63-65 | 63 | 2630 | +/-60 | 1830 | 45 |
| 50100 | VII 21-26 | 256 | 6850 | +/-60 | 6930 | 45 |
| 50101 | VII 63-68 | 449 | 9340 | +/-60 | 9540 | 45 |
| 52002 | VII 87-92 | 473 | 9370 | +/-80 | 9600 | 45 |
| 50102 | VI 0-5 | 536 | 10050 | +/-40 | 10310 | 45 |
| 52003 | VI 12-17 | 548 | 9970 | +/-90 | 10290 | 45 |
| 50103 | V 60-62 | 741 | 13140 | +/-50 | 14400*, 14550§ | 46 |
| 52004 | V 81-86 | 763 | 13070 | +/-80 | 14320*, 14470§ | 46 |
| 50104 | IV 90-92 | 919 | 26360 | +/-150 | 29130*, 29980§ | 46 |
| 50106 | IV 90-92REPL. | 919 | 26360 | +/-150 | 29130*, 29980§ | 46 |
| 52005 | IV 141-143 | 970 | 33420 | +/-250 | 36990*, 37830§ | 46 |
| 50105 | II 50-52 | 1180 | 53720 | +/-3600 | - | |
| 52006 | II 50-52REPL. | 1180 | 52060 | +/-2200 | - | |
| 52007 | I 50-67 | 1289 | >42560 | - | - | |
| - | MIS 4/3 | 1542 | - | - | 59000 | 44 |

Note: Fourteen $^{14}C$ dates on acid-leached monospecific samples of *N. pachyderma* from twelve stratigraphic levels in piston core TTN057-13-PC4 and the MIS 4/3 boundary (Martinson et al., 1987) were used to constrain the glacial chronology for the spliced TTN057-13/1094 record. Piston core TTN057-13-PC4 was spliced to ODP core 1094C-2H at a depth of 9.7 m (equivalent to 33,420 $^{14}C$ yrs B.P.) by adjusting depths in core 1094C-2H upward by 3 meters. Two $^{14}C$ samples, at 9.2 m and 11.8 m, were replicated and yielded radiocarbon ages well within their respective errors. The age model was constructed using dates exhibiting stratigraphic and chronologic internal consistency over the intervals where nearby sample ages are indistinguishable at the 2-sigma level. This choice does not significantly affect the resulting age model. $^{14}C$ dates on samples at and below 1180 cm were not used because this level is below the point where the piston core was spliced to ODP core 1094C-2. Conventional $^{14}C$ ages shown are uncorrected and without the application of a reservoir effect. Calibrated ages were calculated by applying an 800-year reservoir correction and converting to calendar years using either the method of Stuiver et al. (1998) or data from Bard et al. (1998). For the latter, ages were determined by both (*) a least squares regression and (§) a 2nd polynomial fit. CAMS 52007 is from a 160 μg target and did not yield a finite age.

The intermediate site (TTN057-10) at 47°S is located on the western side of the Meteor Rise within the PFZ (Figure 1-2). From this core location (47.1°S, 05.9°E), situated north of the PFZ in 4390 meters water depth, a 12-meter piston core (TTN057-10-PC3) was retrieved in February 1996. Core TTN057-10-PC3 consists of light-gray diatomaceous ooze with calcareous interbeds. Diatoms dominate the biogenic component during glacial periods and calcareous

microfossils dominate during interglacial periods. Carbonate analyses show that the core is nearly devoid of carbonate during the last glaciation, thus limiting the resolution of the oxygen isotope stratigraphy (Figure 2-2). Trigger core TTN057-10-TC3 was collected from the same location and was spliced to the upper portion of TTN057-10-PC3 at a depth of 99 cm on the basis of the oxygen isotopic records. The chronology for core TTN057-10 (47°S) was derived by visually matching its $\%CaCO_3$ record with that of TTN057-21. Sampling of the record was conducted at 3 or 5-cm intervals corresponding to a temporal resolution of approximately 30 to 700 years. The glacial-aged sediments of core TTN057-10 exhibit similar sedimentation rates to those of TTN057-13/1094 (15.9 cm/kyr on average), but the glacial termination is compressed and much of the Holocene is absent in this core. Oxygen isotopic measurements were made on planktic foraminifer *N. pachyderma* (sin) at the University of Florida using a VG Prism Series II mass spectrometer. Analytical precision was ±0.10 per mil. Percent $CaCO_3$ by weight was determined by coulometric titration on a model 5011 carbon analyzer manufactured by Coulometrics (UIC) Inc. (Engelman et al., 1985). Precision was estimated to be ±0.7% (1 standard deviation) on the basis of 104 measurements of reagent-grade (100%) $CaCO_3$.

A 14-meter piston core TTN057-21-PC2 was retrieved during February 1996 from the northernmost site (41.1°S, 07.8°E) in 4980 meters water depth in the southern Cape Basin near the northern flank of the Agulhas Ridge. The deepest of the sites at 4980 meters, it lies very near the calcium compensation depth, yet foraminiferal abundance in the sediments analyzed is fairly constant enabling generation of a continuous stable isotopic stratigraphy. The lithology of core TTN057-21 consists of light gray to gray ooze throughout with varying amounts of calcareous and siliceous components. Correlation of its $\delta^{18}O$ record with that of nearby core RC11-83 (41.6°S, 9.8°E; Figure 1-2), which has a well-constrained AMS-$^{14}C$ chronology, provided age control for this core (Figure 2-2) (Charles et al., 1996; Ninnemann, Charles and Hodell, 1999; Channell et al., 2000). With an average glacial sedimentation rate of 17.3 cm/kyr, a temporal

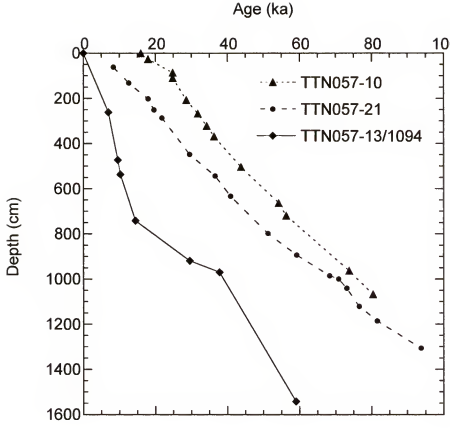


Figure 2-1. Age-depth relationship of each of the three sedimentary records: TTN057-10 (dashed line with triangles), TTN057-21 (dotted line with circles) and TTN057-13/1094 (solid line with squares). The TTN057-13/1094 record exhibits a decrease in sedimentation rates in the latter part of the glaciation followed by a return to higher sedimentation rates across Termination I and into the Holocene.

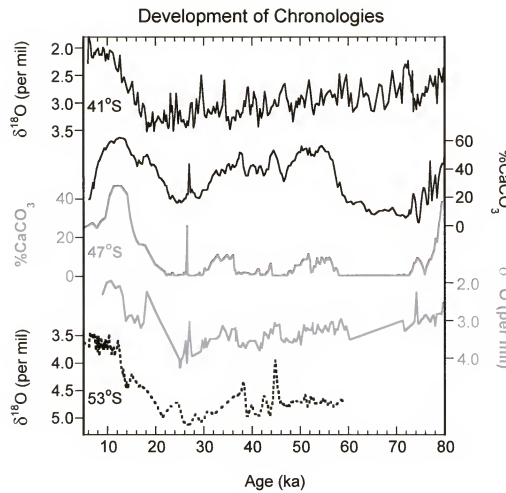


Figure 2-2. Development of Chronologies. Time series of $\delta^{18}O$ (*G. bulloides*) and weight $\%CaCO_3$ in cores TTN057-21 (41°S - solid black) and TTN057-10 (47°S - solid gray) and $\delta^{18}O$ (*N. pachyderma*) in core TTN057-13/ODP Site 1094 (53°S - dotted black). The age scale for TTN057-21 was derived by aligning fine-scale features in the isotopic record with those of nearby piston core RC11-83 which has a well-constrained accelerator mass spectrometry $^{14}C$ chronology (41°S; Charles et al., 1996). The chronology for core TTN057-10 was derived by visual-matching of the weight %CaCO3 record with that of core TTN057-21. The age scale for TTN057-13/1094 is given in Table 2-1.

resolution of 50-100 years was obtained by sampling at 3- or 5-cm intervals. The glacial termination is captured within this core, however Holocene material is lacking. Oxygen isotopic analysis was conducted on the planktic foraminifera *Globigerina bulloides* at the Scripps Institution of Oceanography using a Carousel-48 automatic carbonate device coupled to a Finnegan MAT 252 mass spectrometer with an estimated precision of ±0.1 per mil.

For each of the three sediment records, downcore IRD concentrations were visually determined on the 150μm-to-2mm size fraction (Allen and Warnke, 1991). At least 500 grains were counted including quartz, volcanic ash, fine-grained volcanics, coarse-crystalline rock fragments, metamorphics, radiolaria and foraminifera. In the counts of TTN057-10, the biogenic components were grouped as total non-IRD rather than tallied separately.

## Results

Record TTN057-13/1094 spans the entire last glacial-interglacial cycle, revealing that there were significant changes in IRD flux from the glacial period across the termination into the Holocene (Figure 2-3). Delivery of ice-rafted detritus to 53°S was greatest during the last glacial period. During the last deglaciation IRD accumulation decreased between ~20 and 15 ka, followed by a short pulse at ~13.5 ka. IRD accumulation remained very low from 12 to 5 ka during the early part of MIS 1, and increased again after 5 ka in the late Holocene. Unlike the southernmost record, cores TTN057-10 and TTN057-21 do not contain Holocene sediments (Figures 2-4 and 2-5, respectively).

### Last Glacial Period (Marine Isotope Stages 2-4)

All three cores record discrete episodes of IRD deposition throughout the last glaciation that recur on millennial (~6-10 kyr) time scales (Figure 2-6; Table 2-2). The IRD in the >150μm fraction of TTN057-13/1094 is composed dominantly of volcanic ash (averaging 53.8% of the >150μm fraction, 94% of the total lithics) and quartz (averaging 3.5% of the >150μm fraction,

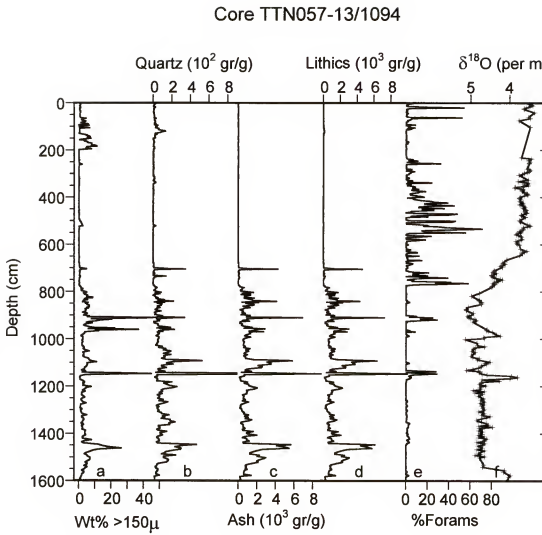


Figure 2-3. Core TTN057-13/1094. Downcore record of sedimentary components, including (a) weight% >150, the concentrations (grains/g) each of (b) total lithics, (c) volcanic ash, (d) quartz, and (e) foraminifera (%) and (f) planktic $\delta^{18}O$ (per mil) (*N. pachyderma* (sin)).

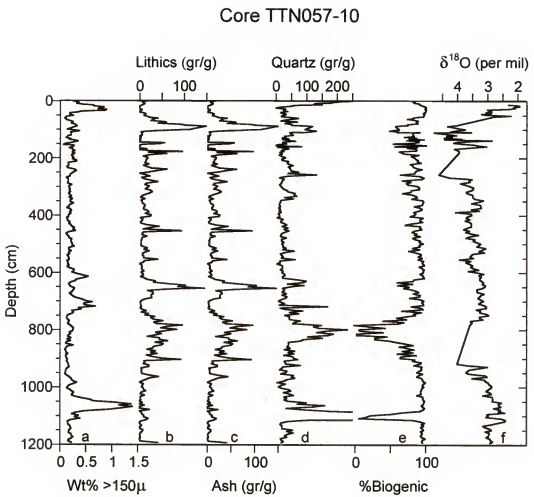


Figure 2-4. Core TTN057-10. Downcore record of sedimentary components, including (a) weight% >150, the concentrations (grains/g) each of (b) total lithics, (c) volcanic ash, (d) quartz, and (e) biogenic components (%; predominantly foraminifera and radiolaria) and (f) planktic $\delta^{18}O$ (per mil; *G. bulloides*). The quartz concentration at 1108 cm is off-scale with a peak value of 781 grains/g.

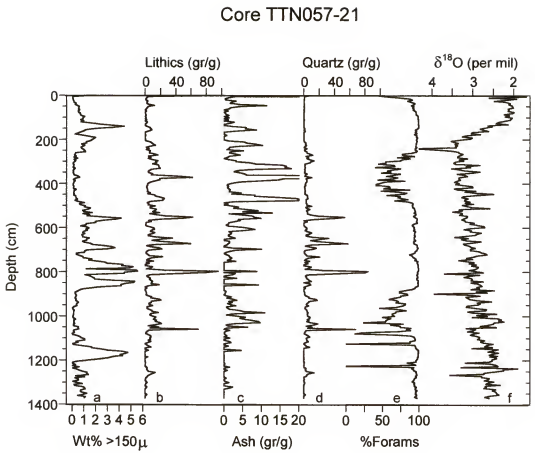


Figure 2-5. Core TTN057-21. Downcore record of sedimentary components, including (a) weight% >150, the concentrations (grains/g) each of (b) total lithics, (c) volcanic ash, (d) quartz, and (e) foraminifera (%) and (f) planktic $\delta^{18}O$ (per mil; *G. bulloides*). Ash concentrations at 372 cm and 477 cm are off-scale with peak values of 48.1 grains/g and 20.4 grains/g, respectively.

5.9% of the total lithics). Also present are minor amounts of fine-grained volcanics, coarse-crystalline rock fragments and mica. Rose quartz and garnet each occur rarely within the sediments, and their presence has been interpreted by some researchers to indicate ice discharge from East Antarctica (Warnke et al., 1992; Teitler et al., 2001). In contrast, although Diekmann and Kuhn (1999) concur that IRD of the South Atlantic has a general petrography consistent with an East Antarctic origin, specifically the a sequence of East Antarctic Paleozoic tillites known as the Beacon Supergroup, they argue that some primary Beacon detritus may have experienced transient storage in the southern Weddell Sea where it was reworked by modern glacial and current activity and subsequently entrained within glacial ice and released to the South Atlantic by ice discharge from West Antarctica. Peaks are composed dominantly of ash and quartz that, despite approximately an order of magnitude difference between their concentrations, were well correlated with each other and with the overall trends in total lithics.

None of the IRD peaks lasts for more than a few thousand years. The weight percent >150μ fraction of the sediment mirrors IRD in TTN057-13/1094 because most of the mass of the >150μ fraction consists of IRD (Figure 2-3). While radiolaria and foraminifera constitute a significant fraction of the grain counts in some parts of the record they contribute little to the mass of the coarse fraction. A plot of both the lithic and oxygen isotopic ($\delta^{18}O$) records from TTN057-13/1094 reveals that IRD is deposited under both full glacial conditions (MIS 4 and 2) and interstadial conditions (MIS 3).

In core TTN057-10 located at 47°S, deposition of both quartz and ash also fluctuates during the glacial period with the highest concentrations occurring within MIS 2 and 4 (Figure 2-4). The IRD events in this core are more similar to one another in magnitude throughout the glacial than those observed in record TTN057-13/1094 (Figure 2-6). The concentration (grains/g) of lithics in core TTN057-10 is more than an order of magnitude smaller than that at 53°S. Unlike the record from 53°S, the two primary lithic components (quartz and ash) do not parallel each

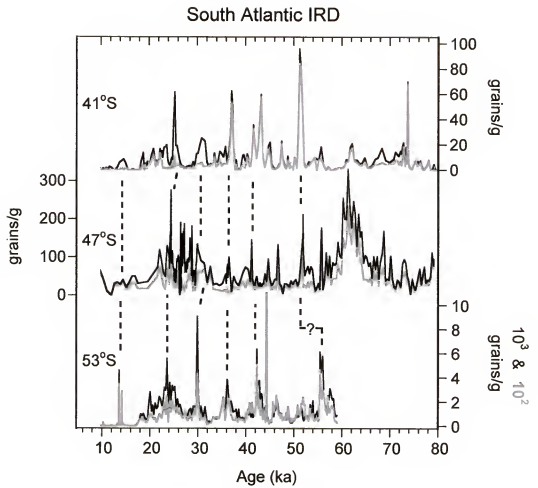


Figure 2-6. South Atlantic IRD. Time series of total lithic concentration (black) and quartz concentration (gray) in cores TTN057-21 (41°S), TTN057-10 (47°S), and TTN057-13/ODP Site 1094 (53°S). Dotted arrows indicate IRD events that correlate across the PFZ. Total lithics and quartz concentrations from 53°S are expressed in $10^3$ and $10^2$ grains/g, respectively, to enable comparison of trends in each parameter. Quartz concentration at ~44 ka is off-scale at 16 x$10^2$ grains/g. Ages shown are calendar years x$10^3$ determined by application of an 800-year reservoir effect and conversion to calendar years using the methods of Stuiver and others (1998) and Bard and others (1998).

other as closely and quartz rather than ash is dominant throughout much of the glacial. Percent $CaCO_3$ is consistently low, near zero, in the stadials (MIS 4 and 2) and high in the interglacial periods (MIS 1and 5a) and interstadial MIS 3.

Within core TTN057-21, quartz is present and fluctuates throughout the glaciation while ash remains relatively low with the exception of a very large peak during each MIS 4 and 2 (Figure 2-5). As noted in TTN057-13/1094 many of the lithics peaks, particularly those of MIS 3, are accompanied by high foraminiferal concentration and are associated with or immediately follow minima in $\delta^{18}O$. Located at 41°S, core TTN057-21 contains the smallest concentration of lithics of the cores analyzed (Figure 2-6). The north-south transect of cores reveals a general trend of decreasing lithic abundance with decreasing latitude, hence increasing distance from the Antarctic continent. Whereas TTN057-10 showed approximately an order of magnitude decrease in overall lithic abundance relative to spliced record TTN057-13/1094, TTN057-21 similarly showed an order of magnitude decrease in lithic content relative to TTN057-10. The northernmost and southernmost cores at 41° and 53°S, respectively, share a basic similarity in the timing of prominent IRD peaks (Figure 2-7). In contrast, the core at 47°S in the PFZ contains additional IRD fluctuations and displays peaks of different amplitudes relative to those observed in the other cores.

**Termination I**

From a maximum at 21.3 ka, $\delta^{18}O$ progressively decreases in TTN057-10 and TTN057-13/1094 (Figure 2-2). In TTN057-21 however, the highest-resolution record, the trend toward lighter $\delta^{18}O$ values does not begin until ~19 ka. An IRD peak occurs in the two southern records at ~21 ka. Following this, IRD in each record exhibits a step-wise decline, reaching a minimum at ~15 ka at 53°S and ~13 ka at 47°S. Biogenic silica concentrations at 53°S increase over Termination I from a low of less than 40% at ~22 ka to a high approaching 100% between 16 and 12 ka (Figure 2-8). From values near zero at the LGM, $\%CaCO_3$ in TTN057-10

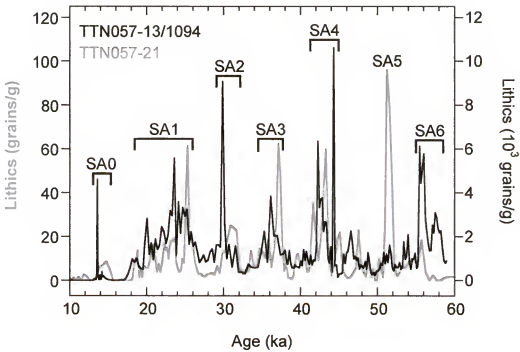


Figure 2-7. Comparison of total lithic peaks in core TTN057-21 (41°S - gray) and TTN057-13/ODP Site 1094 (53°S - black). Prominent glacial IRD events are assigned labels South Atlantic (SA) 1-6. Event SA0 is denoted as such to indicate that it occurs during deglaciation. Brackets illustrate the age range exhibited by IRD peaks within the records from two core sites (41°S and 53°S) interpreted here as regionally correlative depositional events. Brackets also denote that some events (especially SA1 and SA4) consist of several higher-frequency peaks.

rises abruptly beginning at ~16 ka. The sedimentation rates and temporal resolution of core TTN057-10 decline rapidly throughout this period and the record ends shortly after reaching Holocene isotopic values. The sedimentation rates and temporal resolution of TTN057-13/1094 increase throughout this period from a glacial mean of 13 cm/kyr to 32 cm/kyr across the glacial termination. Between ~15 and 13 ka a reversal to higher planktic $\delta^{18}O$ values occurred in TTN057-13/1094 within which is centered two closely-spaced peaks in quartz, the younger of which is accompanied by a peak in ash. This reversal in $\delta^{18}O$ also is recorded in TTN057-10 but is not seen in the $\delta^{18}O$ record of TTN057-21 (Figure 2-2). However, TTN057-21 does contain a minor IRD peak at this time (Figure 2-5). In TTN057-10, percent $CaCO_3$ reaches a maximum at ~13 ka and declines following this to the core top. The %BSi record of TTN057-13 does not exhibit a significant change at this time.

**Holocene (Marine Isotope Stage 1)**

During the Holocene, %BSi was high (averaging 84%) relative to that of the glacial period and the dominant lithology of the IRD switched from ash to quartz (Figures 2-3, 2-9). Ash, which made up over 90% of the total lithics on average during the glacial, dropped to only 21% of the total lithics in the Holocene. Conversely, quartz rose from a secondary component comprising only 6% of the total lithics on average to the dominant lithology at greater than 75% of the lithics. From 12 to 5 ka, IRD delivery to TTN057-13/1094 was minimal (averaging 2.0% of the >150μ fraction) and foraminifera were most abundant (averaging 9.6% of the >150μ fraction). This interval of generally low IRD is punctuated by brief peaks occurring at 10.5 ka, ~8 ka and 7 ka. After 5 ka, IRD returned abruptly to 53°S (increasing to 10.5% of the >150μ fraction on average). Quartz remained dominant relative to ash and quartz reached the highest levels observed in the entire glacial-interglacial record (comprising nearly 50% of the >150μ fraction and accumulating at a rate of >650 $mg/cm^2/kyr$ at 4.7 ka).

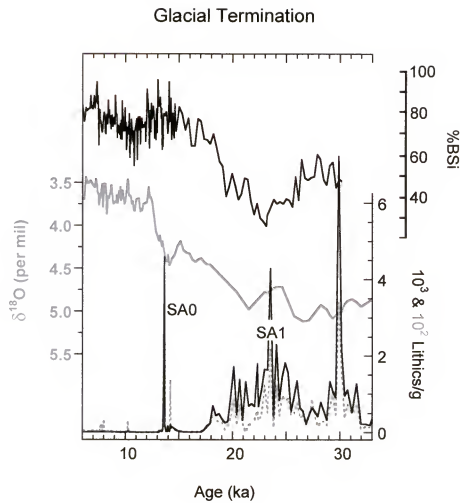


Figure 2-8. Glacial Termination. Comparison of total lithic concentration (black line) and quartz concentration (dotted gray line) in TTN057-13/1094 across the glacial termination with each planktic $\delta^{18}O$ (solid gray line) and percent biogenic silica (black line). Event SA0 occurs during the Antarctic Cold Reversal as indicated by an increase in planktic $\delta^{18}O$ values during Termination I. This event consists of two very brief, closely spaced peaks in IRD, the first dominated by quartz, the second dominated by ash. %Bsi exhibits no pronounced change during the ACR.

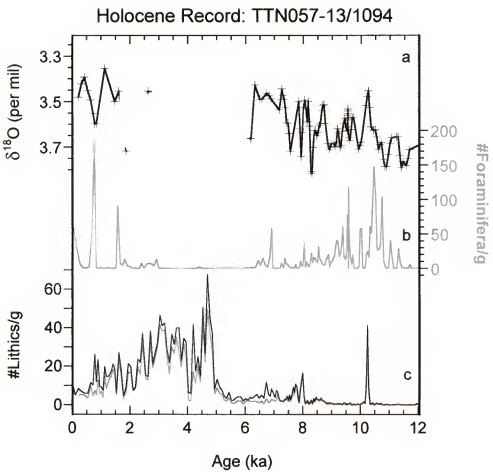


Figure 2-9. Holocene Record: TTN057-13/1094. Comparison of (c) total lithic concentration (black line) and quartz concentration (gray) with each (a) planktic $\delta^{18}O$ and (b) foraminiferal abundance (gray line). Low IRD and high foraminiferal abundance during the early Holocene suggest an early Holocene Hypsithermal. IRD delivery to the site resumes abruptly at ~5ka and is accompanied by a decline in foraminifera suggesting an interval of neoglaciation, or a return toward more glacial-like conditions.

## Discussion

### Interpretation of South Atlantic IRD

Geochemical analysis of volcanic ash in nearby cores suggests it is derived principally from the South Sandwich Islands in the Scotia Arc, with minor contribution from nearby Bouvet Island (Smith et al., 1983). Volcanic eruptions in the South Sandwich Islands produce ash that is carried east by prevailing winds. The size fraction analyzed (150 μm to 2 mm), however, precludes inclusion of ash transported to the core sites by wind or direct fallout from eruptions. The ash settles on ice shelves in the Weddell Sea and on seasonal sea ice, which acts as a conveyor of ash to the South Atlantic sediments during its seasonal advance and retreat.

The quartz and other non-ash lithics detected within the deep-sea cores at 41°S, 47°S and 53°S are sourced from Antarctica by calving of icebergs (Smith et al., 1983; Labeyrie et al., 1986). Today, the majority of Antarctic icebergs originates from ice shelves such as those found in the Weddell Sea (Warnke, 1970). Melting and freezing at the base of these ice shelves can produce debris-rich basal ice that can move upward as new ice is accreted by underplating (Eiken et al., 1994; Bombosch and Jenkins, 1995; Hulbe, 1997). During the last glaciation when sea level was ~120 m lower than today, peripheral ice shelves around Antarctic were more extensive than today as grounding lines moved seaward over the continental shelf (Denton and Hughes, 1983). The greater areal extent of ice shelves could have led to production of greater numbers or sizes of debris-laden icebergs and could in part explain the greater overall flux of IRD to the Southern Ocean during the glacial period than the Holocene. Additionally, cooler sea surface temperatures (SSTs) would be expected to enhance the survival and long-distance transport of icebergs to the core sites as well as the sediment retention for longer distances (El-Tahan et al., 1987; Venkatesh et al., 1994; Matsumoto, 1996, 1997; Azetsu-Scott and Syvitski, 1999).

There are at least two possible processes that might account for the abrupt oscillations in IRD in South Atlantic sediment cores. Labeyrie and others (1986) interpreted increases in quartz

between 17 and 35 ka to reflect increased ice discharge from the AIS. Alternatively, changes in sea surface temperature (SST) in the high-latitude South Atlantic might increase the survivability of icebergs. Keany and others (1976) suggested IRD deposition was related to migration of the PFZ and the zone of rapid melting of icebergs relative to a core's position. Peaks in IRD in Southern Ocean sediments may therefore indicate either increased production of icebergs and/or SST changes that affect their survival. The former has implications for AIS dynamics and predicts similar timing of IRD events across the South Atlantic. Conversely, changes in frontal boundary positions should result in diachronous accumulation of IRD with latitude and a "conjugate region" at intermediate latitudes where the IRD signal is confounded (Keany et al., 1976).

The Polar Front in the study area is presently located at ~49°S, and was apparently displaced northward by ~2° to 4° during the last glacial maximum (Brathauer and Abelmann, 1999). The winter sea ice limit was displaced northward by ~5° to 8° relative to its modern position at ~55° in the study area (Crosta et al., 1998). Changes in SST associated with PFZ migrations may have influenced the position of melting of debris-laden icebergs and sea ice in the South Atlantic during the last glaciation, as predicted by Keany and others (1976). Thus I believe the IRD record from 47°S (TTN057-10) is not solely a record of production of icebergs from the AIS. In contrast, there is no indication that the PFZ migrated north of 45°S during the last glaciation (Crosta et al., 1998), yet the presence of quartz in glacial sediments at 41°S (TTN057-21) clearly indicates icebergs reached this distant site. Similarly, the site at 53°S (TTN057-13/1094) has always been well south of the PFZ and, therefore, the fluctuations in quartz during the last glacial period are most probably the result of iceberg production rather than temperature-controlled variations in melting-zone position.

A prominent glacial-aged (radiocarbon-dated at $\geq$ 26 kyr) IRD layer was discovered in sediment cores collected from the Antarctic continental margin in the vicinity of the Weddell Sea

(Anderson and Andrews, 1999). Since this site is situated well poleward of the influence of melting line migration, it supports the occurrence of ice surges as a controlling mechanism on downcore lithic concentration. A peak in IRD appearing in both TTN057-10 and TTN057-13/1094 near this time that is broad and fluctuating (spanning ~22-26 ka and ~23-27 ka, respectively) overlaps in age with the IRD layer observed on the shelf. A discrete peak in IRD at ~25 ka is observed in TTN057-21. Considering this temporal overlap and the errors associated with radiocarbon dating, it is not unreasonable to suggest that these events are manifestations of the same surge. In contrast, other sediment records of coarse lithic concentration from the Weddell Sea and Antarctic Peninsula were shown to contain a series of millennial fluctuations that are not correlative between individual cores and thus have been interpreted to suggest that rapid ice-sheet collapse did not occur during the late Quaternary (Cofaigh et al., 2001). However, the cores used in the latter study were more proximal to the ice sheet margin and the authors note that the IRD signal recorded in these cores may have been affected by low sedimentation rates and/or current winnowing.

To reconstruct the history of AIS instability during the last glacial period, I compared IRD records between cores situated outside the past dynamic range of the PFZ (Figure 2-7). IRD concentrations in the South Atlantic decrease with increasing distance from Antarctic source areas, such that abundances at 41°S are about two orders of magnitude less than that at 53°S (Figure 2-10). Even so, the pattern of prominent IRD layers in the two sediment records (TTN057-13/1094 and TTN057-21) is remarkably similar, and I interpret them as manifestations of increased ice discharge from the AIS (Figure 2-7, Table 2-2). Radiocarbon ages are precise enough to establish that South Atlantic (SA) events SA0 and SA1 are synchronous between the two sites. I cannot prove that the other events are strictly correlative between sites, but the timing

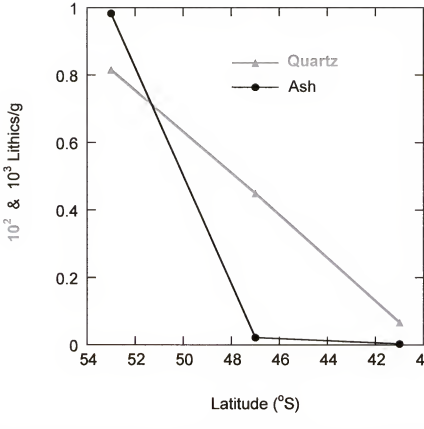


Figure 2-10. Mean glacial IRD concentrations, quartz (gray line with triangles) and ash (black line with circles) with respect to latitude. Concentrations of IRD in the southeast Atlantic decrease with decreasing latitude such that abundances at 41°S are roughly two orders of magnitude less than that at 53°S. The decrease in quartz concentration with latitude is linear. The rate of decrease in ash concentration, in contrast, is steepest from Site 1094 to Site 1091, perhaps due to the proximity of Site 1091 to the PFZ during the glaciation and the consequent rapid melting of ash-bearing sea ice in warm SST.

is close enough to suggest that the major events represent synchronous deposits. Using my most conservative age model, Peak SA5 shows a significant temporal offset between 41° and 53° S, but this offset could be the result of chronological uncertainties in the lower portion of the TTN057-13/1094 record. Between 10 and 60 ka, five (or possibly 6) IRD events occur that have a temporal spacing that ranges between ~6- and 10-kyr (Table 2-2). This millennial-scale spacing is similar to the 7- to 10-kyr recurrence of massive ice discharges associated with Heinrich Events in the North Atlantic (Heinrich, 1988; Andrews and Tedesco, 1992; Bond et al., 1992, 1993; Bond and Lotti, 1995; Fronval et al., 1995).

Table 2-2. Millennial South Atlantic IRD (SA) events and their corresponding calendar ages.

| Event | TTN057-21 (41°S) | TTN057-13/1094 (53°S) | Difference | Mean | Spacing |
|---|---|---|---|---|---|
| SA0 | 14.8 | 13.6 | 1.1 | 14.2 | - |
| SA1 | 18.3-26.5 | 18.1-26.6 | 1.8 | 24.5 | 10.3 |
| SA2 | 30.9 | 29.9 | 1.0 | 30.4 | 5.9 |
| SA3 | 37.1 | 36.1 | 1.0 | 36.6 | 6.2 |
| SA4 | 41.7-45.1 | 42.3-46.5 | 1.1 | 43.8 | 7.2 |
| SA5 | 51.2 | - | - | - | 7.4 |
| SA6 | - | 55.4 | - | - | 4.2 |

Note: All units are kyr. Also shown are the age difference and the mean age of events present in both cores. Where observed in both records, the temporal spacing between successive IRD events was calculated with mean ages.

Clark and Pisias (2000) suggested that SA events are not analogous to the Heinrich events of the North Atlantic, whereby they would imply increased influx of icebergs from the AIS, but rather that SA events have more in common with the non-Heinrich events of the North Atlantic. The non-Heinrich events have low sediment fluxes and have been associated with cold events in the North Atlantic indicating a stable, climatic response of marine ice-sheet margins to climate forcing (Bond and Lotti, 1995). In contrast, the physical properties of the IRD layers representing Heinrich events consist of high sediment fluxes distributed over a large area in a short interval of time (Broecker, 1994). On the basis of this, Clark and Pisias (2000) argued that, at minimum, IRD layers derived from the AIS must show also be characterized by high sediment

fluxes distributed over a large area in a short interval of time to serve as evidence of ice-sheet instability. The full areal extent of the South Atlantic IRD layers as yet remains unknown, however, they correlate across 12 degrees of latitude (greater than 1300 kilometers; Kanfoush et al., 2000a, 2000b). Although a correlative relationship has not been established with the SA events, discrete glacial-aged IRD layers have also been reported in numerous other South Atlantic cores (Watkins et al., 1982; Smith et al., 1983; Labeyrie et al., 1986). The age control of the cores described in this study used linear interpolation between radiometrically-determined ages and ages derived from correlation of the oxygen isotope record to SPECMAP (Martinson et al., 1987). The limited occurrence of carbonate within South Atlantic sediments poses a significant obstacle to high-resolution radiocarbon-dating of such sequences (Shipboard Scientific Party, 1999). Therefore, the chronology is not precise enough to discuss with confidence the duration and sedimentation rates of each of the individual SA events. However, with the exception of SA1 and SA3, accumulation rates of total lithics during SA events rise to ~10 times that of ambient rates (>60 times ambient rates in the case of SA0) (Figure 2-11). Thus, similar to the Heinrich events interpreted as evidence of surging of the Laurentide Ice Sheet, the SA events appear to be both areally extensive and rapidly deposited (Clark and Pisias, 2000; Kanfoush et al., 2000b).

Comparison of the planktic oxygen isotopic ($\delta^{18}O$) and IRD signals at 53°S reveals that most, but not all, of the major peaks in IRD of the last glacial period closely follow low planktic $\delta^{18}O$ values (Figure 2-3). The $\delta^{18}O$ value of planktic foraminifera is potentially a combined signal, being a function of the temperature of growth and/or the $\delta^{18}O$ of seawater, which is in turn a function of continental ice volume and salinity (Emiliani, 1955; Craig, 1965; Shackleton, 1974). Thus, low planktic $\delta^{18}O$ values represent reduced salinity and/or increased temperature of Antarctic surface waters. During the last deglaciation (Termination I, Figure 2-6), South Atlantic IRD Peak SA0 (14.2-13.5 ka) coincides with the Antarctic Cold Reversal (ACR) and global meltwater pulse 1a (~14.4-13.7 ka) (Fairbanks, 1989; Jouzel et al., 1995). Two or three brief

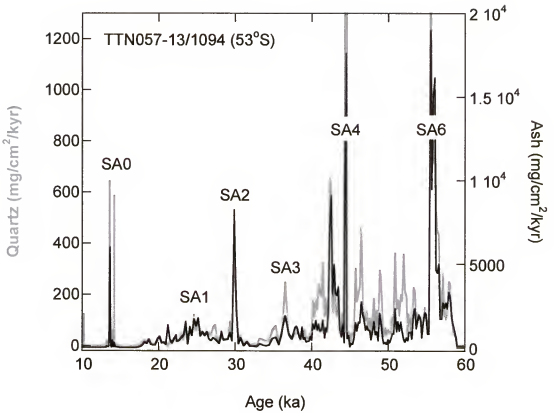


Figure 2-11. Accumulation rates (mg/cm$^2$/kyr) of IRD in TTN057-13/1094 showing that SA events, with the exception of SA1 and SA3, are deposited rapidly in relation to ambient sediments.

intervals of rapid eustatic sea-level rise separated by intervals of lower rates follow the LGM (Fairbanks, 1989; Blanchon and Shaw, 1995) and indicate catastrophic ice-sheet collapse (Blanchon and Shaw, 1995). Which ice-sheet(s) contributed to these rapid pulses remains highly debated (Nakada and Lambeck, 1988; Clark et al, 1996). The IRD deposition at 53°S within the ACR implies an influx of debris-laden icebergs coincident with the earliest and largest of the meltwater pulses observed across the deglaciation (Fairbanks, 1989; Clark et al., 1996). While not eliminating the Laurentide Ice Sheet or other ice-sheets as potential sources of meltwater, this IRD provides evidence that the AIS contributed to the rapid glacio-eustatic sea-level rise observed early in the deglaciation. Additionally, the coincidence of SA0 with the ACR may point to influx of icebergs from the AIS as the cause of this abrupt cooling event.

Peaks SA2 and SA4 in TTN057-13/1094 coincide each with a large increase in the abundance of the planktic foraminifer *N. pachyderma* (sin) (Figure 2-12). In TTN057-21, these as well as many of the other SA events show a similar association with high foraminiferal abundance. The co-occurrence of peaks in IRD and foraminifera in the South Atlantic contrasts with mid-latitude North Atlantic results showing low foraminiferal abundances during Heinrich Events (Ruddiman, 1977; Heinrich, 1988). Foraminifera and IRD in the Irminger Basin of the high-latitude North Atlantic, however, show a similar relationship to that observed in the South Atlantic (Elliot et al., 1998). This may result from iceberg-induced upwelling as has been reported for increased radiolarian productivity in the Southern Ocean (Neshyba, 1977; Labeyrie et al., 1986), or the retreat of sea ice (Grobe and Mackensen, 1992; Elliot et al., 1998). Alternatively, if foraminifera are incorporated into sea ice in significant numbers at the time of its formation they may be ice-rafted and subsequently melted out along with entrained or surficial lithic debris. A study in the Weddell Sea revealed that sea ice is enriched in *N. pachyderma* 70 times per unit volume in comparison to the underlying water column and, on an aerial basis, the

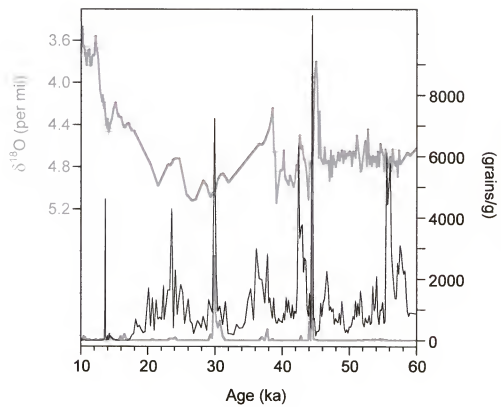


Figure 2-12. Total lithic concentration (black line), $\delta^{18}O$ of *N. pachyderma* (sin) (gray line with crosses) and abundance of foraminifera (gray line) in core TTN057-13/1094 at 53S. Event SA0 occurs during the Antarctic Cold Reversal, as indicated by an increase in planktic $\delta^{18}O$ values during Termination I. Events SA1, SA3 and SA4 are associated with low planktic $\delta^{18}O$ values, which indicate either the influence of meltwater or warm SST. Events SA2 and SA4 are associated with large increases in foraminiferal abundances.

sea-ice cover has approximately the same number of *N. pachyderma* as 60 m of underlying water column (Dieckmann et al., 1991).

The co-occurrence of high IRD and foraminifera during the glacial period contrasts with the pattern observed during the Holocene (Figure 2-9). During interglacial periods, Site 1094 is south of the Polar Front and north of the winter sea-ice margin. Fluctuations in the positions of these boundaries would affect iceberg and sea-ice survivability. Therefore, the controls on IRD during interglacial periods may be different from those during glacial periods. The decreased total flux of IRD to the South Atlantic during the Holocene reflects the landward retreat of grounding lines across the continental shelf relative to LGM positions and consequent decrease in the areal extent of peripheral ice shelves from which icebergs had been calving previously (Figure 2-3). Increased diatom productivity reflected by high %BSi relative to that of the glacial period suggests poleward retreat of the PFZ and perhaps also the sea ice margin. There is a shift in the dominant lithology from ash to quartz from the last glaciation to the Holocene that likely signals a change in the dominant mode(s) of transport of IRD to the site. IRD delivery by both icebergs (carrying both quartz and ash) and sea ice (carrying primarily ash) during the glaciation gave way to dominantly iceberg transport as thin sea ice was not capable of traversing the now warmer water overlying the site. A similar dominance of quartz is observed in MIS 5a.

The early Holocene period is marked by an IRD-free interval with abundant foraminifera occurring at a time when temperature over Antarctica is high (Figure 2-9). Following this, the late Holocene is characterized by a return to more glacial conditions, or a "neoglaciation" in which ice-rafting resumes abruptly and fluctuates irregularly while foraminiferal abundances decline (Kirby et al., 1998; Brachfield and Banerjee, 2000; Yoon, 2000; Hodell et al., 2001). Punctuating the generally low IRD flux of the early Holocene Hypsithermal is a prominent IRD event at ~10.5 ka, which occurs near the time of Heinrich Event H0 reported in North Atlantic sediments (Bond and Lotti, 1995). Whether initially triggered in the northern or southern hemisphere, a sea-level linkage could be responsible for causing coeval ice sheet surge events and attendant IRD delivery

to the two high latitude regions (Denton and Hughes, 1983). The IRD event occurring at ~8 ka in the Southern Ocean occurs at a time of the most prominent climatic event recorded in Holocene Greenland ice core proxies (Alley et al., 1997). Widely recorded in the northern hemisphere, this event is characterized by an atmospheric cooling of 6±2 °C, a 90% increase in forest fire frequency, increases in windblown chemical indicators, a decrease in methane and a freshening of North Atlantic surface waters (Duplessy et al., 1992; Keigwin and Jones, 1995; Alley et al., 1997). The similarities in the spatial pattern of climatic changes with those of the Younger-Dryas and the associated cooling and freshening of North Atlantic surface waters suggest thermohaline circulation played a role in this event (Alley et al., 1997). Suppression of NADW production has been attributed to rapid evacuation of ice and release of meltwater when the ocean broke into Hudson Bay (Street-Perrott and Perrott, 1990; Barber et al., 1999).

The abrupt return of ash, which is largely sea-ice rafted, to 53°S beginning at 5 ka indicates a cooling of SSTs and perhaps a northward advance of the average limit of winter sea ice (Hodell et al., 2001). This interval marks the beginning of the Neoglaciation in the late Holocene (Denton and Karlen, 1973). A similar change from "Hypsithermal" to "Neoglacial" conditions is recorded at 5 ka in sediments from the Bermuda Rise in the northern Sargasso Sea (Keigwin, 1996). Beginning at ~5 ka, weight %carbonate decreases and oxygen isotopic values of planktic foraminifera increase indicating climatic cooling in the northern Sargasso Sea. The onset of cooling at ~5 ka was abrupt and appears synchronous between the North and South Atlantic Oceans indicating a global rather than regional forcing mechanism.

**Relationship to NADW Flux**

To determine the phasing of South Atlantic IRD events relative to variations in the strength of North Atlantic Deep Water (NADW) production and climate in the North Atlantic, I compare the IRD and benthic $\delta^{13}C$ records in piston core TTN057-21 at 41°S (Figure 2-13). This core was taken on the same sediment drift from which core RC11-83 was recovered, and has a

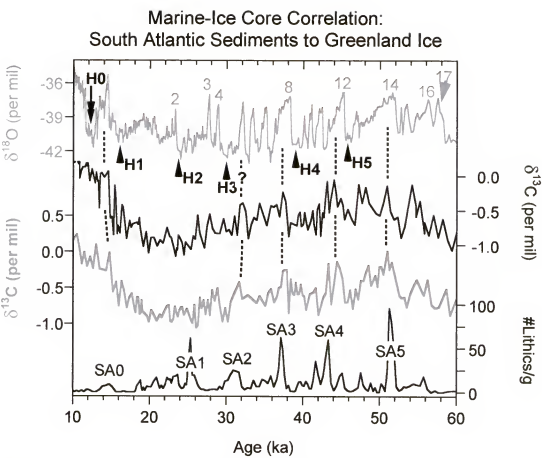


Figure 2-13. Similarities exist between the $\delta^{18}O$ record of the GISP2 Greenland Ice Core (top gray line) and the benthic $\delta^{13}C$ (*Cibicidoides*) records of sediment core RC11-83 (top black line) and TTN057-21 (bottom gray line), with each plotted on their independent chronologies (Charles et al., 1996; Ninnemann et al., 1999). Prominent interstadials as defined in the GISP2 record are numbered and the North Atlantic Heinrich (H) events are indicated relative to climatic events in the Greenland ice cores (Bond et al., 1993; Grootes et al., 1993). South Atlantic IRD events SA0-SA5 are expressed as peaks in the total lithic concentration in core TTN057-21 at 41°S (bottom black line). Events SA2 through SA5 are each associated with high benthic $\delta^{13}C$ values, indicating strong NADW production and inferred warming in the North Atlantic.

stable isotope signal that appears nearly identical in structure to that of RC11-83 (Ninnemann et al., 1999). Charles and others (1996) demonstrated that the benthic $\delta^{13}C$ record of RC11-83 is sensitive to changes in NADW input to the Southern Ocean and bears a striking resemblance to the $\delta^{18}O$ of Greenland ice core records. The two records are similar because both temperature over Greenland and benthic $\delta^{13}C$ in the South Atlantic are sensitive to the formation rate of NADW (Charles et al., 1996; Ninnemann et al., 1999). Each of the IRD events (SA2-5) between 30 and 60 ka is accompanied by an increase in benthic $\delta^{13}C$, suggesting that glacial South Atlantic IRD events are associated with strong NADW production and inferred warming in the North Atlantic.

South Atlantic IRD events tend to occur during the strongest interstadials in Greenland (IS 8, 12, 14 and possibly 16/17) during marine isotopic stage 3 (MIS 3; 28-59 ka). Bender and others (1994) suggested that these long interstadial events (>2 kyr) in Greenland have counterparts in the Vostok ice core of Antarctica. The SA events seem to follow a consistent pattern with the exception of peak SA1 that occurred during the last glacial maximum. During the last deglaciation, SA0 occurred synchronously with the "Antarctic Cold Reversal" (Fig 2-3a) and coincides with warming in Greenland associated with the Bölling/Allerod event. The inferred relationship between South Atlantic IRD events and warm phases of the Dansgaard-Oeschger (D-O) cycles (Dansgaard et al., 1993) implies that SA events were not correlative with North Atlantic IRD deposition because Heinrich Events occurred during the coldest phases of the D-O cycles (Bond et al., 1992, 1993; Bond and Lotti, 1995).

**Interhemispheric Linkage**

The correlation of glacial South Atlantic benthic $\delta^{13}C$ maxima and IRD events with interstadials in Greenland during the last glaciation argues for an interhemispheric linkage that influenced the stability of the AIS, as opposed to internal ice-sheet dynamics (MacAyeal, 1993). Deposition of IRD in the South Atlantic during times of warming in the North Atlantic may be a

manifestation of anti-phase climate behavior between these regions (Manabe and Stoufer, 1997; Broecker, 1998), but not necessarily in the sense normally considered when comparing ice core records of climate. For example, NADW is a major source of heat and salt to the Southern Ocean today (Jacobs et al., 1985; Gordon, 1981), and increased production of NADW during warm D-O events may have been responsible for basal melting of expanded Antarctic ice shelves during the last glaciation (Jenkins et al., 1997). Alternatively, sea-level rise associated with melting of the Laurentide Ice Sheet during warm D-O phases may have unpinned ice shelves that had grounded on the Antarctic continental shelf during times of lowered sea level (Denton and Hughes, 1983; Denton et al., 1986; Hulbe, 1997). Although evidence for the magnitude and timing of sea-level variations during MIS 3 is scarce, millennial-scale fluctuations have been proposed based on oxygen isotopic evidence from the Sulu Sea (Linsley, 1996) and uplifted coral terraces on the Huon Peninsula, New Guinea (Chappell and Shackleton, 1986; Yokoyama et al., 2001; Chappell, 2002). Sea-level rise associated with strong interstadial events may not cause a concurrent unpinning of the LIS as it had already experienced surging and rapid iceberg discharge during the preceding cold D-O phase (i.e. Heinrich Event).

## Conclusions

Ice-rafting delivered quartz and ash to the South Atlantic in a series of discrete millennial-scale pulses throughout the last glacial period. Because the IRD layers are synchronous in sites both north and south of the PFZ, they cannot be the result of migration of the melting line over the site. Rather, I interpret increases in IRD to reflect increases in Antarctic ice discharge on millennial timescales during the last glaciation. In contrast, late Holocene increases in IRD may reflect cooling of the surface South Atlantic.

Whereas D-O cycles and Heinrich events appear to have global signatures (Grimm et al., 1993; Broecker, 1994; Behl and Kennett, 1996; Bensen et al., 1998; Schultz et al., 1998), it remains to be seen if the South Atlantic IRD events identified here will prove to have important regional, hemispheric or even global implications. As yet, I cannot quantify the volume of ice

involved in the rapid calving events or the pattern of discharge in other sectors of the Southern Ocean. Nevertheless, the association of IRD events in the South Atlantic during times of increased NADW and warming in the North Atlantic reflect a consistent response to global climate change during the last glaciation.

# CHAPTER 3
# RELATIONSHIP TO ENVIRONMENTAL AND CLIMATIC PROXIES

## Introduction

If the late Pleistocene history of the AIS included abrupt episodes of instability on millennial timescales (Smith et al., 1983; Labeyrie et al., 1986; Kanfoush et al. 2000a, 2001; see Clark and Pisias, 2000 and Kanfoush et al., 2000b for discussion), then what factors control stability of the AIS? Determination of the leads and lags of changes in the various components of the cryosphere-hydrosphere-atmosphere system has the potential to reveal cause and effect relationships or, at least, to eliminate potential causal relationships. Here I compare the relative timing of peaks in concentration of IRD in the southeast Atlantic with climate proxies from polar ice cores.

In the North Atlantic region, marine-ice correlations have played a key role in understanding the origin and implications of Heinrich and higher-frequency IRD layers. Correlation between North Atlantic cores and the Greenland ice cores reveal that ice-rafting events were associated with brief coolings over Greenland (Heinrich, 1988; Bond et al., 1993; Dansgaard et al., 1993). Here I correlate the South Atlantic IRD record to polar ice cores from Antarctica and Greenland to compare the timing and magnitude of millennial IRD variability with regional changes in atmospheric variables recorded in Antarctica and Greenland. Each correlation is achieved first on the basis of stable isotopes, and then independently tested by correlating sediment paleointensity records with cosmogenic nuclide abundance in polar ice cores.

Limitations in the resolution or accuracy of the chronology may hinder attempts to correlate brief (millennial) events from one core to another. In contrast, comparison of the relative timing of parameters present within a single core serves as an alternate means to potentially infer

the relationship of ice-rafting to environmental and climatic changes (Charles et al., 1996). Consequently, for each of two deep-sea cores I also compare changes in IRD concentration with changes in other parameters within the same core define their sedimentary signature, to determine their impact on surface water hydrology and finally to assess lead-lag relationships. Examination of downcore phase relationships will therefore serve as a test of the climatic interpretations derived via marine-ice correlations.

## Materials and Methods

The material discussed in this study consists of the spliced sedimentary sequence (TTN057-13/1094) from the southernmost site at 53°S south of the present-day position of the PFZ and north of the average limit of winter sea ice (Figure 1-2) (Zwally et al., 1983; Gloerson et al., 1992; Kanfoush et al., 2002; Hodell et al., 2001; Shemesh et al., 2001). Also discussed is the northernmost core (TTN057-21 at 41°S) collected at Site 1089, north of the present-day PFZ. Each core was sampled at 3- or 5-cm intervals, corresponding to a temporal resolution of approximately 200 to 500 years during the glacial period. These core sites were selected for this study because each lies outside both the modern PFZ as well as its past dynamic range throughout the last glaciation, and IRD peaks present in each have been previously demonstrated to result from increased AIS ice discharge rather than temperature controlled changes in the position of melting of debris-laden icebergs (Figure 2-3) (Kanfoush et al., 2000a).

Downcore IRD concentrations were visually determined on the 150μ-to-2mm size fraction following the methodologies of Allen and Warnke (1991). Oxygen isotopic measurements of the planktic foraminifera *Neogloboquadrina pachyderma* (sin) in TTN057-13/1094 were made at the University of Florida using a Finnigan MAT252 mass spectrometer coupled to an automated carbonate preparation system (Kiel III) and measurements of the planktic foraminifera *Globigerina bulloides* in TTN057-21 were made at the Scripps Institution of Oceanography using a Finnigan MAT 252 mass spectrometer and automated common-acid

bath device (Hodell et al., 2001; Mortyn, 2000; Mortyn et al., submitted). Gross features of each of these records were discussed previously (in Chapter 2; Kanfoush et al., 2000a). A more detailed (higher resolution) examination of these records is presented here.

Oxygen isotopic measurements of the benthic foraminifera *Cibicidoides wuellerstorfi* in TTN057-21 were also made at the Scripps Institution of Oceanography Finnigan MAT 252 mass spectrometer (Ninnemann et al., 1999). Isotopic ratios are reported in standard delta notation ($\delta^{18}O$) relative to V-PDB (Coplen, 1996). Analytical precision, estimated by the standard deviation (one sigma) of repeated analysis of a powdered carbonate standard (NBS-19), was ±0.06 per mil for $\delta^{18}O$. Benthic $\delta^{18}O$ data are unavailable for TTN057-13/1094 because of a lack of the benthic foraminifera *Cibicidoides wuellerstorfi* or other appropriate benthic species.

## Results

### Planktic Oxygen Isotopes

Due to sporadic presence or insufficient numbers of *N. pachyderma* (sin), the planktic $\delta^{18}O$ record of TTN057-13/1094 is discontinuous and of lower resolution than the lithic record in the same core (Figure 3-1a). Glacial values of planktic $\delta^{18}O$ range from ~5.1 per mil at the last glacial maximum (LGM) to ~3.8 per mil in MIS 3. The record fluctuates throughout the glaciation on millennial timescales and contains several pronounced minima, particularly in MIS 3. A plot of both the lithic and oxygen isotopic records from core TTN057-13/1094 and TTN057-21 reveals that IRD deposition occurred under both full glacial conditions (MIS 4 and 2) and interstadial conditions (MIS 3) (Figure 3-1).

Many, but not all, of the major peaks in lithic concentration in TTN057-13/1094 immediately follow a low planktic $\delta^{18}O$ event and are associated with increasing planktic $\delta^{18}O$ values (Figure 3-1a). This relationship is strongest during MIS 3, with each of the three large peaks in lithic concentration observed (SA4b, -4a, -3) immediately following a low planktic $\delta^{18}O$ event, and somewhat less consistent at other times during the glacial. A fourth planktic $\delta^{18}O$

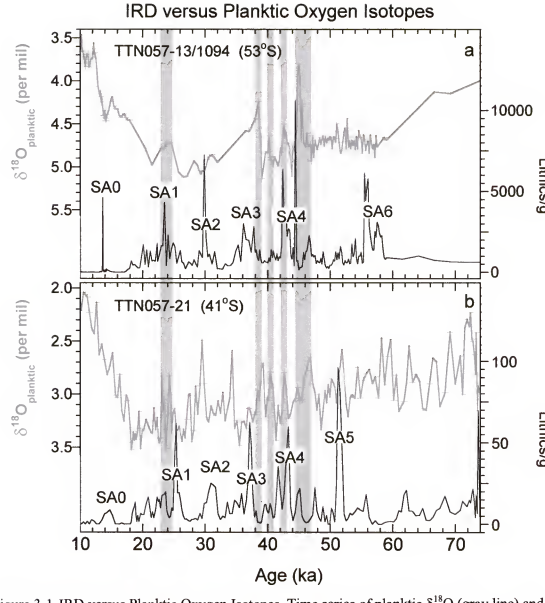


Figure 3-1. IRD versus Planktic Oxygen Isotopes. Time series of planktic $\delta^{18}O$ (gray line) and IRD (lithics/g, black line) in each of the two sediment cores. (a) South of the PFZ (in TTN057-13/1094 at 53°S), SA events consistently lag minima in planktic $\delta^{18}O$. (b) In contrast, although peaks in IRD north of the PFZ (in TTN057-21 at 41°S) are also associated with minima in planktic $\delta^{18}O$, their phase relationship with the isotopic anomalies is variable. Despite the strongly differing resolution of the two records, prominent planktic $\delta^{18}O$ minima (shaded vertical bars) in TTN057-13/1094 correlate with prominent minima in TTN057-21, particularly in MIS 3.

minimum of lesser magnitude, however, is also present in the TTN057-13/1094 record of MIS 3 that has only a minor, un-named associated IRD peak. Early in MIS 3, one prominent IRD event occurs (SA6 at ~56ka) that is not accompanied by a low in the planktic $\delta^{18}O$ signal. Two prominent IRD peaks (SA1 and SA2) are observed within MIS 2 prior to the beginning of the glacial termination. Both lag minima in planktic $\delta^{18}O$ values; however, whereas one isotopic event (SA1 at ~24ka) is very prominent, the other (SA2 at ~31ka) is quite small.

The planktic $\delta^{18}O$ record of TTN057-21 is more continuous and of higher resolution than that of TTN057-13/1094 (Figure 3-1b). It contains several pronounced minima and, similar to TTN057-13/1094, many of these isotopic events is associated with a brief pulse in IRD. In contrast to the pattern observed in TTN057-13/1094, however, the relationship whereby IRD peaks lag somewhat the planktic $\delta^{18}O$ minima is not consistent in TTN057-21. Although many IRD peaks (SA5 and numerous smaller-amplitude peaks) do immediately follow planktic $\delta^{18}O$ minima, other peaks appear to occur synchronously or even precede slightly the light planktic $\delta^{18}O$ events.

**Benthic Oxygen Isotopes**

Scarcity of benthic foraminifera in TTN057-13/1094 precluded the development of a benthic isotope record at this site. Benthic $\delta^{18}O$ values in TTN057-21 are highest in the stadials (ranging from a maximum of ~4.4 at the LGM to ~4.0 per mil in MIS 2 and 4) and exhibit comparably lower values during the interstadial (ranging from ~3.6-3.9 per mil in MIS 3; Figure 3-2) (Charles et al., 1996). Values fluctuate on millennial timescales throughout the glacial period. Maxima in total lithic concentration display an inconsistent relationship with benthic $\delta^{18}O$. Some lithic peaks (SA4b, SA2, SA1 and perhaps also SA0) are associated with benthic $\delta^{18}O$ minima. In contrast, other lithic peaks (peaks at ~62ka and ~56ka as well as SA5 and SA3) coincide with short-lived, typically small-magnitude maxima.

**Benthic Carbon Isotopes**

Benthic $\delta^{13}C$ values in TTN057-21 are lowest during stadials (ranging from a minimum of ~-1.2 per mil in MIS 4 to a stadial maximum of ~ -0.4 per mil in MIS 2) and exhibit comparably higher values during the interstadial (ranging from ~-0.8-0.0 per mil in MIS 3) (Figure 3-3). Values fluctuate on millennial timescales throughout the glacial period. With only the exception of SA1, each peak in total lithics during the glaciation coincides with a brief but pronounced maximum in benthic $\delta^{13}C$. Examination of the relative timing of peaks in each benthic $\delta^{13}C$ and planktic $\delta^{18}O$ reveals that minima in planktic $\delta^{18}O$ frequently precede maxima in benthic $\delta^{13}C$ (Figure 3-4). This offset is most pronounced in the middle part of MIS 3, during which the benthic $\delta^{18}O$ leads by more than ~2 kyr, whereas during MIS 4 and 2 many fluctuations in each record are nearly synchronous.

## Discussion

**Marine-Ice Correlations Using Stable Isotope Records**

The records of benthic $\delta^{13}C$ in the southeast Atlantic and $\delta^{18}O$ in the Greenland ice-core (GISP2) resemble one another on millennial timescales (Figure 3-5a) (Johnsen et al., 1992; Grootes et al., 1993). Maxima in benthic $\delta^{13}C$ represent periods of strong North Atlantic Deep Water (NADW) formation (Oppo et al., 1990; Charles et al., 1996). Strong NADW formation necessitates significant poleward transport of surface water, resulting in the poleward transfer of heat, thus warming the North Atlantic (Manabe and Stoufer, 1997; Broecker, 1998). Such warming of the North Atlantic region is recorded in GISP2 as maxima in $\delta^{18}O$. Therefore, both benthic $\delta^{13}C$ in the South Atlantic sediments and $\delta^{18}O$ in Greenland ice are a function of changes in NADW production (Charles et al., 1996).

Comparison of the records of total lithics and benthic $\delta^{13}C$ in South Atlantic core TTN057-21 reveals that IRD peaks are associated with high benthic $\delta^{13}C$ values (Figure 3-3). Kanfoush and others (2000a) suggested the correlation between maxima in the benthic $\delta^{13}C$

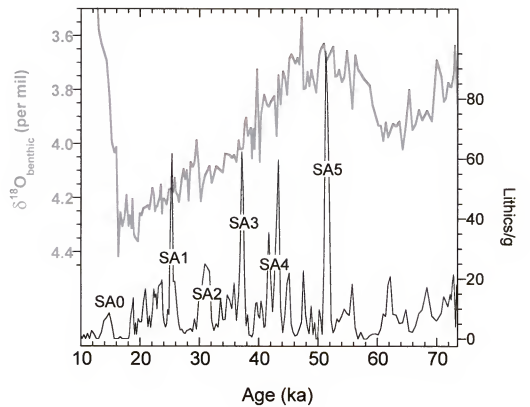


Figure 3-2. Time series of benthic $\delta^{18}O$ (gray line) and IRD (lithics/g, black line) in core TTN057-21 (41°S) for the last glacial period on the chronology of Charles and others (1996).

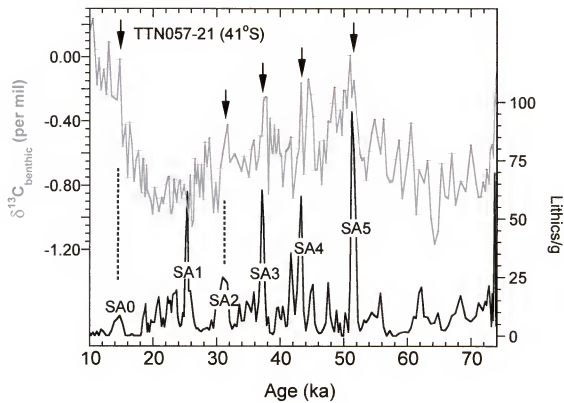


Figure 3-3. Time series of benthic $\delta^{13}C$ (gray line) and IRD (lithics/g, black line) in TTN057-21 (41°S) revealing that, with only the exception of SA1, SA events coincide with prominent maxima in benthic $\delta^{13}C$.

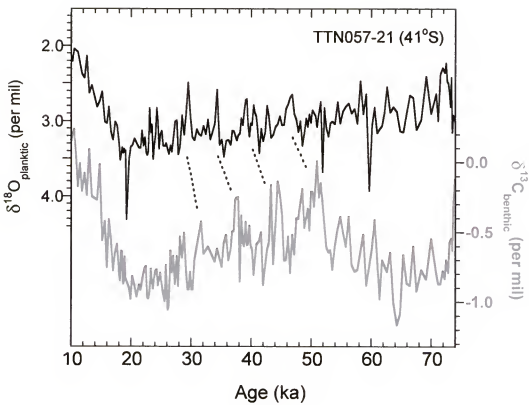


Figure 3-4. Comparison of planktic $\delta^{18}O$ (black line) and benthic $\delta^{13}C$ (gray line) in core TTN057-21 (41°S) demonstrating that oscillations in the carbon isotopic record often lag those within the oxygen isotopic record. The lag appears to be most consistent and of largest magnitude during MIS 3. Alternatively, the relationship between planktic $\delta^{18}O$ and benthic $\delta^{13}C$ can be interpreted as out-of-phase.

record from TTN057-21 and the $\delta^{18}O$ record from GISP2 implied a relationship between South Atlantic ice discharge events and strong interstadial events in the North Atlantic region. In addition to warming of the North Atlantic, the "bipolar see-saw" hypothesis purports that enhanced NADW formation and associated increased cross-equatorial heat transfer leads to consequent cooling in the southern hemisphere (Manabe and Stoufer, 1997; Broecker, 1998). If SA events correlate with warm events over Greenland, as suggested by the benthic $\delta^{13}C$ correlation, then the timing of SA events may coincide with the initiation of cooling over Antarctica.

Even on their independent chronologies, peaks in each benthic $\delta^{13}C$ in TTN057-21 and $\delta^{18}O$ in GISP2 are nearly synchronous (Figure 3-5a). Greenland-Antarctic ice-core correlations have been constructed on the basis of atmospheric methane concentration (Blunier, 1998; Blunier and Brook, 2001). Therefore, plotting the Byrd Ice Core on the GISP2 age model enables us to compare the timing of SA events with regional temperature recorded in Byrd (Figure 3-5b) (Johnsen et al., 1972; Blunier and Brook, 2001). Doing so suggests that many of the millennial-scale South Atlantic IRD events during MIS 3 (SA6, -5, -3 and perhaps also -4) occur on the cooling limb following prominent warm events (A3-A1) recorded in Antarctic ice. Even the smaller IRD peak (at ~56 ka) in TTN057-21 that occurs near SA6 in TTN057-13/1094 also occurs on the cooling following Antarctic warm event A4. Event SA4 is a multiple peak event with each higher-frequency event designated ----4a, -4b and -4c, in chronological order. On the basis of this correlation, the largest of the peaks comprising this event (SA4b) occurs at a time of maximum regional cooling. Alternatively, if the double peak in benthic $\delta^{13}C$ in TTN057-21 at ~43-44 ka is interpreted to correlate with, and hence shifted to align with, the single $\delta^{18}O$ minima in GISP2 that represents Interstadial 12, the timing of SA4b alters such that it would fall on the cooling limb of A2. The SA events of MIS 2 and 4, in contrast, do not display a clear relationship with regional climate on the basis of this correlation.

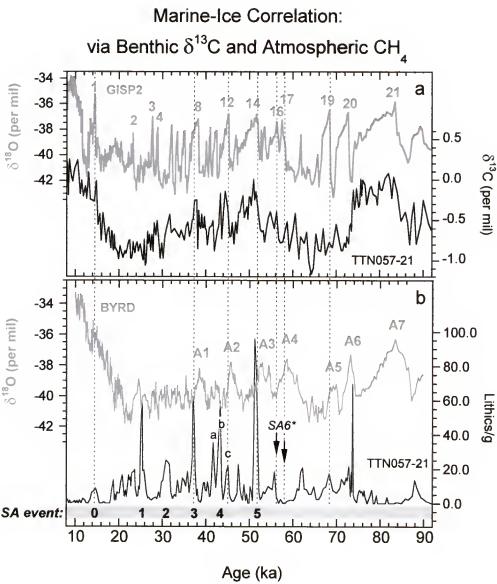


Figure 3-5. Marine-Ice Correlation via Benthic $\delta^{13}C$ and Atmospheric $CH_4$. (a) Comparison of the benthic $\delta^{13}C$ of TTN057-21 (black line) with the $\delta^{18}O$ record of the Greenland ice core GISP2 (gray line, Johnsen et al., 1992; Grootes et al., 1993; Kanfoush et al., 2000a), each plotted on their independent chronologies. The two records bear a striking resemblance, implying both the South Atlantic benthic $\delta^{13}C$ signal and temperature proxy signal are responding to NADW production (Oppo et al., 1990; Charles et al. 1996). (b) The Byrd ice core has been transferred onto the GISP2 chronology by correlation of the methane concentration in each (Blunier and Brook, 2001). Consequently, the timing of SA events (black line) can be compared with climatic events recorded in $\delta^{18}O$ record of Byrd (gray line, Johnsen et al., 1972). The position of SA-6 recorded in TTN057-13/1094 is indicated.

Planktic $\delta^{18}O$ in TTN057-21 bears obvious resemblance to both Vostok $\delta D$ and Byrd $\delta^{18}O$ and provides an independent, and more direct, means to achieve correlation between South Atlantic sediments and Antarctic ice (Johnsen et al., 1972; Jouzel et al., 1987; Ninnemann et al., 1999; Petit et al., 1999; Mortyn, 2000; Mortyn et al., submitted) (Figures 3-6a, 3-7a). The cause of the observed anti-correlation of foraminiferal $\delta^{18}O$ with Vostok $\delta D$ and Byrd $\delta^{18}O$ lies most plausibly in a common response of the climate system to surface temperature. Prominent warm events recorded in the ice-core records (including events A1-A4 within MIS 3) are clearly discernible in the planktic $\delta^{18}O$ record (Mortyn, 2000; Mortyn et al., submitted). Alignment of prominent features common to each the South Atlantic sediment core and Antarctic ice core records enables synchronization of their chronologies, thus allowing comparison of the timing of SA events relative to climatic events over Antarctica. Ice-core records from East and West Antarctica, however, have revealed some differences in climate between the two regions (Steig et al., 1998, 2000). Therefore, the marine record from 41°S was correlated to Vostok of East Antarctica and Byrd of West Antarctica (Figures 3-6a, 3-7a). The resulting correlation to Vostok shows strong agreement with a correlation presented by Mortyn et al. (submitted) between Vostok and a southeast Atlantic planktic isotope stack (of which TTN057-21 is a part). As predicted, the SA events of MIS 3 (SA6, –5, -4c and –3) occur on the cooling limb following peak interstadial warmth. Again, notable exceptions to the pattern are the SA events of MIS 2 (SA1 and SA2), which appear to precede Antarctic warming.

The correlation to Byrd yields a temporal relationship between millennial South Atlantic IRD events and Antarctic climate consistent with that observed in the correlation to Vostok whereby the SA events of MIS 3 occur on the cooling limb following prominent Antarctic warm events (Figure 3-7b). Each of these correlations, however, was based on the reasoning that the anti-correlation of foraminiferal $\delta^{18}O$ with Vostok $\delta D$ and Byrd $\delta^{18}O$ was due to a common response of the climate system to surface temperature (Mortyn, 2000; Mortyn et al., submitted).

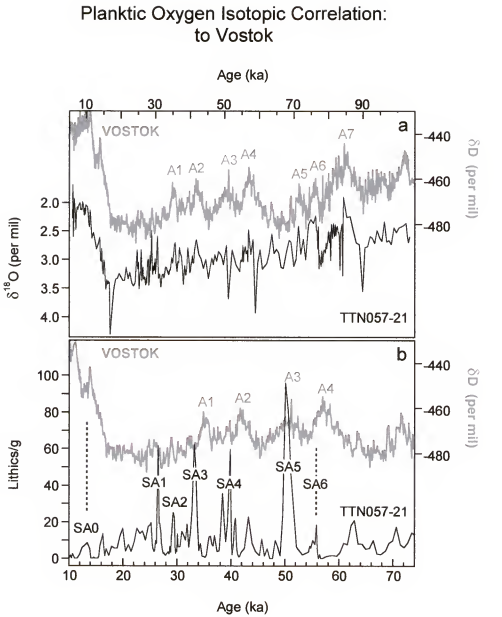


Figure 3-6. Planktic Oxygen Isotopic Correlation to Vostok. (a) The planktic $\delta^{18}O$ record of TTN057-21 (black line) correlated to Vostok δD (gray line), thereby transferring TTN057-21 onto the Vostok chronology (Petit et al., 1999). (b) The resulting correlation thus enables comparison of the IRD record of TTN057-21 (black line) with climatic events recorded in East Antarctic ice (Vostok δD; gray line), each shown on the Vostok chronology.

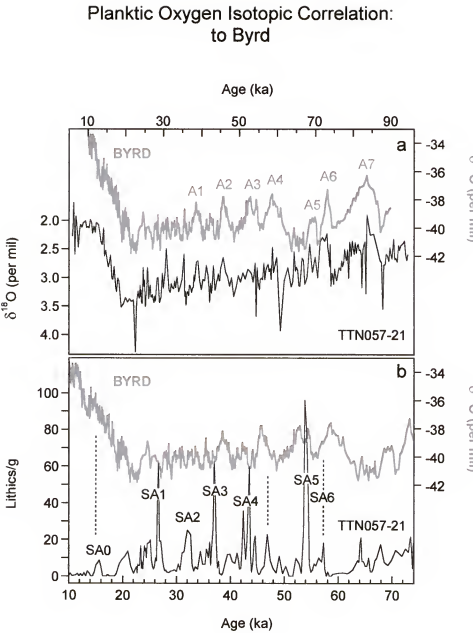


Figure 3-7. Planktic Oxygen Isotopic Correlation to Byrd. (a) The planktic $\delta^{18}O$ record of TTN057-21 (black line) correlated to Byrd $\delta^{18}O$ (gray line), thereby transferring TTN057-21 onto the Byrd (GISP2) chronology (Grootes et al., 1993). (b) The resulting correlation thus enables comparison of the IRD record of TTN057-21 (black line) with climatic events recorded in West Antarctic ice (Byrd $\delta^{18}O$; gray line), each shown on the common chronology (Johnsen et al., 1972; Blunier and Brook, 2001).

Whereas this is the simplest and certainly a plausible explanation, a means by which the relationship between SA events and regional climate can be substantiated is the examination of downcore phase relationships.

In the southeast Atlantic the planktic $\delta^{18}O$ foraminiferal record shows a series of prominent light anomalies associated with each of the SA events. In most cases, at 53°S each millennial IRD peak was deposited a few hundred years to more than a thousand years after the planktic $\delta^{18}O$ minimum (Figure 3-1a). The relationship is strongest during MIS 3 and somewhat less consistent elsewhere. The precise lag amount cannot be accurately determined due to the substantially lower resolution of the isotope record because of the lack of or insufficient numbers of *N. pachyderma* (sin) in some horizons. Nonetheless the lag is consistently observed for each prominent IRD event of MIS 3 recorded at this site, and it cannot be explained by differential settling of the more dense lithic material in relation to the microfossils as that scenario would demand the reverse phase relationship. The $\delta^{18}O$ value of planktic foraminifera is potentially a combined signal, being a function of the temperature of growth and/or the $\delta^{18}O$ of seawater, which is in turn a function of continental ice volume and salinity (Emiliani, 1955; Craig, 1965; Shackleton, 1974). Thus, light planktic $\delta^{18}O$ anomalies can represent either warming or meltwater or some combination thereof. Meltwater contribution to the site by melting of icebergs, however, would yield a near synchronous relationship between IRD and planktic $\delta^{18}O$ minima or the planktic $\delta^{18}O$ anomalies would lag.

In contrast to the TTN057-13/1094 record, the lack of coherence between the timing of IRD and planktic $\delta^{18}O$ minima within the TTN057-21 record suggests caution should be taken in concluding that the isotopic anomalies represent warming (Figure 3-1). The higher resolution of the northern record raises concern in that, on the basis of this fact alone, one would deem it the more reliable record. Alternatively, it appears the rapid isotope fluctuations, inferred warm-cold oscillations, of MIS 3 are grouped into somewhat longer-term (~5-10 kyr on average) bundles of

progressively heavier $\delta^{18}O$ values (Figure 3-8). Each prominent IRD event of MIS 3 is associated with one of these pronounced longer-term $\delta^{18}O$ bundles, with the initiation of IRD deposition lagging the $\delta^{18}O$ minima, thus supporting the marine-ice core correlations. Estimates of summer sea-surface temperature (SSST) derived from alkenones in TTN057-21 and from radiolarian assemblages in nearby Site 1089 each revealed millennial SSST oscillations during MIS 3 on the order of 1-3°C and 3-4°C, respectively (Sachs et al., 2001; Cortese and Abelmann, 2002). The discrepancy in magnitudes may be because alkenones potentially suffer from allocthonous transport of organic matter by bottom water currents (Sachs et al., 2001). Nonetheless, both methods generally support the interpretation of low planktic $\delta^{18}O$ of MIS 3 as warming and also support the interpretation that the rapid warm-cold oscillations are grouped into longer-term bundles of progressively heavier $\delta^{18}O$ values. One potential explanation then of the observed lag between planktic $\delta^{18}O$ minima and IRD is that the ice discharge event terminated the inferred warming. In contrast to the phasing observed in MIS 3, event SA1 of MIS 2 peaks prior to the occurrence of minimum isotope values and SA2 occurs at a time of an isotopic maximum, inferred as a time of peak regional cooling.

In each sediment record, outside the periods of increased IRD deposition, foraminiferal abundance is extremely low (Figure 3-9). In contrast, each of the prominent IRD peaks is accompanied by high foraminiferal abundance (Kanfoush et al., 2000a). Such increases may result either from retreat of the winter sea-ice margin, warming of the surface South Atlantic or from iceberg-induced upwelling (Burckle, 1982; Grobe and Mackensen, 1992). Alternatively, foraminifera may be incorporated into sea ice during its formation and subsequently melted out along with IRD (Dieckmann et al., 1991). Microfossils show no evidence for sea-ice expansion to 41°S even at the LGM (Crosta et al., 1998; Brathauer and Abelmann, 1999). Therefore, retreat of the winter sea-ice margin cannot account for the observed fluctuations in foraminifera in TTN057-21. Close examination of the phase relationship between foraminifera and IRD in

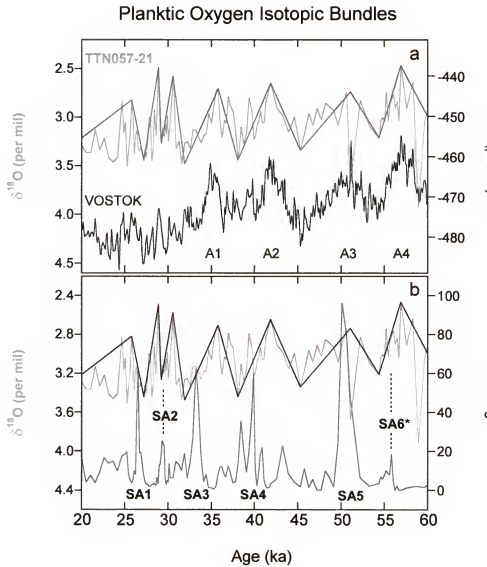


Figure 3-8. Planktic Oxygen Isotopic Bundles. (a) The TTN057-21 planktic $\delta^{18}O$ record (gray line) correlated to the Vostok δD record (solid black line) such that each is shown on the Vostok chronology (Petit et al., 1999). Rapid fluctuations, inferred warm-cold oscillations, are grouped into somewhat longer-term (~5-10 kyr on average) bundles of comparably light $\delta^{18}O$ values (superimposed black line). (b) With only the exception of SA1, each SA event (black line) of the last glaciation occurs on the cooling limb of one of these pronounced longer-term $\delta^{18}O$ minima. The minor peak at ~56 ka within the TTN057-21 record occurs very near in time to Event SA6 recorded within the TTN057-13/1094 record.

TTN057-21 and TTN057-13/1094 reveals that, in each record, peaks in the two components occur synchronously. Coincidence of the foraminifera and IRD would be consistent with either iceberg-induced upwelling or with incorporation of foraminifera during sea ice formation as the cause of the increased abundance. However, peak values in the foraminiferal abundance are substantially higher at both 53°S and 41°S during interstadial MIS 3 as compared to peak abundances during stadials MIS 2 and 4, arguing for at least some temperature control on productivity and again supporting the marine-ice correlations.

Comparison of the benthic $\delta^{18}O$ and the IRD records in TTN057-21 reveals an inconsistent relationship between millennial IRD peaks and benthic $\delta^{18}O$ (Figure 3-2). Shackleton and others (2000) presented a marine sediment record from the North Atlantic in which the planktic $\delta^{18}O$ record closely resembled the record of inferred temperature over Greenland yet, in the same core, the benthic $\delta^{18}O$ closely resembled the record of inferred temperature over Antarctica. However, there is only very limited similarity between the benthic $\delta^{18}O$ record in TTN057-21 and temperature recorded in Antarctic ice implying a factor other than regional temperature dominates the benthic $\delta^{18}O$ signal at this core site (Figure 3-2b).

**Testing Marine-Ice Correlations Using Geomagnetic Paleointensity**

The power of the marine-ice correlations presented here, developed using stable isotopes, is that they enable comparison of the timing of millennial South Atlantic IRD events relative to climatic events recorded in Antarctic and Greenland ice-cores and thus provide an opportunity to potentially identify or eliminate the triggers of SA events. However, these correlations relied on the assumption that each proxy shares the common control of climate. Although this assumption is supported by the downcore phase relationships, yet another promising means of independent verification of the marine core-ice core correlations achieved on the basis of stable isotopic records lies within recent and ongoing studies of geomagnetic paleointensity variations (Stoner et al., 1995a, 1998, 2000; Channell et al., 2000).

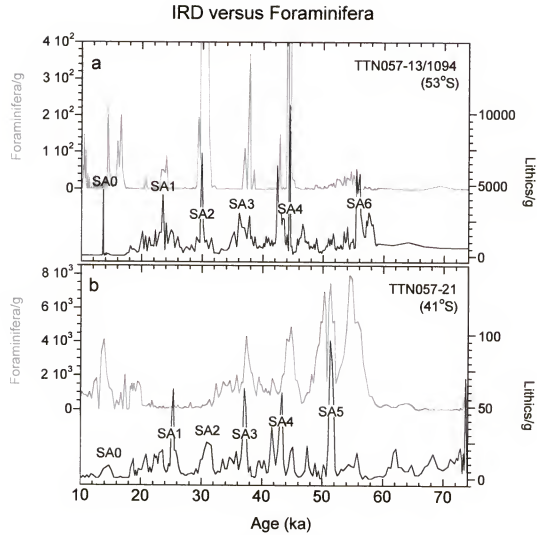


Figure 3-9. IRD versus Foraminifera. Time series of foraminiferal abundances (foraminifera/g, gray line) and IRD (lithic/s, black line) in (a) TTN057-13/1094 (53°S) and in (b) TTN057-21 (41°S).

Geomagnetic paleointensity variations have been shown to display global variance at millennial timescales (Tric et al., 1992; Meynadier et al., 1992; Stoner et al., 1995a; Guyodo and Valet, 1996). Variations in geomagnetic paleointensity control the flux of $^{10}Be$ and $^{36}Cl$, isotopes readily measurable in ice cores (Robinson et al., 1995; Masarik et al, 1999; Yiou et al., 1997; Baumgartner et al., 1998;). Therefore, paleointensity variations recorded within marine sediments can be directly correlated to other sediment records (Channell et al., 1997; 2000; Stoner et al. 1998; Laj et al., 2000) as well as to Antarctic (Raisbeck et al., 1987; Mazaud et al., 1994) and Greenland ice (Baumgartner et al., 1997; Yiou et al., 1997; Voelker et al., 1998; Wagner et al., 2000).

Substantial progress has been made by Stoner and others (2000, 2002) toward developing a common global chronostratigraphy enabling comparison of marine sediment records and ice-core climatic records from the North and South Atlantic regions each transferred onto the GISP2 ice-core age model. Included within this developing global framework is the South Atlantic paleointensity stack (SAPIS) of which TTN057-21 is a part. Stoner and others (2002) placed the marine cores within the common SAPIS stratigraphy using a combination of common lithologic features (from magnetic susceptibility), planktic and benthic isotopic features, and geomagnetic features and then correlated SAPIS to a North Atlantic paleointensity stack (NAPIS; Laj et al., 2000) that has been correlated to Greenland ice using the planktic $\delta^{18}O$ data of Voelker and others (1998) on PS2644-5 (one of the cores comprising the NAPIS stack) and GISP2 $\delta^{18}O$ (Grootes et al., 1993; Stuiver and Grootes, 2000).

Stoner and others (2000; 2002) also individually correlated the paleointensity data of South Atlantic core TTN057-21 to that of MD95-2024 (Labrador Sea) that they had previously correlated to GISP2 using the assumption that detrital layers in MD95-2024 correlate to cold stadials in Greenland ice, thereby transferring South Atlantic core TTN057-21 onto the GISP2 chronology (Figure 3-10) (Bender et al., 1994; Meese et al., 1994). A test of the marine core-ice

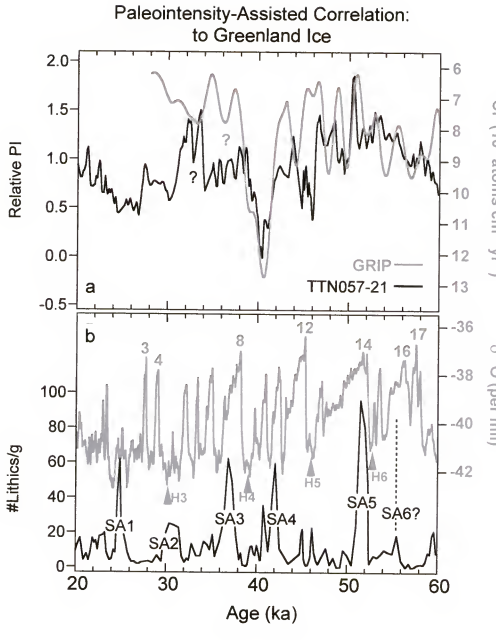


Figure 3-10. Paleointensity-Assisted Correlation to Greenland Ice. (a) Comparison of the records of relative paleointensity (PI; black line) of TTN057-21 and flux of the cosmogenic isotope $^{36}$Cl ($10^4$ atoms/cm$^2$/yr; gray line) in GRIP resulting from the paleointensity-assisted correlation of SAPIS to GRIP (Stoner et al., 2000; 2002). Question marks indicate uncertainty in the correlation for the younger portion of the record. (b) Comparison of the timing of the South Atlantic record of ice-rafting (#lithics/g; black line) relative to inferred climate over Greenland ($\delta^{18}$O per mil; gray line). The chronology for both records is that of GISP2 (Bender et al., 1994; Meese et al., 1994; Stoner et al., 2000; 2002).

core correlation between TTN057-21 and GRIP can be seen in Figure 3-10a in which the resulting correlation between TTN057-21 and GRIP is strongly consistent with the inverse relationship between relative paleointensity and $^{36}Cl$ flux, respectively, for the older portion of the record (>40 ka). For the younger portion of the record the correlation results in poor alignment in prominent features in each paleointensity and $^{36}Cl$ and, thus, remains uncertain.

Comparison of the South Atlantic record of ice-rafting to inferred climate recorded in Greenland ice on the basis of this paleointensity-assisted correlation generally confirms the earlier correlation between benthic $\delta^{13}C$ in TTN057-21 and $\delta^{18}O$ in Greenland ice such that millennial South Atlantic ice-rafting events of the last glaciation, particularly those of MIS 3, are associated with prominent interstadial events in Greenland (Figure 3-10b) (Kanfoush et al., 2000a). The paleointensity-assisted correlation also supports the earlier assertion that SA events are not synchronous with but generally lag the Heinrich events. One exception to this pattern is SA2 that, on the basis of this correlation, is associated with only a very minor warm event occurring between IS4 and IS5 and occurs very near in time to H3. However, the phasing of this event relative to inferred Greenland climate is one of two differences noted between the South Atlantic – Greenland correlation achieved previously on the basis of benthic $\delta^{13}C$ versus the paleointensity-assisted correlation (Figure 3-11) (Kanfoush et al., 2000a; Stoner et al., 2000; 2002). Event SA2 coincided with IS-5 in the former marine-ice core correlation, placing it prior to the occurrence of H-3, thus the phasing of this IRD peak remains uncertain. However, if the paleointensity-assisted correlation of Stoner and others (2000; 2002) is shifted such that between 40 and 30 ka closer alignment is achieved between the prominent maxima and minima in each paleointensity and $^{36}Cl$ flux, respectively, then the two independent correlations show stronger agreement with regard to the phasing of SA2. The other difference between the two correlations is with regard to the relative timing of the largest peak comprising SA-4, which is here associated

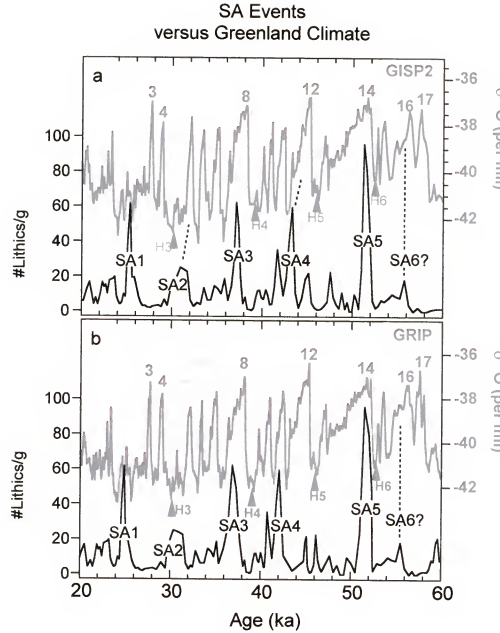


Figure 3-11. SA Events versus Greenland Climate. The phasing of millennial South Atlantic ice-rafting events (black line) relative to inferred Greenland climate (gray line) based upon two independent means of correlation between South Atlantic sediments and Greenland ice: (a) benthic $\delta^{13}C$ correlation (Kanfoush et al., 2000a) and (b) paleointensity-assisted correlation (Stoner et al., 2000; 2002).

with IS-11 whereas it was associated with the more prominent IS-12 in the previous (benthic $\delta^{13}C$) correlation (Kanfoush et al., 2000a).

With TTN057-21 transferred onto the GISP2 chronology, regional marine-ice core correlation between TTN057-21 and Vostok was then accomplished using the synchronization of Greenland and Antarctic ice-core chronologies on the basis of methane concentration in trapped gas (Blunier et al, 1998; Stoner et al., 2000). Despite the substantially lower resolution of the cosmogenic isotope record in Vostok, a convincing comparison results between relative paleointensity measured within TTN057-21 and $^{10}Be$ in Vostok (Figure 3-12a) (Raisbeck et al., 1987; Mazaud et al., 1994). On the basis of this correlation then, the South Atlantic record of ice-rafting can now be compared to inferred regional climate recorded in Antarctic ice to independently (in)validate the correlation achieved on the basis of planktic $\delta^{18}O$ (Figure 3-12b).

The two independent correlations display remarkable similarity, with only the timing of the multi-peaked event SA4 in disagreement between the two (Figure 3-12b). In the isotopic correlation, SA4c falls on the cooling limb of Antarctic warm event A2 and SA4b occurs as Antarctic temperature rise is initiated. In contrast, in the paleointensity-assisted correlation SA4c is shifted such that it occurs earlier, at peak warmth of A2, and SA4b is shifted later to a time of peak Antarctic cool temperature. With only the exception of this multi-peaked event, however, the marine-ice core correlation achieved in part by paleointensity and supported here by direct comparison between paleointensity in South Atlantic sediments and cosmogenic isotopes in Antarctic ice supports the planktic isotopic correlation in suggesting SA events occur on the cooling limb following prominent millennial Antarctic warm events.

**Interhemispheric Relationships**

The coincidence of millennial South Atlantic IRD events with abrupt warming in Greenland and with cooling, particularly with gradual cooling, in Antarctica is precisely what would be predicted by the "bipolar see-saw" hypothesis (Manabe and Stoufer, 1997; Broecker,

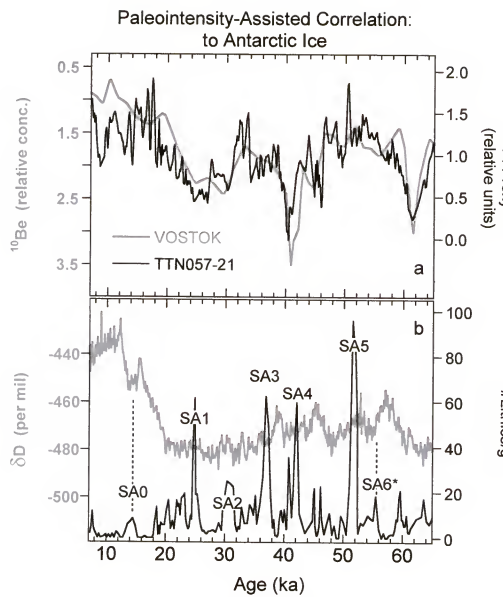


Figure 3-12. Paleointensity-Assisted Correlation to Antarctic Ice. (a) Comparison of the records of relative paleointensity (PI; black line) of TTN057-21 and flux of the cosmogenic isotope $^{10}$Be ($10^4$ atoms/cm$^2$/yr; gray line) in Vostok resulting from combination of the paleointensity-assisted correlation of SAPIS to GRIP (Stoner et al., 2000; 2002) and Greenland-Antarctic ice-core correlations using methane gas concentration (Blunier, 1998). Question marks indicate portions of the correlation that differ substantially from the isotopic correlation. (b) Comparison of the timing of the South Atlantic record of ice-rafting (#lithics/g; black line) relative to inferred climate over Antarctica (δD per mil; gray line). The chronology for both records is that of GISP2 (Bender et al., 1994; Meese et al., 1994; Stoner et al., 2000; 2002).

1998) and by recent interhemispheric correlations (Blunier, 1998; Blunier and Brook, 2001). Such anti-phase temperature of the North and South Atlantic regions as well as the association of a South Atlantic ice-rafting event (SA0) with each peak North Atlantic warmth (the Bölling interstadial; IS-1) and Antarctic cooling (the ACR) are clearly observed across the deglaciation (Figure 3-13).

The pattern of South Atlantic ice-rafting during MIS 3 is similar to that observed during the deglaciation, whereby SA events coincide with warming in Greenland and with cooling in Antarctica. However, in contrast to the deglaciation during which event SA0 appears to be centered within the ACR very near peak cool temperatures, the SA events of MIS 3 occur on the gradual cooling limb of Antarctic interstadials. Unlike Heinrich events of the North Atlantic the SA events of MIS 3 do not typically occur at times of peak Antarctic cooling, nor do they exhibit a consistent amount of lag from peak warmth. IRD concentrations frequently reach peak values and decrease again prior to the maximum of the regional cold phases, signifying that increased SA events of MIS 3 are not simply a reflection of increased iceberg survivorship as ocean surface temperatures dropped. Although SA events of MIS 3 are each associated with a regional cooling trend and, therefore, could be interpreted as simply a linear response to regional climate forcing, the cooling interval prior to an SA event is of variable duration. In contrast, peak IRD delivery consistently coincides with near-peak values of benthic $\delta^{13}C$, interpreted as initiation of enhanced NADW formation and an abrupt rise in Greenland temperatures. If SA events are climatically driven, the more coherent relationship between SA events and changes in climate of the North Atlantic region during MIS 3 implies the origin of the millennial Antarctic ice discharge events during this interval lies there and is somehow transmitted southward.

One potential mechanism is a sea-level linkage whereby melting of Greenland ice associated with enhanced NADW formation and interstadial warmth elevated eustatic sea-level sufficiently to "un-pin" ice shelves of the Weddell Sea region (Denton et al., 1986; Huybrechts, 1990; Kanfoush et al., 2000a). This model is consistent with the observed phase relationships. In

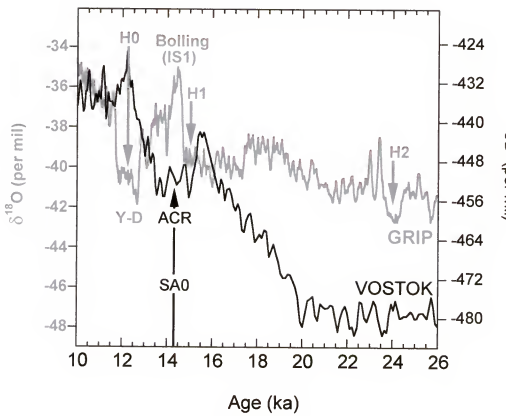


Figure 3-13. Interhemispheric Relationships Across the Glacial Termination. Inferred temperature over Greenland as recorded in the GRIP ice core ($\delta^{18}O$ per mil; gray line) and over Antarctica as recorded in the Vostok ice core (δD per mil; black line), each plotted on the GISP2 equivalent age model (Stoner et al., 2002). The arrows mark the occurrence of ice-rafting events in the North Atlantic (Heinrich event H0; gray arrow) and South Atlantic (event SA0; black arrow). The millennial South Atlantic IRD event coincides with peak North Atlantic warmth (the Bölling interstadial; IS-1) and Antarctic cooling (the ACR).

addition, strong support comes from comparison of the record of South Atlantic ice-rafting with detailed sea-level curves emerging from studies of Barbados and the Huon Peninsula (Figure 3-14) (Lambeck and Chappell, 2001; Yokoyama et al., 2001). The timing of several sea-level highstands recorded each in Barbados (~52-, ~44-, ~37- and ~32-ka) and on the Huon Peninsula (~51.5-, ~43.7-, ~38.3 and ~30.4-ka) relative to that of SA 5-2 (~51-, ~43.5, ~37- and ~31-ka, respectively) is striking. The lack of a clear relationship of the SA events of MIS 2 and 4 with regional climate on the basis of these correlations, in contrast, suggests that sea-level rise was perhaps only an effective trigger of Antarctic ice discharge at times during the last glacial period when sea level was generally high (such as MIS 3) in relation to other times during this period.

Although seemingly not triggered by regional climate change, SA events may play a role in causing regional climate change. An interesting difference between Greenland and Antarctic climate records is that prominent ice-rafting events, Heinrich events, originating in the North Atlantic trigger a much stronger climate response in the Antarctic. Antarctica responds strongly to a dramatic drop in inter-hemispheric heat transport resulting from collapse of the conveyor triggered by freshwater input (Manabe and Stoufer, 1997; Broecker, 1998). In Antarctic ice this is recorded as prominent interstadial events A1-4 during MIS 3 (Blunier et al., 1998). The abrupt resumption of NADW formation coincident with prominent interstadials of the North Atlantic then contributes to the ensuing Antarctic cooling. Greenland, on the other hand, is already in a stadial mode at the start of a Heinrich event and beyond the reach of the glacial configuration of the oceanic conveyor, thus a Heinrich event leads to no further regional cooling (Ganopolski and Rahmstorf, 2001).

Antarctica, unlike Greenland, is not already in a stadial mode at the start of a prominent regional ice-rafting event. Regional insolation is high throughout MIS 3 and, that forcing alone, should lead to generally high regional temperature throughout this interval (Figure 3-15). Intense resumption of NADW formation, leading to increased cross-equatorial heat transport following Heinrich events, combined with ice-discharge into the South Atlantic may have periodically

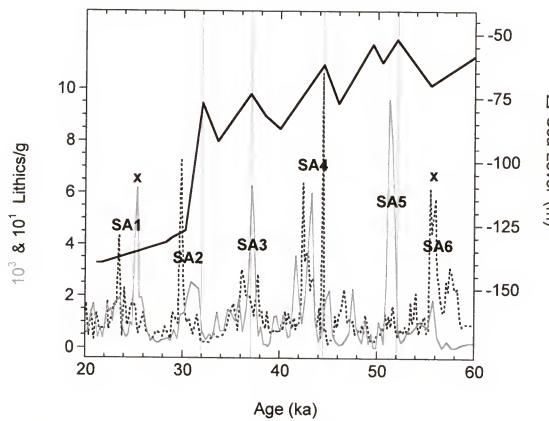


Figure 3-14. Comparison of change in eustatic sea level relative to today (Lambeck and Chappell, 2001; solid black line) with South Atlantic IRD in TTN057-13/1094 (dotted gray line) and TTN057-21 (solid black line). Many SA events (SA-5, -4, -3 and perhaps also –2) during MIS 3 are initiated or peak at times of millennial-scale highstands in eustatic sea level recorded at Barbados and the Huon Peninsula. An "x" indicates presence of a peak in IRD that does not coincide with a millennial highstand in sea level.

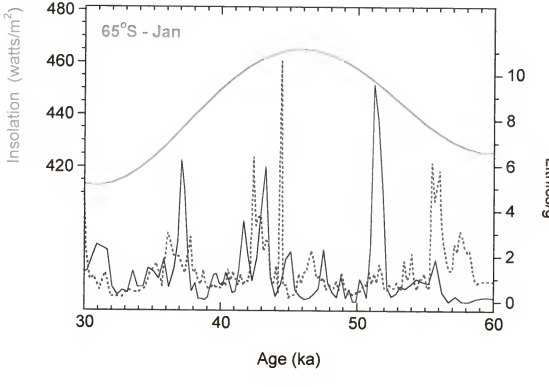


Figure 3-15. Comparison of January insolation at 65°S (Berger and Loutre, 1991; solid gray line) with South Atlantic IRD in TTN057-13/1094 (dotted gray line) and TTN057-21 (solid black line). Despite high regional insolation throughout MIS 3, regional temperature inferred from ice-core data reveals a series of millennial cold oscillations near in time to, and typically lagging slightly, influxes of icebergs responsible for the SA events.

prevailed over the insolation forcing, triggering the observed cold phases of the warm-oscillations that punctuate MIS 3 (Lagerklint and Wright, 1999). This explanation is consistent with the observed lag between planktic $\delta^{18}O$ minima and IRD in MIS 3. The ice-discharge into the South Atlantic evidenced by IRD layer SA0 may have similarly triggered the return to cooler conditions (the ACR) that briefly punctuated the southern hemisphere deglaciation (Kanfoush et al., 2002).

**Conclusions**

The sedimentary signature of the South Atlantic millennial IRD events differs somewhat with latitude. South of the PFZ, simultaneous deposition of ice-rafted quartz and volcanic ash is preceded by light planktic $\delta^{18}O$ anomalies and accompanied by synchronous occurrence of high foraminiferal abundances. Although the planktic $\delta^{18}O$ can represent either warming or meltwater or some combination thereof, the consistent lead-lag relationship suggests they represent in part warming. North of the PFZ, simultaneous deposition of quartz and ash is again accompanied by synchronous deposition of high foraminiferal abundances and associated with light planktic $\delta^{18}O$ anomalies. At this latitude, a peak-to-peak comparison of IRD and planktic $\delta^{18}O$ minima yields a variable phase relationship. However, rapid warm-cold oscillations recorded at 41°S appear to be grouped into longer-term cooling bundles, somewhat analogous to Bond Cycles of the North Atlantic region, and SA events occur on the cooling limb of these longer-term cycles.

The impact of SA events on the surface South Atlantic at each site appears to include an immediate and pronounced local increase in productivity resulting perhaps from iceberg-induced upwelling or warming. South of the PFZ, planktic $\delta^{18}O$ maxima immediately following IRD deposition imply a lowering of SST due to iceberg melting. North of the PFZ, the sediment record indicates that some light planktic $\delta^{18}O$ anomalies follow IRD input and likely represent meltwater contribution from icebergs.

Marine-ice core correlation between the planktic $\delta^{18}O$ signal at 41°S and temperature proxy records in Antarctic ice suggests SA events of marine isotope stage (MIS) 3 occur on the

cooling limb following prominent millennial Antarctic warm events. Both downcore phase relationships and paleointensity-assisted correlations (Stoner et al, 2000; 2002) independently support this correlation and the ensuing interpretations, suggesting the planktic $\delta^{18}O$ signal at 41°S and temperature proxy records in Antarctic ice share a common response to surface temperature such that high-resolution records of planktic $\delta^{18}O$ in this vicinity may be a useful tool for marine-ice correlations (Mortyn et al., submitted). The strong correspondence of the paleointensity-assisted correlations to those achieved on the basis of each planktic $\delta^{18}O$ and benthic $\delta^{13}C$ reinforces its potential as a tool for global chronostratigraphy.

The coincidence of millennial South Atlantic IRD events of MIS 3 with abrupt warming in Greenland and with gradual cooling in Antarctica is precisely what would be predicted by the "bipolar see-saw" hypothesis (Manabe and Stoufer, 1997; Broecker, 1998) and by recent interhemispheric correlations (Blunier, 1998; Blunier and Brook, 2001). The SA events of MIS 3 consistently occur on the gradual cooling limb of Antarctic interstadials yet they do not typically occur at times of peak Antarctic cooling, nor do they exhibit a consistent amount of lag from peak warmth. The observed phase relationships do not eliminate Antarctic climate as the trigger of Antarctic ice discharge. However, if SA events are climatically driven, the synchronous relationship between SA events and North Atlantic interstadials during MIS 3 points to this region as a more likely candidate for this interval. Although perhaps not triggered by regional climate, millennial South Atlantic IRD events may, in combination with the intense resumption of NADW formation following Heinrich events, trigger regional climate change.

CHAPTER 4
THE LAST FOUR CLIMATIC CYCLES

## Introduction

Millennial-scale pulses in IRD delivery to the South Atlantic during the last glaciation have been documented that represent episodes of instability of grounded ice shelves in the Weddell Sea on suborbital timescales (Kanfoush et al., 2000a). Variability of IRD has also been documented for the Holocene from the South Atlantic including an abrupt late-Holocene increase in ice-rafting and decrease in sea surface temperatures (SST) at ~5 ka (Hodell et al., 2001). In this chapter, the high-resolution record of ice-rafting at Site 1094 is extended from marine isotopic stage (MIS) 1 through Termination V (to the MIS 11/12 boundary) to examine the nature of ice-sheet and sea-ice variability over the last four climatic cycles.

The longest, most continuous record of Antarctic climate variability is the Vostok ice core, which extends through the last 420 kyr and captures variability on millennial time-scales (Petit et al., 1999). Here I present a South Atlantic deep-sea record that has a length equaling and resolution approaching, or in some intervals exceeding, that of the Vostok ice core. The utility of such a record is twofold. First, a high-resolution IRD record spanning several climatic cycles provides an opportunity to understand the interactions between variability in the suborbital and Milankovitch bands. Second, correlation of the marine sediment and ice core records will enable comparison of the timing and magnitude of IRD variability in the South Atlantic with changes in atmospheric variables recorded in Vostok. My study is similar to that of Bond and others (1993) who presented a correlation between North Atlantic cores and the Greenland ice cores which showed the relationship between IRD events (Heinrich events -- Heinrich, 1988) and temperature changes over Greenland during the last glaciation (Dansgaard-Oeschger cycles --

Dansgaard et al., 1993). Similarly, correlation of the high-resolution South Atlantic IRD record from Site 1094 will help determine if Antarctic ice-discharge events were linked to external climatic factors.

## Materials and Methods

The material analyzed in this study comes from the spliced TTN057-13/1094C stratigraphy described in chapter 1 and in Kanfoush and others (2000a). The site is located within the biogenic silica belt of the Southern Ocean south of the present-day position of the Polar Frontal Zone (PFZ) and about 2° north of the average limit of winter sea ice (Figure 1-2) (Zwally et al., 1983; Gloerson et al., 1992, Shipboard Scientific Party, 1999). The piston core was sampled at 3- or 5-cm intervals, corresponding to a temporal resolution of approximately 50 to 150 years during the interglacial periods and approximately 300 to 500 years during the glacial periods. To extend the record through the last four climatic cycles, this record was appended to the shipboard-generated composite record that was produced from the same site (Site 1094) during Leg 177 (Shipboard Scientific Party, 1999). The ODP cores were sampled at 5-cm intervals, yielding similar temporal resolution to that of the piston core.

Eleven AMS $^{14}$C-dates on monospecific samples of *Neogloboquadrina pachyderma* (sin) from eight stratigraphic horizons in TTN057-13 provide chronological control to a depth of 9.7 meters below seafloor (mbsf) (to ~38 kyr; explained in Chapter 1). All ages presented subsequently are in calendar years. Using planktic foraminiferal oxygen isotopic records, TTN057-13-PC4 and 1094C were spliced at a depth of 9.7mbsf in the piston core and depths in the piston core were adjusted downward by 3 meters (Table 4-1). This is equivalent to a depth of 12.7 meters composite depth (mcd) in Core 1094C-2, which is not part of the shipboard splice. The downward adjustment of depths in the piston core is necessary to produce a record that is consistent with the depth assignments (i.e., mcd) in ODP site 1094. To the base of 1094C (at 20.5 mcd), the 1094 composite was then spliced extending the record to 73.7 mcd. Below the TTN057-13-PC4/1094C splice position (12.7 mcd), the chronology is constructed by correlating

the oxygen isotopic record to SPECMAP (Imbrie et al., 1984; Martinson et al., 1987) and intervening ages were interpolated assuming linear sedimentation rates between tie points (Figure 4-1) (Hodell et al., 2002).

Table 4-1. Splice table, showing development of the Site 1094 composite stratigraphy.

| Core | Section & Interval | Depth (mbsf) | Depth (mcd) | Age (ka) | Latitude (°S) | Longitude (°S) | Water Depth |
|---|---|---|---|---|---|---|---|
| TTN057-13-PC4 | X 0-2 cm | 0.0 | 3.0 | 0.0 | 53.2 | 5.1 | 2850 |
| | IV 141-143 cm | 9.7 | 12.7 | 37.8 | | | |
| ODP 1094C-2H | 2W 60-62 cm | 11.0 | 12.7 | 37.8 | 53.2 | 5.1 | 2818 |
| | 7W 70-72 cm | 18.7 | 20.5 | 88.0 | | | |
| ODP 1094 splice | A 3H3W 95-97 cm | 18.1 | 20.5 | 88.0 | 53.2 | 5.1 | 2818 |
| | A 8H4W 40-42 cm | 65.6 | 68.6 | 345.0 | | | |

Note: Using planktic foraminiferal oxygen isotopic records, TTN057-13-PC4 and 1094C were spliced at a depth of 9.7 mbsf in the piston core and depths in the piston core were adjusted downward by 3 meters. This is equivalent to a depth of 12.7 meters composite depth (mcd) in Core 1094C-2, which is not part of the shipboard splice. To the base of 1094C (at 20.5 mcd), the 1094 composite was then spliced extending the record to 73.7 mcd. All ages presented are in calendar years.

Downcore IRD concentrations were visually determined on the 150μ-to-2mm size fraction (Allen and Warnke, 1991). At least 500 grains were counted and included quartz, volcanic ash, fine-grained volcanics, coarse-crystalline rock fragments, metamorphics, radiolarians and foraminifera. Relative percent within the 150μ fraction (%), number of grains per gram of total dry sediment (grains/g), milligrams per gram of total dry sediment (mg/g) and accumulation rate (mg/cm$^2$/kyr) were calculated for the individual components (Allen and Warnke, 1991).

Abundance of planktic foraminifera at Site 1094 was variable, resulting in a discontinuous oxygen isotope record, including a gap in late stage 11 and 10 and also in mid stage 5. Oxygen isotopic measurements of the planktic foraminifera *N. pachyderma* (sin) were made at

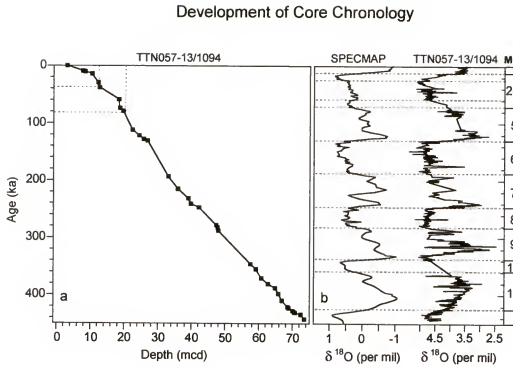


Figure 4-1. Development of Core Chronology. (a) Age-depth model for the Site 1094 stratigraphy derived from piston core TTN057-13, ODP core 1094C-2 and the shipboard splice. Ages were determined by AMS $^{14}C$ to 37ka and beyond this by correlation of the Site 1094 $\delta^{18}O$ record to the SPECMAP record (Martinson et al., 1987). Squares indicate ages determined from radiocarbon or $\delta^{18}O$ correlation points between which ages were interpolated. Dashed lines indicate core splice positions, and that at 37ka also denotes the limit for AMS $^{14}C$ control. Notice in this and all subsequent figures depths in piston core TTN057-13 were adjusted downward by 3 meters, placing the core top at 3 mcd, to keep depths for the composite stratigraphy consistent with the Site 1094 shipboard splice mcd scale. Ages in this and all subsequent figures are in calendar years. (b) (Left) The reference stratigraphy of SPECMAP (Martinson et al., 1987). (Right) Correlation of the Site 1094 planktic $\delta^{18}O$ record to SPECMAP (Hodell et al., 2002).

the University of Florida using a Finnigan MAT252 mass spectrometer coupled to an automated carbonate preparation system (Kiel III). Isotopic ratios are reported in standard delta notation ($\delta^{18}O$) relative to V-PDB (Coplen, 1996). Analytical precision, estimated by the standard deviation (one sigma) of repeated analysis of a powdered carbonate standard (NBS-19), was $\pm 0.06$ per mil for $\delta^{18}O$.

Shipboard measurements of MS and GRA bulk density were made at 2-cm sample intervals using a GEOTEK multisensor core logger (MSCL) on whole-core sections recovered from Site 1094 (Weber et al., 1997; Shipboard Scientific Party, 1999). These parameters were measured on both the piston core and the Leg 177 material. Consequently, MS and GRA bulk density data are from the identical composite stratigraphy used for IRD analysis. Natural gamma radiation (NGR) was collected only on Site 1094 cores, however, therefore the shipboard splice above 12.7 mcd was correlated to the piston core using oxygen isotope stratigraphy. Quantitative estimates of diffuse spectral reflectance were generated on split core sections at 4-6 cm sample intervals using the Oregon State University Split Core Analysis Track (Mix et al., 1992; Shipboard Scientific Party, 1999).

## Results

Ice-rafted debris within late Pleistocene (MIS 1-11) sediments at Site 1094 is composed predominantly of ash (88.3% of the lithic fraction and 600 grains/g on average) and quartz (10.9% and 50 grains/g on average) (Figures 4-2, 4-3). The strong dominance of ash within the total lithic assemblage results in nearly identical records of ash and total lithics. Consequently, hereafter, only plots of quartz and total lithics are shown. IRD levels are generally high during the glacial periods (1200 grains/g on average) and low during the interglacial periods (300 grains/g on average) with a high degree of variability within each of these periods. Expressed as a relative percent of the coarse fraction, the total lithics were roughly equivalent during each of the four glacial periods (reaching >80% in each case). However, expressed as a concentration

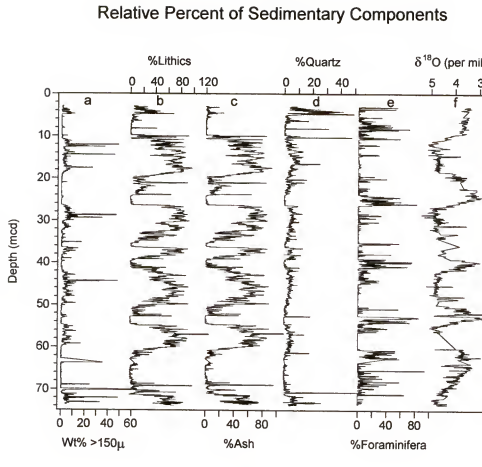


Figure 4-2. Relative Percent of Sedimentary Components. (a) Weight percent of the >150μ sediment fraction, relative percent each within the coarse (>150μ) sediment fraction of (b) total lithics, (c) ash, (d) quartz. (e) Percent of foraminifera within the coarse sediment fraction and (f) $\delta^{18}O$ of the planktic foraminifer *Neogloboquadrina pachyderma* (sin) all versus meters composite depth in the sediment record at Site 1094.

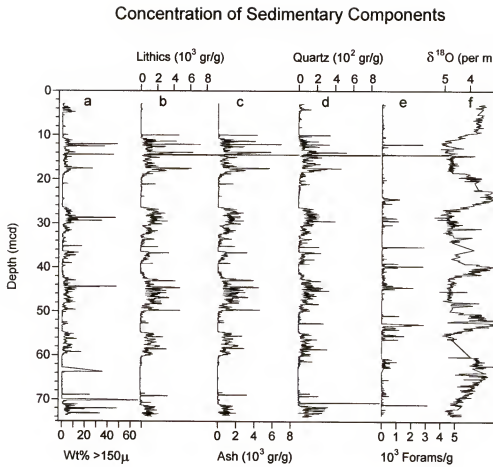


Figure 4-3. Concentration of Sedimentary Components. (a) Weight percent >150μ, (b, c, d and e) concentration (grains/g dry sediment) each of total lithics, ash, quartz and foraminifera. (f) $\delta^{18}$O of the planktic foraminifer *Neogloboquadrina pachyderma* (sin) all versus meters composite depth in the sediment record at Site 1094.

(Figures 4-3, 4-4), peak values of the last glacial period (5,000-10,000 grains/g) were considerably higher than those of MIS 6, 8 and 10 (2,000-4,000 grains/g).

The whole-core sediment physical properties measurements; MS, NGR and GRA bulk density, are each high during the glacial periods (averaging 38.1x$10^{-5}$ SI, 4.8 cps and 1.25 g/$cm^3$, respectively) and low during the interglacials (averaging 10.2 x$10^{-5}$ SI, 1.9 cps and 1.20 g/$cm^3$) (Figure 4-4). The highest levels (nearing 200 x$10^{-5}$ SI, 11.5 cps and 1.5 g/$cm^3$) occurred during the last glacial period. Both MS and GRA bulk density exhibit a degree of variability within each marine isotopic stage similar to that of the visually-determined IRD, capturing many of the prominent features displayed by that record. The NGR record exhibits a prominent saw-toothed pattern whereby values increase gradually throughout each glacial period and then decrease abruptly at glacial terminations. The %reflectance record is low during glacial period and high during interglacial periods, paralleling the $\delta^{18}O$ record. It also exhibits a saw-toothed pattern, although the relationship is inverted relative to that of the NGR. The general saw-toothed structure displayed by both NGR and %reflectance has numerous millennial-scale oscillations superimposed on this pattern.

**Glacial Periods**

Throughout the last glacial period, discrete episodes of IRD deposition recur on millennial timescales (~6-10 kyr; Figures 4-3, 4-5; Kanfoush et al., 2000a). None lasts for more than a few thousand years, and the concentration typically returns to baseline values before increasing again. Peaks are composed predominantly of ash and quartz, with ash abundances roughly an order of magnitude greater than those of quartz (surpassing 5,000 grains/g and 400 grains/g, respectively), and the two primary constituents closely parallel each other throughout. As in the IRD record of the last glacial period, MS and GRA bulk density also contain discrete peaks recurring on millennial timescales. Values of these whole-core physical properties generally do return to baseline values before increasing again but, unlike the IRD record, the baseline is substantially elevated above the values of the contiguous interglacial

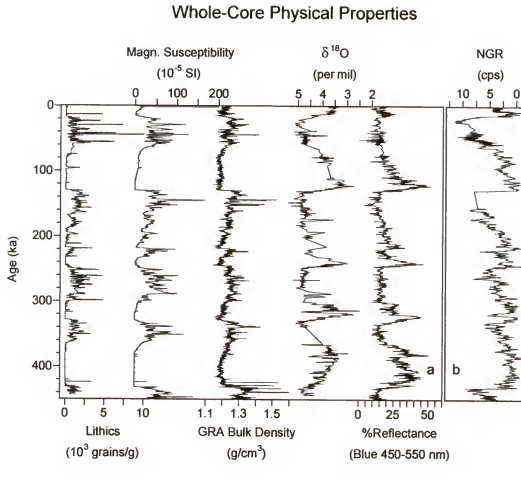


Figure 4-4. Whole-Core Physical Properties. (a) Time series in the spliced TTN057-13/1094C-2/1094 shipboard splice of total lithic concentration (grains/g), magnetic susceptibility $10^{-5}$ SI, GRA bulk density (g/cm$^3$), $\delta^{18}O$ of the planktic foraminifer *Neogloboquadrina pachyderma* (sin) and percent reflectance of the blue (450-550nm) band. (b) Time series of NGR in the Leg 177 Site 1094 shipboard splice correlated to the composite splice used for IRD analysis.

periods (MIS 5 and the Holocene). In all parameters, higher-frequency oscillations are also superimposed on the ~6-10 kyr events.

Discrete peaks in IRD, dominantly ash and quartz, occurred during MIS 6, MIS 8 and MIS 10 with a temporal spacing (~3-12, ~2-9 kyr and ~2-8 kyr, respectively) similar to that observed for the last glacial period (Kanfoush et al., 2000a). Unlike the last glaciation, however, the magnitude of the IRD peak concentrations in the three older glaciations (MIS 6, 8 and 10) is smaller (~2,000-3,000 grains/g, 3,000-4,000 grains/g and 1,500-3,000 grains/g, respectively). The records of MS and GRA bulk density do not parallel the IRD record as closely as they did in the records of the last glaciation. In both parameters, the peaks are often much greater than those found in the IRD record, particularly at ~145-155ka. As in the last glacial period, higher-frequency oscillations are superimposed on the ~3-12 kyr, ~2-9 kyr and ~2-8 kyr events displayed in all measured sediment parameters.

**Interglacial Periods**

Within each of the past five interglacial periods there is an early interval during which IRD values approach zero then rise abruptly. The early Holocene (Figure 4-3, 4-6) is marked by a period in which foraminiferal abundances are high (>45%) and IRD is extremely low (~5.4 grains/g on average). At ~5.5 ka, percent IRD increases abruptly (to >60%). With the exception of two brief events (at ~1500 and ~600 yrs BP), foraminiferal abundances accompanying this late-Holocene increase in IRD are very low (~8.2%). Highest %IRD occurs at ~4.7 ka and there is a decrease in IRD following this although levels remain higher than those of the early Holocene. Expressed as a concentration, the large increase in IRD (to >140 grains/g) occurs later, beginning at ~4 ka and peaking at ~3 ka. Unlike the last glacial period, in which ash dominated IRD deposition at the site, the composition of the IRD in the late Holocene is dominantly quartz. Magnetic susceptibility, NGR and GRA bulk density are each low during the early Holocene (averaging 0.0 $x10^{-5}$ SI, 1.2 cps and 1.150 $g/cm^3$, respectively) and show an increase in the latter part of the Holocene (averaging 9.9 $x10^{-5}$ SI, 3.2 cps and 1.163 $g/cm^3$). Similar to the record

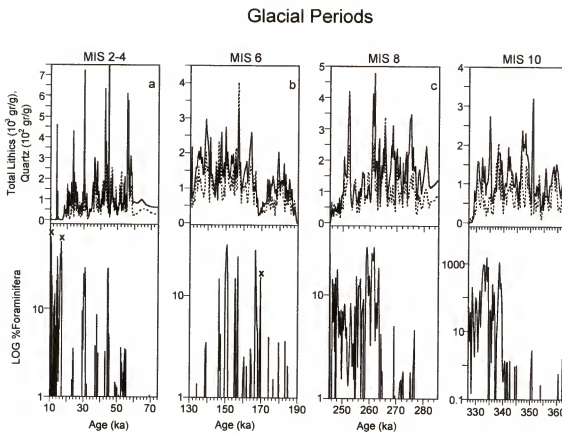


Figure 4-5. Glacial Periods. Comparison of lithics and quartz concentrations and relative percent foraminifera in the >150μ size fraction within each of the past four glacial periods; (a) MIS 2-4, (b) MIS 6 (c) MIS 8 and (d) MIS 10. Ash strongly dominates the record in each period, making up >90% of the total lithic concentration, and is therefore not shown. Quartz closely parallels ash and total lithics throughout each. IRD peaks are associated with high foraminiferal abundances during MIS 2-4 and MIS 6 except where indicated with an "x". In MIS 8 and 10, this association is not as clearly identifiable due to the widely varying magnitudes of peaks in foraminiferal abundance.

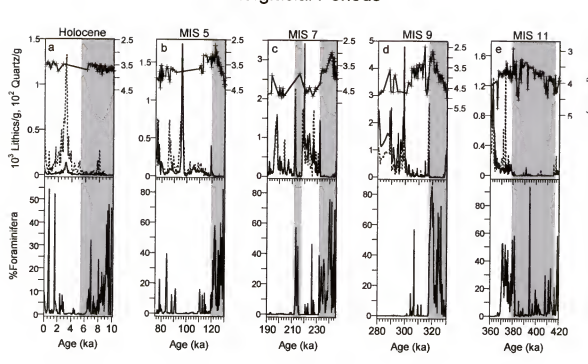


Figure 4-6. Interglacial Periods. (Top) Comparison of lithics and quartz concentrations and $\delta^{18}O$ of the planktic foraminifer *Neogloboquadrina pachyderma* (sin) in each of the past five interglacial periods. (Bottom) High relative percent foraminifera accompanies IRD values approaching zero during the early part of each interglacial period (indicated by shading). Following these times of apparent hypsithermal conditions, IRD delivery to Site 1094 resumes and foraminiferal abundances decline suggesting the occurrence of a neoglaciation that characterized the latter part of each interglacial period. Notice the resumption of ice-rafting during MIS 5 begins prior to the end of the substage 5e (the Eemian) as defined by $\delta^{18}O$ values that remain low and constant relative to the neoglaciations of MIS 7 and 9. Similarly, IRD returns to Site 1094 during the Holocene at a time when $\delta^{18}O$ values are unchanged.

of foraminiferal abundances, high %reflectance marks the early Holocene (27.5% on average) and is followed by lower %reflectance values in the late Holocene (23.9% on average). Unlike the IRD and whole-core physical properties, the $\delta^{18}O$ signal is relatively constant throughout the Holocene.

The patterns of IRD and foraminiferal abundance during MIS 5 are similar to those observed for the Holocene. IRD values are near zero early in substage 5e (the Eemian) and increase to greater values at ~120 ka. High foraminiferal abundances (>60%) in the early Eemian are replaced by generally lower foraminiferal abundances (<40%) throughout the remainder of the interglacial. MIS 5 is marked by large fluctuations in IRD abundances, with total lithics peaking at >80% and >1600 grains/g. High IRD and low foraminiferal abundances occur in substages 5d and 5b. A general reversal of these conditions occurs in substages 5c and 5a, although levels do not return to those observed in the early Eemian. The composition of the IRD in the latter part of MIS 5 is dominated by ash. As in the Holocene, MS, NGR and GRA bulk density during MIS 5 each increase (to ~7 $x10^{-5}$ SI, ~6 cps and ~1.18 $g/cm^3$, respectively) following low Eemian values (~ -1 $x10^{-5}$ SI, ~0.5 cps and ~1.19 $g/cm^3$). The opposite pattern (decreasing from >50% to ~25%) is displayed by %reflectance.

Marine Isotope Stage 7 shows two substages centered on ~240ka and ~215ka, of high foraminiferal abundances (>55% in each case) and essentially no IRD. As in MIS 5, the record is marked by periods of high IRD occurring during the stadials (>1500 grains/g in each case). Ash is the dominant component of the IRD throughout. From values approaching zero, MS reaches values of 95 $x10^{-5}$ SI and 53 $x10^{-5}$ SI during the stadials. Similarly, GRA bulk density values rise from ~1.17 $g/cm^3$ to greater than 1.25 $g/cm^3$ during stadials; NGR values rise from <0 cps to > 4 cps. From values greater than 30% during MIS 7, %reflectance drops to less than 20% during stadials. Similar to MIS 7, two pronounced substages occur in MIS 9. Each is marked by an abrupt increase in IRD following intervals of low IRD. The earliest part of MIS 9 is essentially "IRD-free". Unlike MIS 7, however, %reflectance values remain relatively constant throughout,

whereas MS and GRA bulk density increase from 20 x$10^{-5}$ SI to >35 x$10^{-5}$ SI and from about 1.23 to 1.3 g/$cm^3$.

The early part of Marine Isotope Stage 11 was marked by a period of very little IRD. Although punctuated at ~405 ka by a brief reversal in planktic $\delta^{18}O$, IRD remains low throughout the early part of MIS 11. The pattern of foraminiferal abundances during MIS 11 is different from that seen in subsequent interglacials, with the early part of the stage characterized by generally low abundances (< 50%) punctuated by only two brief peaks in foraminiferal abundances greater than 50%. Following this, as IRD values increase, there is an abrupt increase in foraminifera. The planktic $\delta^{18}O$ minimum of MIS 11 remained heavier than those observed in MIS 9 and 5e (>2.9 per mil versus <2.7 and ~2.7 per mil, respectively). Ash is the dominant component of the IRD throughout MIS 11. From concentrations near zero in the earliest part of the stage, ash begins to gradually increase at ~395 ka. Quartz displays an abrupt, large-magnitude (~150 grains/g) peak at ~383 ka. From a minimum of <0 cps at ~407 ka, NGR values increase to 3.7 cps at ~390 ka and from less than 25% at 405 ka, %reflectance rapidly increases to >50% by 400 ka. MS begins at ~395 ka to gradually increase from values approaching zero and reaches values of >15 x$10^{-5}$ SI by the end of the interglacial period. Similarly, GRA bulk density values rise from <1.20 g/$cm^3$ to greater than 1.25 g/$cm^3$ at ~400 ka and continue to fluctuate near that value throughout the remainder of MIS 11.

**Glacial Terminations**

From high glacial concentrations, IRD decreases across each of the glacial terminations. This decrease occurs in a somewhat gradual "step-wise" manner in some cases (terminations I, III and V) and abruptly in others (terminations II and IV). In all cases, however, the decrease in IRD occurs early during the termination. As $\delta^{18}O$ values decline across termination I, they display a brief reversal toward heavier values before again declining (Figure 4-7). Within this $\delta^{18}O$

reversal, there is a prominent IRD peak. Only Termination V contains a similar IRD peak centered within a reversal in $\delta^{18}O$. The IRD peak within Termination V is strongly dominated by quartz.

## Discussion

### Whole-Core Physical Properties as Proxies of IRD

Analysis of IRD is a time-consuming procedure. Consequently, several researchers have sought, with success, to use other sediment parameters as a proxy of IRD in North Atlantic sediments (Robinson et al., 1995; Stoner et al., 1995b, 1996; Chi and Mienert, 1996). An opportunity exists here to compare directly IRD concentrations with other sediment parameters in Site 1094 to assess their utility as IRD proxies in the South Atlantic. This also includes weight percent of the coarse sediment fraction (wt% >63μ and wt%>150μ), which is routinely measured during sample processing.

In general, the glacial-interglacial pattern displayed by MS and GRA bulk density is similar to that for IRD (Figure 4-4). This implies these whole-core physical properties are controlled by terrigenous influx, largely via ice-rafting (Shipboard Scientific Party, 1999). Discrepancies between the visually-counted IRD and the whole-core physical properties may be attributed in part to grain size differences resulting from the selected upper and lower sieve limits (2mm and 150μ, respectively) used for IRD analysis. Specifically, the substantially elevated glacial baseline values of the whole-core physical properties may reflect the presence of terrigenous fines omitted in the visual IRD counts. Examination of the weight percent of the various size fractions of the sediment supports this conclusion (Figure 4-8). Because of the greater weight of the lithics as compared to the biogenic components, the weight percent of the >150μ fraction provides a good approximation of the IRD. However, inclusion of finer sediments (the weight percent 63-150μ fraction) approaches more closely the structure of the MS and GRA bulk density records, specifically the elevated baseline of glacial periods (Figure 4-5).

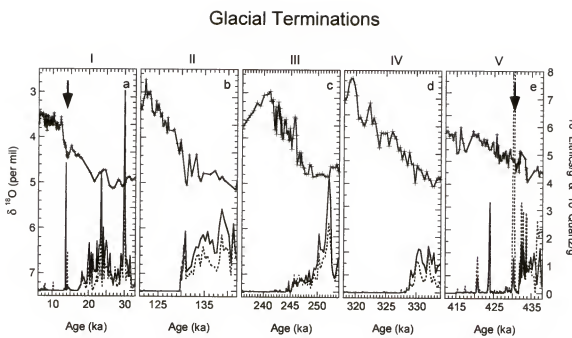


Figure 4-7. Glacial Terminations. Comparison of $\delta^{18}O$ and IRD (total lithics and quartz) concentrations across the past five glacial terminations. Terminations I, III and IV (and perhaps II) each is punctuated by a reversal to heavier $\delta^{18}O$ values suggesting a brief return toward more glacial conditions. Termination V also is punctuated by a reversal to heavier $\delta^{18}O$ values, but it is of smaller magnitude than in the other terminations. In terminations I and V, this $\delta^{18}O$ reversal is accompanied by an influx of IRD (marked with arrows).

Both the start of glacial periods and glacial terminations are recorded as an abrupt change in the records of IRD, MS and GRA bulk density (Figure 4-4). Each of the past three glacial terminations are also abrupt in the records of $\delta^{18}O$, %reflectance and NGR. However, the transition from interglacial to glacial conditions in these parameters is recorded as a gradual change. Natural gamma radiation is derived from decay of natural radioisotopes, including potassium, uranium and thorium and reflects influx of terrigenous materials containing these radioisotopes. The strong anti-correlation between the prominent saw-toothed patterns of NGR and %reflectance, therefore, implies that gradual decreases in %reflectance result from either an increase in terrigenous influx or a decrease in biogenic input (Shipboard Scientific Party, 1999). All other factors being equal, however, both processes would impact the other indicators of terrigenous influx as well. Their lack of anti-correlation with %reflectance, therefore, implies that the NGR signal is dominated by fine-grained sediments delivered to the site via ice-rafting, focusing by deep currents, advection within the nephaloid layer and/or eolian transport. Alternatively, the NGR signal may reflect dilution by biosiliceous sediment (diatom productivity).

Discrete IRD peaks observed within each of the past four glaciations begin and end abruptly and are very brief, on the order of a few thousand to even a few hundred years in duration. Even with the high sedimentation rates at Site 1094 (averaging ~40 cm/yr and ~18 cm/yr during interglacial and glacial periods, respectively), the ice-rafting events are recorded within only a few centimeters sediment thickness. This, in conjunction with slightly offset sampling depths and differing sampling intervals for the different sediment measurements, may explain discrepancies between the millennial-scale events present within the IRD and the whole-core physical properties records. For example, the records of MS and GRA bulk density, while also containing discrete millennial-scale peaks, display some peak magnitudes much higher than peaks within the IRD record, particularly at ~145-155ka (Figure 4-5).

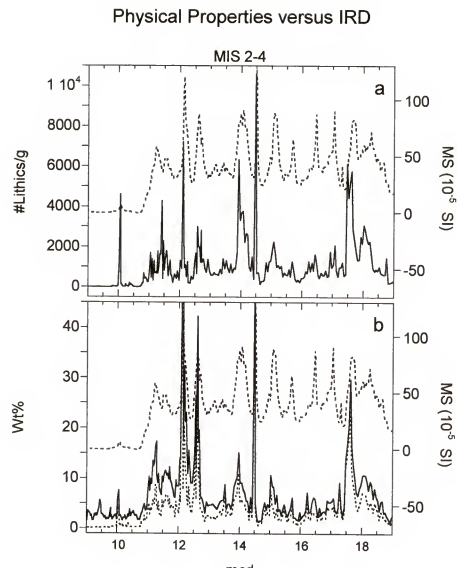


Figure 4-8. Physical Properties versus IRD. (a) Comparison of total lithic concentration (solid line) and magnetic susceptibility (dashed line) during the last glaciation (MIS 2-4) demonstrates that MS provides a good approximation of visually-determined IRD. (b) Comparison of the >63μ sediment fraction (solid line) with magnetic susceptibility (dashed line) reveals elevated baselines of MS and GRA bulk density (not shown) relative to the IRD counts. This may be attributed to influence of the fine size fraction that is omitted in the arbitrarily selected upper and lower sieve limits used in the IRD analysis.

The sediment parameter that most closely approximates the IRD concentration is weight% >150μ, displaying most (but not all) of the discrete IRD peaks (Figures 4-3, 4-8). Although the majority of IRD peaks is present within the weight% >150μ signal, the magnitude of some of the events differs from the IRD counts. Because larger lithic grains typically weigh more, their presence is reflected by greater values of weight% >150μ. Within IRD counts, however, each lithic grain is counted once regardless of size and weight. This problem is exacerbated by the selection of upper and lower size limits for IRD analysis. Nonetheless, because the other sediment parameters incorporate fine sediments omitted in the IRD counts, weight% >150μ provides the best approximation of IRD at Site 1094.

**Glacial-to-Interglacial Variability**

Ice-rafted debris in sediments at Site 1094 is composed overwhelmingly of ash and quartz. Geochemical analysis of IRD in nearby sediment cores suggests the ash in South Atlantic sediments is derived principally from volcanic eruptions in the South Sandwich Islands in the Scotia Arc, West Antarctica, with minor contribution from nearby Bouvet Island (Cooke and Hays, 1982; Smith et al., 1983). Carried to the east by prevailing winds, ash then settles on ice shelves in the Weddell Sea and on seasonal sea ice, which acts as a conveyor of ash to the South Atlantic Ocean during its seasonal advance and retreat. The quartz and other non-ash lithics are sourced from Antarctica by calving of icebergs (Smith et al., 1983; Labeyrie et al., 1986). The majority of icebergs originate from ice shelves such as those found in the Weddell Sea where debris-rich basal ice can be produced by melting and freezing at the base of these ice shelves (Warnke, 1970; Hulbe, 1997).

If IRD transport were exclusively by icebergs, the relative proportions of the primary components, ash and quartz, would be the same throughout the South Atlantic. However, ash is the dominant component in Site 1094 at 53°S, whereas quartz is the dominant component in core TTN057-21 at 41°S. Site 1094 is situated south of the polar front where cool SST permits sea-ice

rafting. In contrast, core TTN057-21 at 41°S is situated north of both the present-day polar front and the glacial position of the polar front where the comparably warm SST inhibits sea-ice rafting (Brathauer and Abelmann, 1999; Kanfoush et al., 2000a). Consequently, although ash is transported both by icebergs and sea ice, sea-ice rafting appears to be an important mechanism in the South Atlantic.

Strong glacial-interglacial distinctions occur in the record of IRD delivery to Site 1094, with very high IRD levels during the glacial periods and very low levels during the interglacial periods (Figures 4-5, 4-6). The increase in IRD during glacial may be due to increased production of icebergs, increased survival of icebergs and sea ice, or dilution by biogenic material.

During the last glaciation when sea level was ~120 m lower than today, peripheral ice shelves around Antarctica were more extensive as grounding lines advanced seaward over the continental shelf (Denton and Hughes, 1983; Bindschadler et al., 1998). Expansion of the WAIS during the glacial period increased the proportion of marine-based ice, and attendant delivery of IRD to the South Atlantic. Additionally, isostatic depression of the continental shelf beneath the large glacial WAIS could render it susceptible to relative sea-level rise and subsequent buoyancy increase and unpinning along its margins (Andrews and Peltier, 1989; Anderson and Thomas, 1991).

In addition to the higher calving rates associated with increased ice volume in the Weddell Sea region, cooler glacial SST would enhance the survival and long-distance transport of debris-laden icebergs and sea ice to the core site (Matsumoto, 1996). Increased survivability associated with cool glacial SST may have resulted in an increase in the relative percent of IRD within the sediments, even without an increase in the rate of iceberg production (Keany et al., 1976).

Sea-ice coverage and frontal boundary positions control biosiliceous sedimentation to South Atlantic sediments (Burckle et al., 1982; Westfall and Fenner, 1991; Charles et al., 1991;

Asmus et al., 1999) and, consequently, IRD content. During cool intervals, the polar front migrated northward and sea ice expanded over the site resulting in a decline in biosiliceous productivity (Crosta et al., 1998; Brathauer and Abelmann, 1999). As a result, the relative percent of IRD within the sediments increased, even without an increase in their rate of delivery to the site. However, IRD expressed as an accumulation rate corrects for dilution and shows increases during cool intervals similar to that observed in the concentration data.

**Suborbital Variability**

In addition to well-defined glacial-interglacial cycles, suborbital variability is clearly present in the records of IRD and whole-core physical properties measurements at Site 1094. For the last glacial period, these prominent events have been correlated with IRD layers in cores situated north of the Polar Frontal Zone and have been interpreted as evidence of abrupt episodes of instability of the AIS in the Weddell Sea region (Kanfoush et al., 2000a). Examination of the past four glaciations reveals that, in addition to generally high IRD, each is characterized by discrete pulses in IRD delivery to Site 1094 that occurred on millennial timescales (Figure 4-5). With few exceptions, the abrupt IRD events are accompanied by brief episodes of high foraminiferal abundances originating from iceberg-induced upwelling or high SST (Labeyrie et al., 1986; Grobe and Mackensen, 1992).

Based on my chronology derived from SPECMAP tie-points, the temporal spacing of discrete peaks in IRD during MIS 6, MIS 8 and MIS 11 appears to be ~3-12, ~2-9 and ~2-8 kyr, respectively. However, two factors make it difficult to ascertain if this differs significantly from that observed for the last glacial period (~6-10 kyr; Kanfoush et al., 2000a). First, the IRD fluctuations during MIS 6 and 8 are less distinct making it difficult to identify individual events and, second, the chronology is coarse. It can be ascertained, however, if the relationship between these events and other suborbital changes within the same record is consistent for different glacial periods. For example, do the millennial-scale IRD peaks "march" through the changing climatic conditions of MIS 2, 3 and 4 as well as similar (unnamed) changes within MIS 6? Whereas MIS 3

is marked by several rapid $\delta^{18}O$ fluctuations, the variability in MIS 2 and 4 is comparably reduced. A similar pattern occurs in estimated temperatures at Vostok during the last glaciation. Millennial-scale IRD events do occur during each of the three stages, but their magnitude and frequency is greatest during MIS 3. This is consistent with McManus and others (1999) who argue for relative climatic stability in the northern hemisphere during full glacial periods and interglacial periods, and increased variability in the intervening climate states. As in the last glaciation, IRD variability occurs throughout MIS 6. However, unlike the last glaciation, IRD events of greater magnitude and frequency do not occur during the interval containing numerous rapid $\delta^{18}O$ fluctuations.

Suborbital variability within the interglacial periods exists with less regularity than the glacial periods (Figure 4-6). Within the glacial periods SST was near freezing year-round and I interpret IRD, therefore, as a signal of iceberg production. During interglacial periods, Site 1094 is south of the Polar Front and north of the winter sea-ice margin. Fluctuations in the positions of these boundaries would affect iceberg and sea-ice survivability. Therefore, the controls on IRD during interglacial periods may be different from those during glacial periods. Each of the last five interglacial periods begins similarly, marked by an IRD-free interval with abundant foraminifera occurring at a time when temperature over Antarctica is high (Figures 4-3, 4-6). Following this, each interglacial is characterized by a return to more glacial conditions, or a "neoglaciation" in which ice-rafting resumes abruptly and fluctuates irregularly while foraminiferal abundances decline (Kirby et al., 1998; Brachfield and Banerjee, 2000; Yoon, 2000).

The nature of the hypsithermal, however, differs among the interglacial periods. Previous studies implied that MIS 11 was the warmest interglacial period of the late Pleistocene (Oppo et al., 1990; Hodell, 1993). In contrast, the planktic $\delta^{18}O$ minimum of MIS 11 at Site 1094 remained heavier than minimum values observed in MIS 9 and 5e which suggests, all other factors being

equal, that SST in the southeast Atlantic were not significantly warmer during MIS 11 compared to the subsequent interglacial stages (Hodell et al., 2000). Although not unique with respect to the magnitude of its SST, the MIS 11 hypsithermal exhibited relatively IRD-free conditions that appear to have persisted for a substantially longer period of time than observed in the later interglacial periods. One possible exception to this is MIS 5 that had measurable, but extremely low, IRD amounts for a similarly long period of time. My age model, derived from correlation to SPECMAP, is admittedly coarse, particularly during MIS 11 (Figure 4-1). However, based on this chronology, indicators of ice-rafting to the southeast Atlantic appear to have remained near zero for more than 30 kyr, compared to ~5-15 kyr in the hypsithermal intervals of subsequent interglacial periods. Such a particularly IRD-free interval implies diminished calving or size of the ice-sheet or both (McManus et al., 1999). The duration of sustained IRD-free conditions at Site 1094 may be due to orbital configuration. Eccentricity at MIS 11 was low and the amplitude of the precession cycle was damped with the result that fewer cold substages punctuated the interglacial (Hodell et al., 2000).

The nature of the neoglaciation also differs among the interglacial periods. Although the two youngest interglacial periods (MIS 5 and 1) and MIS 9 and 11 were marked by a resumption of ice-rafting, delivery of IRD remained low relative to those of the glacial periods. In contrast, the neoglaciation of MIS 7 exhibits IRD concentrations approaching values typical of full glacial periods. The $\delta^{18}O$ during MIS 7 increased concomitantly with the IRD. Again, this difference between the interglacial periods is likely a reflection of the different orbital configurations of each (Figure 4-9). Precession is large during MIS 7 with the result that the magnitude of cold substages are much stronger.

Millennial-scale variability on Termination I is characterized by a reversal to cooler temperatures or the so-called Antarctic Cold Reversal (ACR) (Jouzel et al., 1987). In the Site 1094 record, the ACR is marked by greater $\delta^{18}O$ values and a brief, but prominent pulse in IRD

delivery to the core site (Figure 4-7) (Kanfoush et al, 2000a). Ice-rafted detritus within the ACR consists of two rapid peaks in quartz, the younger of which is accompanied by a single large peak in ash. Termination V is the only other glacial termination punctuated by a pronounced quartz peak. The rate of IRD decrease across the terminations differs also, with a gradual, step-wise decrease across terminations I and V and an abrupt decrease across terminations II and IV. In each case, however, concentrations of IRD decrease very early in the terminations with values approaching zero well prior to the end of each glacial termination. This implies a rapid and early response of sea ice in relation to SST, which continued to warm throughout the terminations (Shemesh et al., in press).

Estimates of SST derived from diatoms in Site 1094 sediments indicate that substantial warming of South Atlantic surface waters and reduction of sea ice occurred early in terminations I and V (Kunz-Pirrung, 2001; Shemesh et al., in press). Consequently, high biosiliceous productivity may have led to dilution of IRD delivered to Site 1094 sediments. In addition, SST increase early in the termination may have decreased survivability and transport distances of debris-laden icebergs resulting in a decrease in IRD delivery to Site 1094 early in the termination. The brief reversal to cooler SST associated with the ACR may have caused an expansion of sea ice and increased survivability of icebergs, both of which may have increased IRD concentrations in sediments at Site 1094. If SST increase is responsible for the reduction in IRD delivery to Site 1094 during glacial terminations, the gradual, step-wise IRD decrease across terminations I and V implies SST increase occurred in a gradual, step-wise manner. In contrast, the abrupt IRD decrease early in terminations II and IV suggests SST increase was abrupt and began early in the terminations.

**Marine-Ice Correlation**

Site 1094 at 53°S can be correlated to the Vostok ice core using sodium concentration in Vostok and %ash in South Atlantic sediments because both parameters are influenced by the extent of sea-ice cover in the South Atlantic Ocean. Atmospheric circulation, driven by the

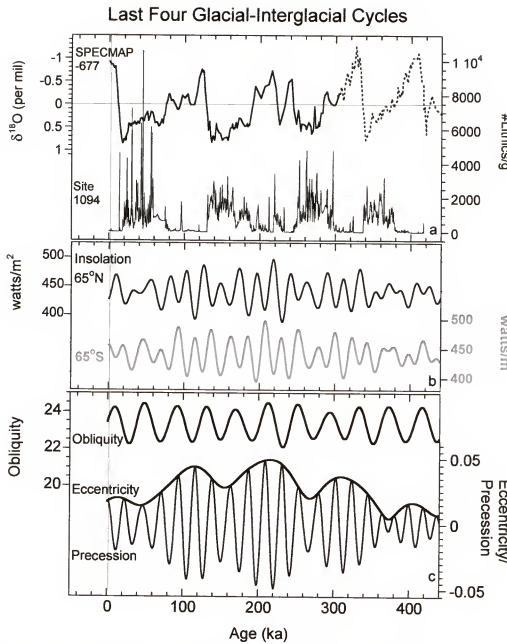


Figure 4-9. Last Four Glacial-Interglacial Cycles. (a) Comparison of IRD at Site 1094 and SPECMAP, (b) July solar insolation at 65°N, (c) December solar insolation at 65°S and (d) the earth's orbital parameters throughout the period spanned by the Site 1094 IRD record (440,000 years) (Modified after Hodell et al., 2000). This figure illustrates that the past four glacial periods occurred under different orbital configurations and different insolation values. Similarly, the past five interglacial periods and glacial terminations occurred under different orbital configurations and different insolation values as well. IRD decrease early in terminations II and IV suggests SST increase was abrupt and began early in the terminations.

ocean-Antarctica temperature gradient, is most vigorous during the austral winter when sea ice is at its maximum extent. This results in efficient transport of this marine aerosol to the South Pole (Petit et al., 1999). In Site 1094, ash and radiolarians strongly dominate the coarse sediment fraction and both are related to sea-ice cover at Site 1094. Ash is transported in part by sea ice, and sea-ice cover inhibits radiolarian productivity (Keany et al., 1976; Smith et al., 1983; Gersonde and Zielinski, 2000). Consequently, as sea-ice cover increases, %ash increases and radiolarian abundance falls. I elected to use %ash to correlate the Site 1094 record to Vostok, but could have used %radiolaria as it is essentially the inverse of the %ash signal (Figure 4-10).

The correlation yields close agreement between changes in Vostok inferred temperature and $\delta^{18}O$ of the marine record on both orbital and millennial timescales (Figure 4-10). On glacial-interglacial timescales, regional atmospheric temperature controls changes in ice-rafting via its influence on SST and, hence, survivorship and transport distances of sea ice and icebergs. Reconstructions of SST based on South Atlantic diatoms and radiolarians reflect the regional atmospheric temperature control on SST, showing much similarity with temperature recorded at Vostok (Pichon et al., 1992; Brathauer and Abelmann, 1999). In general (but not always), IRD delivery to Site 1094 is high when inferred temperature at Vostok is cool (less than ~-3.5 to -4.0°C). IRD often drops precipitously, sometimes approaching zero, at times when temperatures over Antarctica warm to greater than this. Such declines in ice-rafting occur during the two most prominent warm intervals within MIS 7, much of MIS 5, the brief warm interval at ~14.5ka and the early Holocene.

Dominated by quartz, the IRD of the late Holocene differs in composition relative to that of the previous interglacials and the majority of the record (which is dominated by ash). Termination V is punctuated by a brief but large peak in quartz and is the only other instance in which quartz is dominant. One possible explanation is a difference in provenance. However, for the Holocene, the correlation to Vostok suggests this may result from SSTs too warm to allow

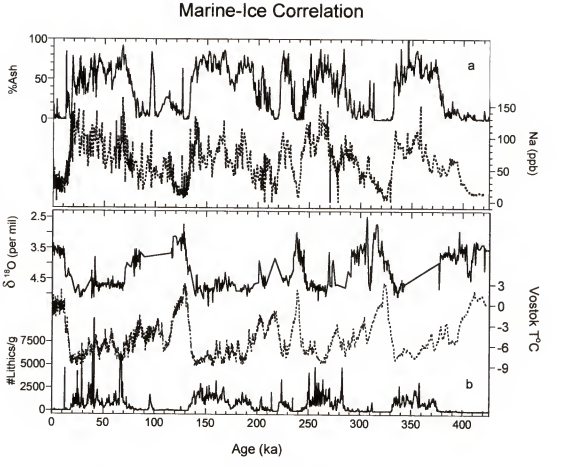


Figure 4-10. Marine-Ice Correlation. (a) Correlation of %ash in the marine sediment record from Site 1094 and sodium concentration in the Vostok ice core. Both are controlled by areal extent of sea ice, and therefore provided a means for correlation between the South Atlantic sediments and Antarctic ice at resolution sufficient to examine the interaction of ice discharge and atmospheric climate on millennial-scales. (b) The resulting comparison of $\delta^{18}O$ and lithic concentration at Site 1094 with inferred atmospheric temperature in Vostok on the GT4 Vostok chronology (Petit et al., 1999).

significant sea-ice rafting of ash. Similarly, estimates of SST derived from diatoms in Site 1094 sediments indicate that substantial warming of South Atlantic surface waters and reduction of sea ice occurred in termination V (Kunz-Pirrung et al., 2002).

Resumption of IRD delivery to Site 1094 in the late Holocene occurs when inferred temperature at Vostok remains warm (> ~0°C) and $\delta^{18}O$ remains relatively unchanged. Ice-rafting to Site 1094 resumes during MIS 5 even before the end of the Eemian following an essentially IRD-free interval. Similar to the Holocene, the first neoglacial IRD peak during the Eemian occurs while inferred temperature at Vostok is ~0°C. However, it does follow a rapid drop in temperature from the early Eemian maximum (>3°C). During MIS 11, IRD delivery increases while $\delta^{18}O$ remains relatively unchanged, however temperature at Vostok has decreased substantially by this time (from more than +2°C to less than –4°C). In MIS 7 and 9, the neoglaciation corresponds to substantially heavier $\delta^{18}O$ values and cooler Vostok temperatures (less than ~-3.5 to -4.0°C) that likely enhanced long-distance transport of sea ice.

The record of IRD concentration exhibits broad similarities with the dust record in Vostok (Figure 4-11). There is similarity on timescales somewhat intermediate between orbital and suborbital. Glacial-interglacial patterns are clearly evident in each and some (but not all) of the millennial-scale events match. High dust concentrations during glacial periods reflect continental aridity, dust mobilization and transport, whereas the presence of larger particles indicates more turbulent atmospheric circulation in the high southern latitudes (Petit et al., 1999). Petit and others (1999) suggested that peaks in dust in Vostok correspond to periods of steepened winter ocean-Antarctica temperature gradient resulting from expansion of sea ice in the South Atlantic. The general correspondence of %ash with dust in Vostok may be explained by sea-ice expansion because ash is rafted, in part, by sea ice (Keany et al., 1976; Smith et al., 1983). Quartz, which is not dominantly rafted by sea ice, also exhibits a similar broad-scale correspondence with dust. This may be explained by increased iceberg survivorship and transport

distances at times when SSTs are cool enough to permit sea-ice expansion. The MS and GRA bulk density, which approximate the IRD record, show a corresponding degree of similarity with the dust record.

Comparison of NGR and log Vostok dust reveals striking similarity (Figure 4-11). The prominent saw-toothed pattern displayed by NGR is present in the dust record and many of the millennial-scale peaks are represented in both. NGR reflects influx of uranium- and thorium-bearing terrigenous materials, including dust, much of which is sourced from the Patagonia region of South America (Grousset et al., 1992; Basile et al., 1997). The NGR signal, therefore, is dominated by fine-grained terrigenous particles largely of eolian origin whereas the other proxies of terrigenous influx to Site 1094 (IRD, MS and GRA bulk density) reflect terrigenous material transported to the site via ice-rafting. Other processes that may also contribute terrigenous fines to Site 1094 include eolian transport, focusing by deep currents, advection within the nephaloid layer, or a combination of these.

**Conclusions**

(1) The whole-core measurements of sediment physical properties, MS and GRA bulk density, displayed much (but not all) of the variability present within the visually-determined IRD record for both glacial and interglacial periods. Consequently, for Site 1094, and likely others situated south of the present-day polar frontal zone where sedimentation is controlled by similar processes, these parameters are to a limited extent a proxy of IRD. Weight% >150 yielded the best estimate of IRD. The NGR signal is not a proxy for IRD but rather exhibited strong similarity with the record of dust concentration in Vostok on millennial timescales.

(2) Suborbital variability in ice-rafting at Site 1094 characterizes glacial periods and interglacial periods of the late Pleistocene. Millennial-scale pulses in IRD delivery to the South Atlantic, interpreted as episodes of instability of the Antarctic Ice Sheet, occurred during each of the last four glacial periods (MIS 2-4, MIS 6, MIS 8 and MIS 10). Variability within each of the last five interglacial periods (the Holocene, MIS 5, MIS 7, MIS 9 and MIS 11) includes an early

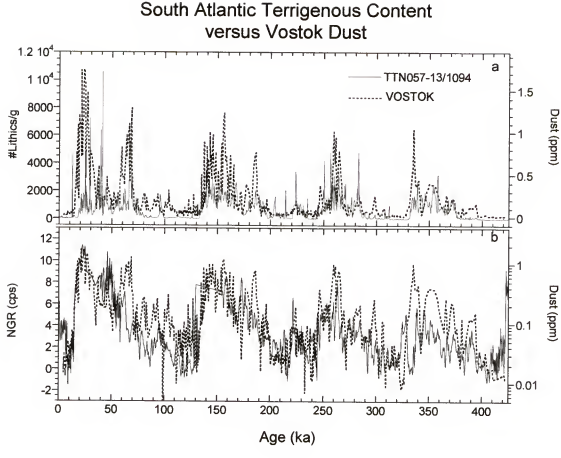


Figure 4-11. South Atlantic Terrigenous Content versus Vostok Dust. Comparisons of (a) total lithic concentration at Site 1094 (solid line) and dust in Vostok (dashed line). (b) NGR at Site 1094 (solid line) is smoothed with a 5-point moving average and compared with LOG dust in Vostok (dashed line), both on the GT4 chronology (Petit et al., 1999).

hypsithermal period characterized by low IRD, MS and GRA bulk density and high foraminiferal abundance and %reflectance. A reversal of these conditions characterized the latter parts of the interglacial periods and is interpreted as a return to more glacial conditions, a neoglaciation.

(3) Suborbital variability in ice-rafting at Site 1094 differs among glacial periods and among interglacial periods. Thus, the nature (magnitude, frequency, perhaps even composition) of IRD peaks is to some extent dependent on orbital configuration. Within the limitations of my chronology, the duration of hypsithermal conditions appears to have been greater for MIS 11 than other interglacial periods of the late Pleistocene. The neoglaciations of MIS 7 and 9 were associated with a substantial increase in $\delta^{18}O$, however the neoglaciation of MIS 5 began prior to the end of the Eemian and was accompanied by only a modest increase in $\delta^{18}O$. Oxygen isotopic values during the late Holocene neoglaciation are unchanged. Precession is large during MIS 7 with the result that the magnitude of cold substages was much larger and ice-rafting more abundant than in other interglacial periods of the past 420,000 years.

(4) Percent ash in the marine sediment record from Site 1094 and sodium concentration in the Vostok ice core are both controlled by areal extent of sea ice. They, therefore, provided a means for correlation between the South Atlantic sediments and Antarctic ice at resolution sufficient to examine the phasing of marine and atmospheric changes on millennial-scales. NGR exhibits similarities with dust concentration in Vostok. One possible explanation is that it is attributed to periods of vigorous atmospheric circulation resulting from steepened ocean-Antarctica thermal gradients associated with sea-ice expansion. Peaks in IRD also show broad-scale (on timescales somewhat intermediate between Milankovitch and suborbital) similarities with Vostok dust and likely reflect enhanced sea ice and iceberg survivability in cooler SSTs at times of sea-ice expansion.

# CHAPTER 5
# SYNTHESIS

The purpose of this synthesis is, first, to briefly summarize the conclusions of this study. Second, the conclusions of this study will be placed in the broader context of climate change and its implications for Antarctic Ice Sheet stability as well as the contrary; the implications of an unstable Antarctic Ice Sheet for both sea level and climate. Lastly, I will briefly discuss remaining debates and gaps in our understanding of the delivery of ice-rafted debris to the South Atlantic Ocean on millennial timescales that serve as an impetus for future work.

## Synthesis of Late Pleistocene Ice-Rafting and AIS Dynamics

Discrete IRD layers (SA events), consisting overwhelmingly of volcanic ash and quartz, recur on millennial timescales during the last glacial period. Peaks in IRD are synchronous north and south of the Polar Frontal Zone. Therefore, such layers are not simply the result of temperature-controlled shifts in the locus of iceberg melting. Rather their synchroneity, combined with their association with light planktic $\delta^{18}O$ anomalies, implies the IRD layers represent increases in Antarctic ice discharge. Suborbital variability in ice-rafting at Site 1094 characterizes each glacial period (MIS 2-4, 6, 8, 10) of the late Pleistocene.

Although different in both magnitude and recurrence interval than that observed for glacial periods, suborbital variability in ice-rafting at Site 1094 also characterizes each interglacial period of the late Pleistocene. Variability within interglacial periods includes an early hypsithermal period, characterized by low IRD and high foraminiferal abundance, followed by an abrupt reversal of these conditions interpreted as a neoglaciation. In addition to these glacial-interglacial differences, suborbital variability in ice-rafting also differs among glacial periods and among interglacial periods. This suggests that delivery of ice-rafted debris to the southeast Atlantic is, to

some extent, dependent on orbital configuration. The similarity between the Holocene and MIS 11 in both basic orbital configuration and pattern of ice-rafting on suborbital timescales suggests MIS 11 is perhaps a reasonable analogue to our present interglacial, if temperatures warmer than present existed within MIS 11. However, this is a topic that remains the subject of debate (Burckle, 1993; Howard, 1997; Oppo et al., 1998; Hodell et al., 2000).

The impact of millennial South Atlantic ice-rafting events on the surface South Atlantic during glacial periods appears to includes an immediate and pronounced local increase in productivity, resulting perhaps from iceberg-induced upwelling or warming. Additional impacts include meltwater contribution from icebergs and a lowering of SST due to iceberg melting. Both downcore phase relationships and marine-ice core correlations suggest that SA events occur on the cooling limb following millennial Antarctic warm events but often not at times of peak cool temperatures. Because IRD concentrations typically reach a maximum and subsequently return to near baseline values prior to times of peak cool temperatures, increased IRD deposition cannot be simply the result of increased iceberg survivorship and, hence, transport distance.

SA events coincide with near-peak warmth of brief interstadial events recorded in Greenland ice. Because they display a more coherent temporal relationship with abrupt changes in climate of the North Atlantic region than with Antarctic climate, the origin of the millennial Antarctic ice discharge events appears to lie in the North Atlantic region and be somehow transmitted southward. Comparison of SA events with high-resolution eustatic sea-level records supports the existence of a sea-level linkage whereby melting of Greenland ice associated with enhanced NADW formation and interstadial warmth elevated sea level sufficiently to "un-pin" ice shelves of the Weddell Sea region.

Regional insolation is high throughout MIS 3, yet inferred temperature recorded in Antarctic ice indicates that MIS 3 was punctuated by several millennial-scale warm-cold oscillations. Intense resumption of NADW formation and consequent cooling of the southern hemisphere associated with strong interstadials of the North Atlantic region combined with ice-

discharge into the South Atlantic may have periodically prevailed over the insolation forcing, triggering the observed cold phases of the warm-cold oscillations that punctuate MIS 3. Thus, although seemingly not triggered by regional climatic events, the SA events may have led to millennial changes in regional climate.

## Future Work

### Interpretation of IRD Layers

This study suggests that the so-called SA events are both areally extensive, spanning twelve degrees of latitude, and rapidly deposited in relation to ambient sedimentation rates (Kanfoush et al., 2000b). These are two of the criteria used to suggest Heinrich layers of the North Atlantic were indicative of Laurentide Ice Sheet instability (Broecker, 1994; McManus et al., 1998). However, whereas progress has been made in ascertaining the spatial and temporal variability of IRD in Southern Ocean sediments, much more work on these rudimentary issues remains. The full spatial extent of SA events will only be revealed by obtaining and analyzing additional deep-sea cores of sufficient resolution throughout the South Atlantic region. The results presented here which suggest whole-core physical properties measurements of magnetic susceptibility and GRAPE bulk density closely mirror downcore IRD changes at Site 1094 in the South Atlantic may aid in this goal, because such measurements are much quicker and much less labor-intensive than visual IRD counts enabling analysis of a greater number of cores in an equal amount of time. Because the WAIS discharges ice into the South Pacific Ocean as well as the South Atlantic, a complete understanding of its late Pleistocene dynamics must include examinations of high-resolution deep-sea records from this basin as well. Furthermore, although the EAIS is land-based and thus presumably more stable than its marine-based counterpart, this needs to be ascertained by corresponding studies within the Indian Ocean. In comparison to the core distribution and assessment of the spatial variations of IRD throughout the North Atlantic region, the appraisal of IRD in the Southern Ocean is in its infancy.

Sediment accumulation rates during IRD events within the southeast Atlantic records described here increase ten-fold in relation to ambient rates. However, this apparent increase is based on the chronologies of the sediment cores, constructed by linear interpolation between radiometrically-determined ages and ages derived from correlation to a standard reference curve (SPECMAP; Martinson et al., 1987; Kanfoush et al., 2000). There is an obvious need for better age control during the SA events. If IRD layers are in fact the result of substantially increased ice discharge rather than temperature-controlled variations in the position of iceberg melting, then the apparent 10-fold increase in accumulation rate during the SA events is likely a minimum estimate and a closer look using techniques such as $Th_{ex}$ dating may yield similar or even higher rates.

A common assumption is that all icebergs carry the same sediment load such that high IRD concentration implies high iceberg flux (Alley and MacAyeal, 1994; Dowdeswell et al., 1995). However, there is some evidence to suggest that spatial variability of IRD load may exist. For example, icebergs originating from outlet glaciers of East Antarctica have been reported to carry substantially greater amounts of debris than those originating from the ice shelves of West Antarctica (Warnke, 1970; Anderson et al., 1980; Kellogg and Kellogg, 1988). Thus a change in the dominant source area of icebergs and IRD, perhaps due to a change in surface currents, could result in an increase in IRD concentration at a site without any increase in ice discharge. This is a possibility currently overlooked and further examination of this issue needs to and can be addressed through geochemical analysis to identify the source area(s) of IRD observed in South Atlantic sediments (Gwiazda et al., 1996a, 1996b; Hemming et al., 1998, 2000).

In addition to spatial variability, temporal variability of IRD load within icebergs could similarly result in an increase in IRD accumulation with even a constant ice flux. There is some evidence to suggest that sediment entrainment and sediment retention within glacial ice varies as a function of such factors as basal temperature and, hence, ice flow velocity (Clarke et al., 1999). If so, then sediment entrainment would be expected to vary through time as periodic (or quasi-periodic) ice surging occurs (Alley and MacAyeal, 1994). However, the characteristics of an IRD

signal as a function of ice-sheet dynamics is not well understood (Clark and Pisias, 2000). Thus, it remains an assumption widely made in IRD studies of both the northern and southern hemispheres that an increase in IRD represents greater iceberg flux versus a greater amount of debris incorporation (Dowdeswell et al., 1995). Whereas, in the event of a surge, an interpretation of increased ice discharge from observed increases in IRD concentration would not be incorrect, such a scenario clearly renders untrue an assumption of a linear relationship between IRD concentration and ice flux. The occurrence of light planktic $\delta^{18}O$ anomalies coincident with or following IRD deposition provides evidence for at least some increased ice discharge (Labeyrie et al., 1986; Kanfoush et al., in preparation). Yet for some IRD peaks an associated planktic $\delta^{18}O$ anomaly is not observed, and so there remains a need to better understand temporal variability in debris incorporation within glacial ice and the impacts of this on the interpretation of the IRD signal. This question must be resolved before one could successfully quantify the volume of ice involved in the rapid discharge events.

Another common assumption is that continentally-derived lithics are delivered to the deep sea primarily by icebergs rather than sea ice. The mechanics and relative importance of sediment entrainment and rafting by sea ice in the North Atlantic region is beginning to receive some attention (Kempema et al., 1989; Nürnberg et al., 1994; Eicken et al., 1996; Reimnitz et al., 1998; Hebbeln, 2000). Although I have briefly discussed the fact that sea ice is another potential means by which at least some IRD is transported to the southeast Atlantic, the relative importance of sea ice versus iceberg rafting within the region remains largely unaddressed (Lizitzin, 1978; Smith et al., 1983). Assumptions such as these obviously remain important questions that should serve as an impetus for future research.

**Identification of Source Areas**

Geochemical analysis and dispersal patterns of volcanic ash in southeast Atlantic sediments suggest it is derived principally from the South Sandwich Islands in the Scotia Arc,

with minor contribution from nearby Bouvet Island (Cooke, 1978; Smith et al., 1983). Smith and others (1983) hypothesized that volcanic eruptions in the South Sandwich Islands produce ash that is carried east by prevailing winds, settles on ice shelves in the Weddell Sea and on seasonal sea ice, which acts as a conveyor of ash to the South Atlantic sediments during its seasonal advance and retreat. If true, then while the concentration of volcanic ash within South Atlantic sediments may harbor important information about the controls on formation, dispersal and melting of sea ice, it is not an indicator of AIS dynamics.

In contrast, the quartz and other non-ash components within South Atlantic IRD probably originate from the Antarctic continental crust (Labeyrie et al, 1986). Therefore, the origin of these components is of direct importance to development of an understanding of AIS dynamics. In the North Atlantic region, for example, lead isotopes in feldspar grains and argon isotope ratios in amphiboles were instrumental in identifying the source of the IRD characterizing the Heinrich layers to be the Canadian shield's Churchill Province (Gwiazda et al., 1996; Hemming et al., 1998). In addition, the presence of 20 to 30% detrital carbonate within the IRD further pinpointed the source to specifically within Hudson Bay and Hudson Strait (Andrews and Tedesco, 1992; Broecker et al., 1992; Bond et al., 1993). The identification of source area lead to the interpretation of Heinrich layers as recorders of "armadas of icebergs" launched from the Laurentide Ice Sheet (Heinrich, 1988; Broecker et al., 1992; Bond et al., 1993).

Because the AIS comprises two morphologically and behaviorally distinct ice-sheets, the EAIS and WAIS, identification of source area(s) of South Atlantic IRD will also shed light on whether these very different ice-sheets operated independently of one another or in tandem and what factors controlled such behavior. For example, the presence of rose quartz and garnet within sediments of the South Atlantic has been interpreted by some researchers to indicate ice discharge from East Antarctica (Listizin, 1978; Warnke et al., 1992; Teitler et al., 2001).

Because the sources of the majority of icebergs in the South Atlantic today are ice shelves such as those found in the Weddell Sea region and the location of my sediment cores is

downdrift of icebergs originating in the Weddell Sea region, the occurrence of rose quartz and garnet observed within some horizons within my sediment cores appears to disagree with an East Antarctic origin for such minerals in my cores. Alternatively, Diekmann and Kuhn (1999) argue that IRD of the South Atlantic does have a general petrography consistent with an East Antarctic origin (East Antarctic Paleozoic tillites known as the Beacon Supergroup) but that some primary East Antarctic detritus experienced transient storage in the southern Weddell Sea where it was subsequently entrained within glacial ice and released to the South Atlantic by ice discharge from West Antarctica. Yet another alternative explanation is that icebergs from East Antarctica are transported westward by easterly winds where they may become entrained within the Weddell Gyre and transported toward the southeast Atlantic, to the vicinity of my core locations (Listizin, 1978). Unfortunately, <1% of the Antarctic continent reveals rock outcrops, with the remaining surface covered entirely by ice (Listizin, 1978). Consequently, very few studies have been conducted on IRD source areas in the South Atlantic region and this remains a topic that needs to be addressed.

**Potential Causes of Increased Ice Discharge**

Among the possible mechanisms of increased IRD accumulation is increased ice flow (surging), disintegration of ice-shelves, ice-sheet expansion in response to climatic forcing, or greater distance of iceberg transport. Identification of, and differentiation between, surging and disintegration of ice shelves on the basis of distal IRD evidence remains difficult. Although complicated by a variety of additional nearshore processes, evidence for these mechanisms is perhaps more likely to be found in the proximal rather than distal marine environment. However, as in the distal environment, different proxies within proximal deposits may not be of equal utility in reconstructing ice-sheet dynamics. As discussed previously, for example, diatom and Beryllium-10 evidence from subglacial sediments suggests the existence of an open marine environment beneath the modern Ross ice-shelf at some time during the late Pleistocene (Scherer

et al., 1998). In contrast, layers enriched in coarse lithics may be the result of winnowing rather than a signal of ice-sheet collapse (Cofaigh et al., 2001).

Clark and Pisias (2000) suggested that an increase in ice discharge does not necessarily indicate AIS instability, which they interpreted to mean ice surging, but rather could be a stable response of marine ice-sheet margins to climatic forcing. Many IRD layers (exclusive of the Heinrich layers) of the North Atlantic, for example, have been shown to have low sediment fluxes and to be associated with cold events in the North Atlantic (Bond and Lotti, 1995). Ice-sheet expansion in response to climatic forcing and also greater distance of iceberg transport are each potential causes of increased IRD concentration that can be tested by correlating South Atlantic sediment records to Antarctic ice. Each would require a consistent temporal relationship between SA events and climatic events recorded in Antarctic ice-cores. For example, all other factors being equal, cooler sea-surface temperatures yield greater iceberg transport distances and retention of entrained debris for greater distances (El-Tahan et al., 1987; Venkatesh et al., 1994; Matsumoto, 1996, 1997; Azetsu-Scott and Syvitski, 1999).

Correlations presented here between South Atlantic sediment records and Antarctic ice suggest that SA events do not occur at peak cool temperatures, thus eliminating greater distance of iceberg transport as the mechanism of increased IRD deposition. However, both marine-ice core correlation and downcore phase relationships revealed prominent South Atlantic millennial ice-rafting events (SA events) do coincide with times of regional cooling (Kanfoush et al., in preparation). I have argued that the more consistent relationship between SA events and changes in climate of the North Atlantic region implies the origin of the millennial Antarctic ice discharge events lies there and is somehow transmitted southward, perhaps via a sea-level linkage (Denton et al., 1986; Huybrechts, 1990; Kanfoush et al., 2000a; Kanfoush et al., in preparation). Yet the correlations between South Atlantic sediments and Antarctic ice presented here do not eliminate the possibility that increased ice discharge is the result of increased ice-sheet expansion in response to regional climatic forcing and this, as yet, remains a possibility awaiting (in)validation.

## REFERENCES


Adkins, J.F., Cheng, H., Boyle, E.A., Druffel, E.R.M., Edwards, R.L., 1998. Deep-sea coral evidence for rapid change in ventilation of the deep North Atlantic 15,400 years ago. Science 280, 725-728.

Allen, C.P., Warnke, D.A., 1991. History of ice-rafting at Leg 114 Sites, Subantarctic South Atlantic. In: Ciesielski, P.F., Kristofferson, Y. (Eds.), Proceedings of the Ocean Drilling Program, Scientific Results Leg 114, Subantarctic South Atlantic. Ocean Drilling Program, College Station, TX, pp. 599-607.

Alley, R.B., MacAyeal, D.R., 1994. Ice-rafted debris associated with binge/purge oscillations of the Laurentide Ice-sheet. Paleoceanography 9(4), 503-511.

Alley, R.B., Mayewski, P.A., Sowers, T., Stuiver, M., Taylor, K.C., Clark, P.U., 1997. Holocene climatic instability: a prominent, widespread event 8200 yr ago. Geology 25, 483-486.

Alley, R.B., Whillans, I.M., 1991. Changes in the West Antarctic ice sheet. Science 254, 959-963.

Anderson, J.B., Andrews, J.T., 1999. Radiocarbon constraints on ice sheet advance and retreat in the Weddell Sea, Antarctica. Geology 27(2), 179-182.

Anderson, J.B., Domack, E.W., Kurtz, D.D., 1980. Observations of sediment-laden icebergs in Antarctic waters: Implications to glacial erosion and transport. J. Glaciol. 25, 387-396.

Anderson, J.B., Thomas, M.A., 1991. Marine ice-sheet decoupling as a mechanism for rapid, episodic sea-level change: the record of such events and their influence on sedimentation. Sedimentary Geology 70, 87-104.

Andrews, J.T., Tedesco, K., 1992. Detrital carbonate-rich sediments, northwestern Labrador Sea: implications for ice-sheet dynamics and iceberg rafting (Heinrich) events in the North Atlantic. Geology 20, 1087-1090.

Asmus, T. Frank, M., Koschmieder, C., Frank, N., Gersonde, R., Kuhn, G., Mangini, A., 1999. Variations in biogenic particle flux in the southern Atlantic section of the subantarctic zone during the late Quaternary: evidence from sedimentary $^{231}Pa_{ex}$ and $^{230}Th_{ex}$, Marine Geol. 159, 63-78.

Atlas Antarktiki (Atlas of Antarctica, vol. 2), 1969, GURK, Moskow.

Azetsu-Scott, K., Syvitski, S.P.M., 1999. Influence of melting icebergs on distribution, characteristics and transport of marine particles in an East Greenland fjord. J. Geophys. Res. C: Oceans 104(3), 5321-5328.

Barber, D.C., Dyke, A., Hillaire-Marcel, C., Jennings, A.E., Andrews, J.T., Kerwin, M.W., Bilodeau, G., McNeely, R., Southon, J., Morehead, M.D., Gagnon, J.-M., 1999. Forcing of the cold event of 8,200 years ago by catastrophic drainage of Laurentide lakes. Nature 400, 344-348.

Bard, E., Arnold, M., Hamelin, B., Tisnerat-Laborde, N., Cabioch, G., 1998. Radiocarbon calibration by means of mass spectrometric $^{230}Th/^{234}U$ and $^{14}C$ ages of corals: an updated database including samples from Barbados, Mururoa and Tahiti. Radiocarbon 40, 1085-1092.

Basile, I., Grousset, F.E., Revel, M., Petit, J.R., Biscaye, P.E., Barkov, N.I., 1997. Patagonian origin of glacial dust deposited in East Antarctica (Vostok and Dome C) during glacial Stages 2, 4 and 6. Earth Planet. Sci. Lett. 146, 573-589.

Baumgartner, S., Beer, J., Masarik, J., Wagner, G., Meynadier, L., Synal, H.-A., 1998. Geomagnetic modulation of the $^{36}Cl$ flux in the GRIP ice core, Greenland. Science 279, 1330-1332.

Baumgartner, S.J., Beer, M., Suter, M., Dittrich-Hannen, B., Synal, H.-A., Kubik, P.W., Hammer, C., Johnsen, S., 1997. 36Cl fallout in the Summit Greenland Ice Core Project ice core. J. Geophys. Res. 102, 26659-26662.

Behl, R.J., Kennett, J.P., 1996. Brief interstadial events in the Santa Barbara basin, NE Pacific, during the past 60 kyr. Nature 379, 243-246.

Bender, M.B., Sowers, T., Dickson, M.-L., Orchardo, J., Grootes, P., Mayewski, P.A., Meese, D.A., 1994. Climate correlations between Greenland and Antarctica during the past 100,000 years. Nature 372, 663-666.

Benson, L.V., Burnett, J.W., Kashgarian, M., Lund, S.P., Phillips, F.M., Rye, R.O., 1996. Climatic and hydrologic oscillations in the Owens Lake basin and adjacent Sierra Nevada, California. Science 274, 746-749.

Bindschadler, R., 1998. Future of the West Antarctic Ice Sheet. Science 282, 428-429.

Bindschadler, R., Alley, R.B., Anderson, J., Shipp, S., Borns, H., Fastook, J., Jacobs, S., Raymond, C.F., Shuman, C.A., 1998. What is happening to the West Antarctic Ice Sheet? Eos, Trans. Am. Geophys. Union 257, 264-265.

Bindschadler, R.A., Fahnestock, M.A., Skvarka, P., Scambos, T.A. 1994. Surface-velocity field of the northern Larsen ice-shelf, Antarctica. Ann. Glaciol. 20, 319-326.

Binford, M.W., Kolata, A.L., Brenner, M., Janusek, J., Seddon, M.T., Abbott, M., Curtis, J.H., 1997. Climate variation and the rise and fall of an Andean civilization, Quat. Res. 47(2), 235-248.

Blanchon, P., Shaw, J., 1995. Reef drowning during the last deglaciation: Evidence for catastrophic sea-level rise and ice-sheet collapse. Geology, 23, 4-8.

Blunier, T., Brook, E.J., 2001. Timing of millennial-scale climate change in Antarctica and Greenland during the last glacial period. Science 291, 109-112.

Blunier, T., Chappellaz, J., Schwander, J., Dallenbach, A., Stauffer, B., Stocker, B., Raynaud, D., Jouzel, J., Clausen, H.B., Hammer, C.U., Johnsen, S.J., 1998. Asynchrony of Antarctic and Greenland climate change during the last glacial period. Nature 394, 739-743.

Bombosch, A., Jenkins, A., 1995. Modeling the formation and deposition of frazil ice beneath Filchner-Ronne Ice Shelf. J. Geophys. Res. 100(C4), 6983-6992.

Bond, G., Broecker, W., Johnsen, S., McManus, J., Labeyrie, L., Jouzel, J., Bonani, G., 1993. Correlations between climate records from the North Atlantic sediments and Greenland ice. Nature 365, 143-147.

Bond, G., Heinrich, H., Broecker, W., Labeyrie, L., McManus, J., Andrews, J., Huon, S., Jantschik, R., Clasen, S., Simet, C., Tedesco, K., Klas, M., Bonani, G., Ivy, S., 1992. Evidence for massive discharges of icebergs into the North Atlantic ocean during the last glacial period. Nature, 360, 245-249.

Bond, G., Kromer, B., Beer, J., Muscheler, R., Evans, M.N., Showers, W., Hoffmann, S., Lotti-Bond, R., Hajdas, I., Bonani, G., 2001. Persistent Solar Influence on North Atlantic Climate During the Holocene. Science 294, 2130-2136.

Bond, G.C., Lotti, R., 1995. Iceberg discharges into the North Atlantic on millennial time scales during the last glaciation. Science 267, 1005-1010.

Bond, G.C., Showers, W., Cheseby, M., Lotti, R., Almasi, P., deMenocal, P., Priore, P., Cullen, H., Hajdas, I., Bonani, G., 1997. A pervasive millennial-scale cycle in North Atlantic Holocene and Glacial climates. Science 278, 1257-1266.

Brachfield, S.A., Banerjee, S.K., 2000. Rock-magnetic carriers of century-scale susceptibility cycles in glacial-marine sediments from the Palmer Deep, Antarctic Peninsula. Earth Planet. Sci. Lett. 167 (3-4), 443-455.

Bramlette, M.N., Bradley, W.H., 1941. Lithology and geologic interpretations, in: Bradley, W.H. (Ed.), Geology and biology of North Atlantic deep-sea cores between Newfoundland and Ireland. U.S. Geol. Survey Prof. Paper 198, Washington D.C., U.S. Government Printing Office, p. 1-34.

Brathauer, U., Abelmann, A., 1999. Late Quaternary variations in sea-surface temperatures and their relationship to orbital forcing recorded in the Southern Ocean (Atlantic sector). Paleoceanography 14(2), 15-148.

Broecker, W.S., 1994. Massive iceberg discharge as triggers for global climate change. Nature 372, 421-424.

Broecker, W.S., 1995. Ice-cores cooling the tropics. Nature 376, 212-213.

Broecker, W.S., 1997. Thermohaline circulation, the achilles heel of our climate system: will man-made CO2 upset the current balance? Science 278, 1582-1588.

Broecker, W.S., 1998. Paleocean circulation during the last deglaciation: a bipolar seesaw? Paleoceanography 13(2), 119-121.

Broecker, W.S., Bond, G., McManus, J., Klas, M., Clark, E., 1992. Origin of the Northern Atlantic's Heinrich events. Climate Dynamics 6, 265-273.

Broecker, W.S., Denton, G.H., 1989. The role of ocean-atmosphere organizations in glacial cycles. Geochimica Cosmochimica Acta 53, 2465-2501.

Broecker, W.S., Henderson, G.M., 1998. The sequence of events surrounding Termination II and their implications for the cause of glacial-interglacial CO2 changes. Paleoceanography 13(4), 352-364.

Burckle, L.H., 1993. Late Quaternary interglacial stages warmer than present. Quat. Sci. Rev. 12, 825-831.

Burckle, L.H., Robinson, D., Cooke, D., 1982. Reappraisal of sea-ice distribution in Atlantic and Pacific sectors of the Southern Ocean at 18,000 yr BP. Nature 299, 435-437.

Cane, M.A., 1998. A role for the tropical Pacific. Science 281, 59-61.

Channell, J.E.T., Charles, C.D., Stoner, J.S., Hodell, D.A., 2000. Geomagnetic paleointensity for the last 100 kyr from the sub-antarctic South Atlantic: A tool for interhemispheric correlation. Earth Planet. Sci. Lett. 175(1-2), 145-160.

Channell, J.E.T., Hodell, D.A., Lehman, B., 1997. Relative geomagnetic paleointensity and $\delta^{18}O$ at ODP Site 983 (Gardar Drift, North Atlantic) since 350 ka. Earth Planet. Sci. Lett. 153, 103-118.

Chappell, J., 2002. Sea level changes forced ice breakouts in the last glacial cycle: new results from coral terraces. Quat. Sci. Rev. 21, 1229-1240.

Chappell J., Shackleton, N.J., 1986. Oxygen isotopes and sea-level. Nature 324, 137-140.

Charles, C.D., Froelich, P.N., Zibello, M.A., Mortlock, R.A., Morley, J.J., 1991. Biogenic opal in Southern Ocean sediments over the last 450,000 years: implications for surface water chemistry and circulation. Paleoceanography 6(6), 697-728.

Charles, C.D., Lynch-Stieglitz, J., Ninnemann, U.S., Fairbanks, R.G., 1996. Climate connections between the hemispheres revealed by deep sea sediment core/ice core correlations. Earth Planet. Sci. Lett. 142, 19-27.

Chi, J., Mienert, J., 1996. Linking physical property records of Quaternary sediments to Heinrich events. Marine Geology 131, 57-73.

Clapperton, C.M., Sugden, D.E., 1988. Holocene glacier fluctuations in South America and Antarctica. Quat. Sci. Rev. 7, 185-198.

Clark, P.U., Alley, R.B., Keigwin, L.D., Licciardi, J.M., Johnsen, S.J., Wang, H., 1996. Origin of the first global meltwater pulse following the last glacial maximum. Paleoceanography, 11, 563-577.

Clark, P.U., Bartlein, P.J., 1995. Correlation of late Pleistocene glaciation in the western United States with North Atlantic Heinrich events. Geology 23, 483-486.

Clark, P.U., Pisias, N.G., 2000. Interpreting Iceberg Deposits in the Deep Sea; Comment on "Millennial-scale instability of the Antarctic Ice Sheet during the last glaciation." by Kanfoush, S.L., Hodell, D.A., Charles, C.D., Guilderson, T.P., Mortyn, P.G., Ninnemann, U.S. Science 290, 51-52.

Clarke, G.K.C., Marshall, S.J., Hillaire-Marcel, C., G. Bilodeau, Veiga-Pires, C., 1999. A glaciological perspective on Heinrich events, In: Clark, P.U., Webb, R.S., Keigwin, L.D. (Eds.), Mechanisms of global climate change at millennial time scales. Am. Geophys. Union Geophys. Monograph Series 112, 243-262.

Cofaigh, C.O., Dowdeswell, J.A., Pudsey, C.J., 2001. Late Quaternary ice-rafting along the Antarctic Peninsula continental rise and in the Weddell and Scotia Seas. Quat. Res. 56, 308-321.

Conolly, J., Ewing, M., 1965a. Pleistocene glacial-marine zones in North Atlantic deep-sea sediments. Nature 208, 135-138.

Conolly, J., Ewing, M., 1965b. Ice-rafted detritus as a climatic indicator in Antarctic deep-sea cores. Science 150, 1822-1824.

Conolly, J.R., Ewing, M., 1970. Ice-rafted detritus in northwest Pacific deep-sea sediments. in: Hays, J.D. (Ed.), Geological Investigations of the North Pacific. GSA Memoir 126, 219-231.

Conway, H., Hall, B.L., Denton, G.H., Gades, A.M., Waddington, E.D., 1999. Past and future grounding-line retreat of the West Antarctic Ice Sheet. Science 286, 280-283.

Coplen, T.B., 1996. More uncertainty than necessary. Paleoceanography 11, 369-370.

Cooke, D.W., 1978. Variations in the seasonal extent of sea ice in the Antarctic during the last 140,000 years. Unpublished dissertation, Columbia University, 287pp.

Cooke, D.W., Hays, J.D., 1982. Estimates of Antarctic Ocean seasonal sea-ice cover during glacial intervals. In: Proceedings of the 3rd Symposium on Antarctic Geology and Geophysics (ed. Craddock, C.), Univ. Wisconsin Press, Madison, 1017-1025.

Cortese, G., Abelmann, A., 2002. Radiolarian-based paleotemperatures during the last 160 kyr at ODP Site 1089 (Southern Ocean, Atlantic Sector). Palaeogeog., Palaeoclimatol., Palaeoecol. 182(3-4), 259-286.

Cortijo, E., Chapman, M., Duplessy, J.-C., Elliot, M., Arnold, M., Turon, J.-L., Auffret, G., Labeyrie, L., Vidal, L., Vautravers, M., 1997. Changes in sea surface hydrology associated with Heinrich event 4 in the North Atlantic Ocean between 40° and 60°N. Earth Planet. Sci. Lett. 146(1-2), 29-45.

Craig, H., 1965. The measurement of oxygen isotope paleotemperatures. In: Tongiorgi, E. (Ed.), Stable Isotopes in Oceanographic Studies and Paleotemperatures. Spoleto, Pisa, pp. 161-282.

Crosta, X., Pichon, J.-J., Burckle, L.H., 1998. Application of modern analogue technique to marine Antarctic diatoms: Reconstruction of maximum sea-ice extent at the last glacial maximum. Paleoceanography 13(3), 284-297.

Cullen, H. M., deMenocal, P. B., Hemming, S., 2000. Climate change and the collapse of the Akkadian empire: evidence from the deep sea. Geology 28(4), 379-82.

Curtis, J.H., Hodell, D.A., Brenner, M., 1996. Climate variability on the Yucatan Peninsula (Mexico) during the last 3500 years, and implications for Maya cultural evolution. Quaternary Res. 46, 37-47.

Dansgaard, W., Johnson, S.J., Clausen, H.B., Dahl-Jensen, D., Gundestrup, N., Hammer, C.U., Hvidberg, C.S., Steffensen, J.P., Sveinbjornsdottir, A.E., Jouzel, J., Bond, G., 1993. Evidence for general instability of past climate from a 250 kyr ice core record. Nature 364, 218-220.

Davis, C.H., Kleuver, C.A., Haines, B.J., 1998. Elevation change of the southern Greenland ice-sheet. Science 279, 2086-2088.

DeMaster, D.J., 1981. The supply and accumulation of silica in the marine environment. Geochim. Cosmochim. Acta, 45, 1715-1732.

Denton, G.H., Hughes, T.J., 1983. Milankovitch theory of ice ages: Hypothesis of ice-sheet linkage between regional insolation and global climate. Quaternary Res. 20, 125-144.

Denton, G.H., Hughes, T.J., Karlen, W., 1986. Global ice-sheet system interlocked by sealevel. Quat. Res. 26, 3-26.

Denton, G.H., Karlen, W., 1973. Holocene climatic variations—their patterns and possible cause. Quat. Res. 3, 155-205.

Diekmann, B., Kuhn, G., 1999. Provenance and dispersal of glacial-marine surface sediments in the Weddell Sea and adjoining areas, Antarctica: Ice-rafting versus current transport. Marine Geology 158(1-4), 209-231.

Dieckmann G.S., Eicken H., Spindler M., Lange M.A., Ackley S.F., 1991. Antarctic sea ice: a habitat for the foraminifer Neogloboquadrina pachyderma. J. Foraminiferal Res. 21(2), 182-189.

Doake, C.S.M., Vaughn, D.G. 1991. Rapid disintegration of the Wordie ice-shelf in response to atmospheric warming. Nature 350,328-330.

Domack, E.W., Jull, A.J.T., Nakao, S., 1991. Advance of East Antarctic outlet glaciers during the Hypsithermal: Implications for the volume state of the Antarctic Ice Sheet under global warming. Geology 19, 1059-1062.

Dowdeswell, J.A., Elverhoi, A., Andrews, J.Y., Hebbein, D., 1999. Asynchronous deposition of ice-rafted layers in the Nordic seas and North Atlantic Ocean. Nature 400, 348-351.

Dowdeswell, J.A., Hagen, J.O., Bjornsson, H., Glazovsky, A.F., Harrison, W.D., Holmlund, P., Jania, J., Koerner, R.M., Lefunconnier, B., Ommanney, C.S.L., Thomas, R.H., 1997. The mass balance of circum-arctic glaciers and recent climate change. Quaternary Res. 48, 1-24.

Dowdeswell, J.A., Maslin, M.A., Andrews, J.T., McCave, I.N., 1995. Iceberg production, debris rafting, and the extent and thickness of Heinrich layers (H-1, H-2) in North Atlantic sediments. Geology 23(4), 301-304.

Drewry, D.J., Cooper, A.P.R., 1981. Processes and models of Antarctic glaciomarine sedimentation. Ann. Glaciol. 2, 117-122.

Dyurgerov, M.B., Meier, M.F., 2000. Twentieth century climate change: Evidence from small glaciers. Proceedings of National Academy of Sciences, USA 97(4), 1406-1411.

Eicken, H., Martin, T., Kassens, H., Viehoff, T., Reimnitz, Alexandrov, V., 1996. Sea-ice processes in the Laptev Sea and their importance for sediment export. Cont. Shelf Res. 17(2), 205-233.

Elliot, M., Labeyrie, L., Bond, G., Cortijo, E., Turon, J.-L., Tisnerat, N., Duplessy, J.-C., 1998. Millennial-scale iceberg discharges in the Irminger Basin during the last glacial period: Relationship with the Heinrich events and environmental settings. Paleoceanography 13(5), 433-446.

El-Tahan, M., Venkatesh, S., El-Tahan, H., 1987. Validation and quantitative assessment of the deterioration mechanisms of Arctic icebergs. J. Offshore Mech. Arct. Eng. 109, 102-108.

Emiliani, C., 1955. Pleistocene temperatures. J. Geology 63, 538-578.

Engelman, E.E., Jackson, J.J., Norton, D.R., 1985. Determination of carbonate carbon in geologic materials by coulometric titration. Chemical Geol. 53, 125-128.

Erikson, D.B., Ewing, M., Wollin, G., Heezen, B.C., 1961. Atlantic deep-sea sediment cores. GSA Bulletin 72, 193-286.

Fairbanks, R.G., 1989. A 17,000-year glacio-eustatic sea-level record: Influence of glacial melting rates on the Younger Dryas event and deep-ocean circulation. Nature 342, 637-642.

Ferrigno, J.G., Swithinbank, C., Williams, R.S., Jr., Rosanova, C.E., Lucchitta, B.K., 1998. Analysis of coastal change in Marie Byrd Land and Ellsworth Land, West Antarctica, using Landsat imagery. Ann. Glaciology 27, 33-40.

Fitzsimons S.J., McManus K.J., Lorrain, R.D., 1999. Structure and strength of basal ice and substrate of a dry-based glacier: Evidence for substrate deformation at sub-freezing temperatures. Ann. Glaciology 28, 236-240.

Frezzotti, M., Cimbelli, A., Ferrigno, J.G., 1998. Ice-front change and iceberg behaviour along Oates and George V Coasts, Antarctica, 1912-96. Ann. Glaciology 27, 643-650.

Fronval, T., Jansen, E., Bloemendal, J., Johnsen, S., 1995. Oceanic evidence for coherent fluctuations in Fennoscandian and Laurentide ice-sheets on millennium timescales. Nature 374, 443-446.

Gersonde, R., Zielinski, U., 2000. The reconstruction of late Quaternary Antarctic sea-ice distribution—The use of diatoms as a proxy for sea-ice. Palaeogeogr. Palaeoclimatol. Palaeoecol. 162(3-4), 263-286.

Gloerson, P., Campbell, W.J., Cavalieri, D.J., Comiso, J.C., Parkinson, C.L., Zwally, H.J., 1992. Arctic and Antarctic Sea Ice, 1978-1987: Satellite Passive Microwave Observations and Analysis. NASA, Washington, D.C.

Grimm, E.C., Jacobson Jr., G.L., Watts, W.A., Hansen, B.C.S., Maasch, K.A., 1993. A 50,000-year record of climate oscillations from Florida and its temporal correlation with Heinrich events. Science 261, 198-200.

Grobe, H., Mackensen, A., 1992. Late Quaternary climatic cycles as recorded in sediments from the Antarctic continental margin. In: Kennett, J.P., Warnke, D. (Eds.), The Antarctic Paleoenvironment: A Perspective on Global Change. AGU Antarctic Research Series, Washington D.C., pp. 349-376.

Grootes, P.M., Steig, E.J., Stuiver, M., Waddington, E.D., Morse, D.L., 1994. A new ice core record from Taylor Dome, Antarctica. EOS Transactions 75, 225-228.

Grootes, P.M., Stuiver, M., White, J.W.C., Johnsen, S.J., Jouzel, J., 1993. Comparison of oxygen isotope records from the GISP2 and GRIP Greenland ice cores. Nature 366, 552-554.

Grousset, F.E., Biscaye, P.E., Revel, M., Petit, J.R., Pye, K., Joussaume, S., Jouzel, J., 1992. Antarctic (Dome C) ice-core dust at 18 k.y. B.P.: Isotopic constraints on origins. Earth Planet. Sci. Lett. 111: 175-182.

Gwiazda, R.H., Hemming, S.R., Broecker, W.S., 1996a. Tracking the sources of icebergs with lead isotopes: the provenance of ice-rafted debris in Heinrich layer 2. Paleoceanography 11(1), 77-93.

Gwiazda, R.H., Hemming, S.R., Broecker, W.S., 1996b. Provenance of icebergs during Heinrich event 3 and the contrast to their sources during other Heinrich episodes. Paleoceanography 11(4), 371-378.

Guyodo, Y., Valet, J.-P., 1996. Relative variations in geomagnetic intensity from sedimentary records: the past 200 thousand years. Earth Planet. Sci. Lett. 143, 23-26.

Hebbeln, D., 2000. Flux of ice-rafted detritus from sea-ice in the Fram Strait. Deep-Sea Res. Part II: Tropical Studies in Oceanogr. 47(9-11), 1773-1790.

Heinrich, H., 1988. Origin and consequences of cyclic ice rafting in the northeast Atlantic Ocean during the past 130,000 years. Quaternary. Res. 29, 142-152.

Hemming, S.R., Bond, G.C., Gwiazda, R.H., McManus, J.F., Klas, M., Hajdas, I., Broecker, W.S., Sharp, W.D., 1998. Provenance of Heinrich layers in core V28-82, northeastern Atlantic: $^{40}Ar/^{39}Ar$ ages of ice-rafted hornblende, Pb isotopes in feldspar grains, and Nd-Sr-Pb isotopes in the fine sediment fraction. Earth Planet. Sci. Lett. 164(1-2), 317-333.

Hemming, S.R., Jennings, A.E., Onstott, T.C., Gwiazda R.H., Andrews, J.T., Broecker, W.S., 2000. $^{40}Ar/^{39}Ar$ and Pb-Pb study of individual hornblende and feldspar grains from southeastern Baffin Island glacial sediments: Implications for the provenance of the Heinrich layers. Can. J. Earth Sci. 37(6), 879-890.

Hendy, E.J., Gagan, M.K., Alibert, C.A., McCulloch, M.T., Lough, J.M., Isdale, P.J., 2002. Abrupt Decrease in Tropical Pacific Sea Surface Salinity at End of Little Ice Age. Science 295, 1511-1514.

Hodell, D.A., 1993. Late Pleistocene paleoceanography of the South Atlantic sector of the Southern Ocean: Ocean Drilling Program Hole 704 A. Paleoceanography 8, 47-67.

Hodell, D.A., Charles, C.D., Ninnemann, U.S., 2000. Comparison of interglacial stages in the South Atlantic sector of the southern ocean for the past 450 kyr: implications for Marine Isotope Stage (MIS) 11. Global and Planetary Change 24, 7-26.

Hodell, D.A., Curtis, J.H., Brenner, M., 1995. Possible role of climate in the collapse of the Maya civilization. Nature 375, 391-394.

Hodell, D.A., Gersonde, R., Blum, P., 2002. Proceedings of the Ocean Drilling Program, Scientific Results, ODP Leg 177 Synthesis: Insights into Southern Ocean Paleoceanography on Tectonic to Millennial Timescales. Ocean Drilling Program, College Station, Texas.

Hodell, D., Shemesh, A., Crosta, X., Kanfoush, S., Charles, C., Guilderson, T., 2001. Evidence for late Holocene neoglaciation in the Southern Ocean and its implications for future climate change. Quaternary Research 56(2), 191-198.

Hollin, J.T., 1962. On the glacial history of Antarctica. J. Glaciol. 4, 173-195.

Hostetler, S.W., Pisias, N.J., Clark, P.U., Bartlein, P.J., Mix, A.C., 1999. Atmospheric transmission of North Atlantic Heinrich events. J. Geophys. Res. D: Atmosph. 104(4), 3947-3952.

Howard, W.R., 1997. A warm future in the past. Nature 338, 418-419.

Hulbe, C.L., 1997. An ice-shelf mechanism for Heinrich layer production. Paleoceanography 12(5), 711-717.

Huybrechts, P., 1990. The Antarctic Ice Sheet during the last glacial-interglacial cycle: a three-dimensional experiment. Annals of Glaciology 14, 115-119.

Imbrie, J., Hays, J.D., Martinson, D.G., McIntyre, A., Mix, A.C., Morley, J.J., Pisias, N.G., Prell, W.L., Shackleton, N.J., 1984. The orbital theory of Pleistocene climate: support from a revised chronology of the marine $\delta^{18}O$ record, In: Berger, A., Imbrie, J., Hays, J., Kukla, G., Saltzman, B. (Eds.), Milankovitch and Climate, Part I., D. Reidel, Dordrecht, pp. 269-305.

International Panel on Climate Change (IPCC), 1996. Climate Change 1995. In: The Science of Climate Change, J.T. Houghton, L.G. Meira Filho, B.A. Callander, N. Harris, A. Kattenberg, Maskell, K. (Ed.), Cambridge University Press, 572 pp.

Irion, R., 2001. The melting snows of Kilimanjaro. Science 291, 1690-1691.

Iverson, N.R., 1993. Regelation of ice through debris at glacier beds: implications for sediment transport. Geology 21, 559-62.

Jenkins, A., Keys, J.R., Vaughan, D.G., Jacobs, S.S., Hellmer, H.H., 1997. Glaciological and oceanographic evidence of high melt rates beneath Pine Island Glacier, West Antarctica. J. Glaciol. 43(143), 114-121.

Johnsen, S.J., Clausen, H.B., Dansgaard, W., Fuhrer, K., Gundestrup, N., Hammer, C.U., Iversen, P., Jouzel, J., Stauffer, B., Steffensen, J.P., 1992. Irregular glacial interstadials recorded in a new Greenland ice core. Nature 359, 311-313.

Johnsen, S.J., Dansgaard, W., Clausen, H.B., Langway Jr., C.C., 1972. Oxygen isotope profiles through the Antarctic and Greenland ice-sheets. Nature 235, 429-434.

Jouzel, J., Lorius, C., Petit, J.R., Genthon, C., Barkov, N.I., Kotyakov, V.M., Petrov, V.M., 1987. Vostok ice core: a continuous isotope temperature record over the last climatic cycle (160,000 years). Nature 329, 403-408.

Jouzel, J., Vaikmae, R., Petit, J.R., Martin, M., Duclos, Y., Stievenard, M., Lorius, C., Toots, M., Melieres, M.A., Burckle, L.H., Barkov, N.I., Kotyakov, V.M, 1995. The two-step shape and timing of the last deglaciation in Antarctica. Climate Dynamics 11, 151-261.

Kanfoush, S.L., Hodell, D.A., Charles, C.D., Guilderson, T.P., Mortyn, P.G., Ninnemann, U.S., 2000a. Millennial-scale instability of the Antarctic Ice Sheet during the last glaciation. Science 288,1815-1819.

Kanfoush, S.L., Hodell, D.A., Charles, C.D., Janecek, T.R., Rack, F.R., 2002. Comparison of ice-rafted debris and physical properties in ODP Site 1094 (South Atlantic) with the Vostok Ice Core over the last four climatic cycles. Paleogeogr. Paleoclimatol. Paleoecol. 182(3-4), 329-349.

Kanfoush, S.L., Hodell, D.A., Guilderson, T.R., 2000b. Interpreting iceberg deposits in the deep sea: Reply to Comment on "Millennial-scale instability of the Antarctic Ice Sheet during the last glaciation." Clark, P.U., Pisias, N.G. Science 290, 51-52.

Keany, J., Ledbetter, M., Watkins, N., Huang, T.-C., 1976. Diachronous deposition of ice-rafted debris in sub-Antarctic sediments. Geol. Soc. Am.. Bull. 87, 873-882.

Keigwin Jr., L.D., 1996. The Little Ice Age and Medieval Warm Period in the Sargasso Sea. Science 274, 1504-1508.

Keigwin Jr., L.D., Lehman, S.J., 1994. Deep circulation change linked to Heinrich event 1 and Younger Dryas in a middepth North Atlantic core. Paleoceanography 9, 189-194.

Kellogg, T.B., Kellogg, D.E., 1988. Antarctic cryogenic sediments: Biotic and inorganic facies of ice-shelf and marine-based ice-sheet environments. Paleogeogr., Paleoclimatol., Paleoecol. 67, 51-74.

Kempema, E.W., Reimnitz, E., Barnes, P.W., 1989. Sea ice sediment entrainment and rafting in the Arctic. J. Sedimentary Petrol. 59(2), 308-317.

Kent, D., Opdyke, N.D., Ewing, M., 1971. Climate change in the North Pacific using ice-rafted detritus as a climatic indicator. GSA Bulletin 82, 2741-2754.

Kindle, E.M., 1924. Observations in ice-borne sediments by the Canadian and other Arctic expeditions. Am. J. Sci. 207, 251-286.

Kirby, M.E., Domack, E.W., McClennen, C.E., 1998. Magnetic stratigraphy and sedimentology of Holocene glacial marine deposits in the Palmer Deep, Bellingshausen Sea, Antarctica: implications for climate change? Marine Geology 152(4), 247-259.

Krabill, W., Frederick, E., Manizade, S., Martin, C., Sonntag, J., Swift, R., Thomas, R., Wright, W., Yungel, J., 1999. Rapid thinning of parts of the southern Greenland ice-sheet. Science 283, 1522-1524.

Krajick, K., 2001. Tracking icebergs for clues to climate change. Science 292, 2244-2245.

Kumar, N., Anderson, R.F., Mortlock, R.A., Froelich, P.N., Kubick, P, Dittrichhannen, B., Suter, M., 1995. Increased biological productivity and export production in the glacial Southern Ocean. Nature 378, 675-680.

Kunz-Pirrung, M., Gersonde, R., Hodell, D.A., 2002. Mid-Brunhes century-scale diatom sea surface temperature and sea ice records from the Atlantic sector of the Southern Ocean (ODP Leg 177, Sites 1093, 1094 and core PS2089-2). Palaeogeog. Palaeoclimatol. Palaeoecol. 182(3-4), 305-328.

Labeyrie, L.D., Pichon, J.J., Labracherie, M., Ippolito, P., Duprat, J., Duplessy, J.C., 1986. Melting history of Antarctica during the past 60,000 years. Nature 322, 701-706.

Lackschewitz K.S., Wallrabe-Adams, H.-J., 1997. Composition and origin of volcanic ash zones in late Quaternary sediments from the Reykjanes Ridge: evidence for ash fallout and ice-rafting. Marine Geology 136(3-4), 209-224.

Lagerklint, I.M., Wright, J.D., 1999. Late glacial warming prior to Heinrich event 1: the influence of ice rafting and large ice sheets on the timing of initial warming. Geology 27(12), 1099-1102.

Laj, C., Kissel, C., Mazaud, A., Channell, J.E.T., Beer, J., 2000. North Atlantic paleointensity stack since 75 ka (NAPIS-75) and the duration of the Laschamp event. Philos. Trans. Royal Soc., A358, 1009-1025.

Lambeck, K., Chappell, J., 2001. Sea-level change through the last glacial cycle. Science 292, 679-686.

Lazzara, M.A., van der Veen, C.J., Jezek, K.C., Scambos, T.A., MacAyeal, D.R., 1999. On the recent calving of icebergs from the Ross ice-shelf. Polar Geography 23(3), 201-212.

Leuschner, D.C., Sirocko, F., 2000. The low-latitude monsoon climate during Dansgaard-Oeschger cycles and Heinrich Events. Quaternary Science Rev. 19, 243-254.

Levitus, S., Antonov, J.I., Wang, J., 2001. Anthropogenic warming of Earth's climate system. Science 292, 267-270.

Linsley, B.K., 1996. Oxygen-isotope record of sea-level and climate variations in the Sulu Sea over the past 150,000 years. Nature 380, 234-237.

Lizitzin, A.P., 1978. Oceanic Sedimentation: Lithology and Geochemistry. English translation by Woolhiser, C. (1996), Kennett, J.P. (Ed.), Washington D.C., AGU, 391pp.

Lowell, T.V., Heusser, C.J., Anderson, B.G., Moreno, P.I., Hauser, A., Heusser, L.E., Schluchter, C., Marchant, D.R., Denton, G.H., 1995. Interhemispheric correlation of late Pleistocene glacial events. Science 269, 1541-2549.

MacAyeal, D.R., 1992. Irregular oscillations of the West Antarctic Ice Sheet. Nature 359, 29-32.

MacAyeal, D.R., 1993. Binge/purge oscillations of the Laurentide Ice Sheet as a cause of the North Atlantic's Heinrich events. Paleoceanography 8, 775-784.

Manabe, S., Stoufer, R.J., 1997. Coupled ocean-atmosphere model response to freshwater input: comparison to Younger Dryas event. Paleoceanography 12, 321-336.

Margolis, S.V., Kennett, J.P., 1971. Cenozoic paleoglacial history of Antarctica recorded in subantarctic deep-sea cores. Am. J. Sci. 271, 1-36.

Marshall, S.J., Tarasov, L., Clarke, G.K.C., Peltier, W.R., 2000. Glaciological reconstruction of the Laurentide Ice-sheet: Physical processes and modelling challenges. Canadian Journal of Earth Sciences 37(5), 769-793.

Masson, V., Vimeux, F., Jouzel, J., Morgan, V., Delmotte, M., Ciais, P., Hammer, C., Johnsen, S., Ya Lipenkov, V., Mosley-Thompson, E., Petit, J.-R., Steig, E.J., Stievenard, M., Vaikmae, R., 2000. Holocene climate variability in Antarctica based on 11 ice-core isotopic records. Quat. Res. 54(3), 348-358.

Martinson, D.G., Pisias, N.G., Hays, J.D., Imbrie, J., Moore, Jr., T.C., Shackleton, N.J., 1987. Age dating and the orbital theory of the ice ages: development of a high-resolution 0 to 300,000-year chronostratigraphy. Quaternary Research 27, 1-29.

Masarik, J., Beer, J., 1999. Simulation of particle fluxes and cosmogenic nuclide production in earth's atmosphere. J. Geophys. Res. 104, 12099-13012.

Matsumoto, K., 1996. An iceberg drift and decay model to compute the ice-rafted debris and iceberg meltwater flux: application to the interglacial North Atlantic. Paleoceanography 11(6), 729-742.

Matsumoto, K., 1997. Modeled glacial North Atlantic ice-rafted debris pattern and its sensitivity to various boundary conditions. Paleoceanography 12(2), 271-280.

Mazaud, A., Laj, C., Bender, M., 1994. A geomagnetic chronology for Antarctic ice accumulation. Geophys. Res. Lett. 21, 337-340.

McManus, J.F., Oppo, D.W., Cullen, J.L., 1999. A 0.5 million year record of millennial-scale climate variability in the North Atlantic. Science 283, 971-975.

Meese, D.A., Alley, R.B., Gow, A.J., Grootes, P.M., Mayewski, P.A., Ram, M., Taylor, K.C., Waddington, I.E., Zielinski, G.A., 1994. Preliminary depth-age scale for the GISP2 ice core. Spec. Rep. 94-1, Cold Reg. Res. Eng. Lab., Hanover, NH.

Meier, M.F., 1983. Snow and ice in a changing hydrological world. J. des Sci. Hydrologiques 28(1), 3-22.

Meier, M.F., 1984. Contribution of small glaciers to global sea-level. Science 226, 1418-1421.

Meier, M.F., 1993. Ice, climate and sea-level: Do we know what is happening? In: Peltier, W.R. (Ed.), Ice in the Climate System. Springer-Verlag, Berlin, pp. 141-260.

Mercer, J. H. 1978. West Antarctic Ice Sheet and CO2 greenhouse effect: A threat of disaster. Nature 271, 321-325.

Meynadier, L., Valet, J.-P., Weeks, R., Shackleton, N.J., Hagee, V.L., 1992. Relative geomagnetic intensity of the field during the last 140 ka. Earth Planet. Sci. Lett. 114, 39-57.

Mix, A.C., Rugh, W., Pisias, N.G., Veirs, S., Leg 138 Shipboard Sedimentologists (Hagelberg, T., Hovan, S., Kemp, A., Leinen, M., Levitan, M., Ravelo, C.) and Leg 138 Scientific Party, 1992. Color reflectance spectroscopy: a tool for rapid characterization of deep-sea sediments, In: Mayer, L., Pisias, N., Janecek, T. et al., Proc. ODP Init. Repts. 138, Part 1, College Station, Texas, Ocean Drilling Program, pp. 67-77.

Mortyn, P.G., 2000. Planktonic foraminifera and upper water column variability in the South Atlantic: a multiple species approach to the deep sea sedimentary record of climate change. Ph.D. dissertation, Scripps Inst. of Oceanography, Univ. Calif., San Diego, 2000.

Mortyn, P.G., Charles, C.D., Ninnemann, U.S., Hodell, D.A.. Deep sea sedimentary analogs for the Vostok ice core. J. Geophys. Res., submitted.

Murray, J., Renard, A.F., 1884. On the nomenclature, origin and distribution of deep-sea sediments. Royal Soc. Edinburgh Proc. 12, 474-495.

Nakada, M., Lambeck, K., 1988. The melting history of the late Pleistocene ice-sheet. Nature 333, 36-40.

Neshyba, S., 1977. Upwelling by icebergs. Nature 267, 507-508.

Neuman, A.C., Hearty, P.J., 1996. Rapid sea-level changes at the close of the last interglacial (substage 5e) recorded in Bahamian Island geology. Geology 24, 775-778.

Ninnemann, U.S., Charles, C.D., Hodell, D.A., 1999. Origin of global millennial scale climate events: constraints from the southern ocean deep sea sedimentary record, In: Clark, P.U., Webb, R.S., Keigwin, L.D. (Eds.), Mechanisms of global climate change at millennial time scales. Am. Geophys. Union Geophysical Monograph Series 112, 99-112.

O'Brien, S.R., Mayewski, P.A., Meeker, L. D., Meese, D. A., Twicker, M. S., Whitlow, S.I., 1995. Complexity of Holocene climate as reconstructed from a Greenland ice core. Science 270, 1962-1964.

Oppenheimer, M., 1998. Global Warming and the Stability of the West Antarctic Ice Sheet. Nature 393, 325-332.

Oppo, D.W., Fairbanks, R.G., Gordon, A.L., Shackleton, N.J., 1990. Late Pleistocene Southern Ocean $\delta^{13}C$ variability. Paleoceanography 5, 43-54.

Peterson, L.C., Haug, G.H., Hughen, K.A., Röhl, U., 2000. Rapid Changes in the Hydrologic Cycle of the Tropical Atlantic During the Last Glacial. Science 290, 1947-1951.

Petit, J.R., Jouzel., J., Raynaud, D., Barkov, N.I., Barnola, J.-M., Basille, I., Bender, M., Chappellaz, Davis, M., Delaygue, G., Delmotte, M., Kotlyakov, Legrand, M., Lipenkov, V.Y., Lorius, C., Pepin, L., Ritz, C., Saltzman, E., Stievenard, M., 1999. Climate and atmospheric history of the past 420,000 years from the Vostok ice core, Antarctica. Nature 399, 429-436.

Pfeffer, W.T., Dyurgerov, M., Kaplan, M., Dwyer, J., Sassolas, C., Jennings, A., Raup, B., Manley, W., 1997. Numerical modeling of late Glacial Laurentide ice advance across Hudson Strait: Insights into terrestrial and marine geology, mass balance, and calving flux. Paleoceanography 12, 97-110.

Phillippi, E., 1910. Die Grundproben der deutschen Sudpolar Expedition 1901-2903. in: Deutsche Sudpolar-Expedition 1901-2903, v. 2, Berlin, Geographie und Geologie, p. 415-616.

Pichon, J.-J., Labeyrie, L.D., Bareille, G., Labracherie, M., Duprat, J., Jouzel, J., 1992. Surface water temperature changes in the high latitudes of the southern hemisphere over the last glacial-interglacial cycle. Paleoceanography 7(3), 289-318.

Porter, S.C., 2000. Onset of Neoglaciation in the Southern Hemisphere. J. Quat. Sci. 15, 395-408.

Porter, S.C., Denton, G.H., 1967. Chronology of Neoglaciation in the North American cordillera. Am. J. Sci. 265, 177-210.

Porter, S.C., An, Z.S., 1995. Correlation between climate events in the North Atlantic and China during the last glaciation. Nature 375, 305-308.

Rasibeck, G.M., Yiou, F., Bourles, D., Lorius, C., Jouzel, J., Barkov, N.I., 1987. Evidence for two intervals of enhanced $^{10}$Be deposition in Antarctic ice during the last glacial period. Nature 326, 273-277.

Reimnitz, E., McCormick, M., Bischof, J., Darby, D.A., 1998. Comparing sea-ice sediment load with Beaufort Sea shelf deposits: Is entrainment selective? J. Sedimentary Res., Sect. A: Sedimentary Petrol. Processes 68(5), 777-787.

Rignot, E.J., 1998. Fast recession of a west Antarctic glacier. Science 281, 549-551.

Robinson, C., Raisbeck, G.M., Yiou, F., Lehman, B., Laj, C., 1995. The relationship between $^{10}$Be and geomagnetic field strength records in central North Atlantic sediments during the last 80 ka. Earth Planet. Sci. Lett. 136, 551-557.

Robinson, S.G., Maslin, M.A., McCave, I.N., 1995. Magnetic susceptibility variations in upper Pleistocene deep-sea sediments of the NE Atlantic: Implications for ice rafting and paleocirculation at the last glacial maximum. Paleoceanography 10(2), 221-250.

Rott, H., Skvarca, P., Nagler, T., 1996. Rapid collapse of northern Larsen ice-shelf, Antarctica. Science 271, 788-792.

Ruddiman, W.F., 1977. Late Quaternary deposition of ice-rafted sand in the subpolar North Atlantic (lat. 40° to 65°N). GSA Bulletin 88, 1813-1827.

Ruddiman, W.F., Glover, L.K., 1972. Vertical mixing of volcanic ash in North Atlantic sediments. GSA Bulletin 83, 2817-2836.

Sachs, J.P., Lehman, S.J., 1999. Subtropical North Atlantic Temperatures 60,000 to 30,000 Years Ago. Science 286, 756-759.

Scherer, R.P., Aldahan, A., Tulaczyk, S., Possnert, G., Engelhardt, H., Kamb, B., 1998. Pleistocene collapse of the West Antarctic Ice Sheet. Science 281, 82-85.

Schulz, H., von Rad, U., Erlenkeuser, H., 1998. Correlation between Arabian Sea and Greenland climate oscillations of the past 110,000 years. Nature 393, 54-57.

Severinghaus, J.P., Brook, E.J., 1999. Abrupt climate change at the end of the last glacial period inferred from trapped air. Science 286, 930-934.

Shackleton, N.J., 1974. Attainment of isotopic equilibrium between ocean water and the benthic foraminifera genus Uvigerina: isotopic changes in the ocean during the last glacial. In: Labeyrie, J. (Ed.), Les Méthodes Quantitatives d'Etudes des Variations du Climat au Cours du Pléistocène. Cent. Nat. de la Rech. Sci., Paris.

Shackleton, N.J., 2001. Climate change across the hemispheres. Science 291, 58-59.

Shackleton, N.J., Hall, M.A., Vincent, E., 2000. Phase relationships between millennial-scale events 64,000-24,000 years ago. Paleoceanography 15, 565-569.

Shemesh, A., Burckle, L.H., Hays, J.D., 1994. Meltwater input to the Southern Ocean during the last glacial maximum. Science 266, 1542-1544.

Shemesh, A., Hodell, D.A., Crosta, X., Kanfoush, S.L., Charles, C., Guilderson, T., 2002. The sequence of events during the last deglaciation in Southern Ocean sediments and Antarctic ice cores. Paleoceanography, in press.

Shepherd, A., Wingham, D.J., Mansley, J.A.D., Corr, H.F.J., 2001. Inland thinning of Pine Island glacier, West Antarctica. Science 291, 862-864.

Shimada I., Schaaf, C.B., Thompson L.G., Mosley-Thompson, E., 1991. Cultural impacts of severe droughts in the prehistoric Andes: application of a 1500-year ice core precipitation record. World Archaeology 22(3), 247-270.

Shipboard Scientific Party, 1999. Leg 177 summary: Southern Ocean paleoceanography. In: Gersonde, R., Hodell, D.A., Blum, P. (Eds.), Proceedings of the Ocean Drilling Program, Initial Reports Leg 177. Ocean Drilling Program, College Station, TX, pp. 1-67.

Skvarca, P. 1993. Fast recession of the Northern Larsen ice-shelf monitored by space images. Ann. Glaciology 17, 317-321.

Smith, D.G., Ledbetter, M.T., Ciesielski, P.F., 1983. Ice-rafted volcanic ash in the South Atlantic sector of the Southern Ocean during the last 100,000 years. Marine Geology 53, 291-312.

Stahle, D.W., Cleaveland, M.K., Blanton, D.B., 1998. The Lost Colony and Jamestown droughts. Science 280, 564-567.

Steig, E.J., Brook, E.J., White, J.W.C., Sucher, C.M., Bender, M.L., Lehman, S.J., Morse, D.L., Waddington, E.D., Clow, G.D., 1998. Synchronous climate changes in Antarctica and the North Atlantic. Science 282, 92-95.

Steig, E.J., Morse, D.L., Waddington, E.D., Stuiver, M., Grootes, P.M., Mayewski, P.M., Whitlow, S.I., Twickler, M.S., 2000. Wisconsinan and Holocene climate history from an ice core at Taylor Dome, western Ross Embayment, Antarctica. Geografiska Annaler 82A, 213-235.

Stoner, J.S., Channell, J.E.T., Hillaire-Marcel, C., 1995a. Late Pleistocene relative geomagnetic paleointensity from the deep Labrador Sea: Regional and global correlations. Earth Planet. Sci. Lett. 134(3-4), 237-252.

Stoner, J.S., Channell, J.E.T., Hillaire-Marcel, C., 1995b. Magnetic properties of deep-sea sediments off southwest Greenland: evidence for major differences between the last two deglaciations. Geology 23, 241-244.

Stoner, J.S., Channell, J.E.T., Hillaire-Marcel, C., 1996. The magnetic signature of rapidly deposited detrital layers from the deep Labrador Sea: Relationship to North Atlantic Heinrich layers. Paleoceanography 11(3), 309-325.

Stoner, J.S., Channell, J.E.T., Hillaire-Marcel, C., 1998. A 200 ka geomagnetic chronostratigraphy for the Labrador Sea: Indirect correlation of the sediment record to SPECMAP. Earth Planet. Sci. Lett. 159(3-4), 165-181.

Stoner, J.S., Kissel, C., Channell, J.E.T., Hillaire-Marcel, C., 2000. Geomagnetic paleointensity and environmental record from Labrador Sea core MD95-2024: Global marine sediment and ice core chronostratigraphy for the last 110 kyr. Earth Planet. Sci. Lett. 183(1-2), 161-277.

Stoner, J.S., Laj C., Channell, J.E.T., Kissell, C., 2002. South Atlantic and North Atlantic geomagnetic paleointensity stacks (0-80 ka): implications for inter-hemispheric correlation. Quat. Sci. Rev. 21, 1141-1151.

Stuiver, M., Grootes, P.M., 2000. GISP2 oxygen isotope ratios. Quaternary Res. 53, 277-284.

Stuiver, M., Reimer, P.J., Bard, E., Beck, J.W., Burr, G.S., Hughen, K., Kromer, B., McCormac, G., van der Plicht, J., Spurk, M., 1998. INTCAL98 radiocarbon age calibration, 24,000-0 cal BP. Radiocarbon 40(3), 1041-2084.

Taylor, K.C., Mayewski, P.A., Alley, R.B., Brook, E.J., Gow, A.J., Grootes, P.M., Meese, D.A., Saltzman, E.S., Severinghaus, J.P., Twickler, M.S., White, J.W.C., Whitlow, S., Zielinski, G.A., 1997. The Holocene-Younger Dryas Transition Recorded at Summit. Greenland. Science 278, 825-827.

Thompson, L.G., Davis, M.E., Mosley-Thompson, E., Sowers, T.A., Henderson, K.A., Zagorodnov, V.S., Lin, P.-N., Mikhalenko, V.N., Campen, R.K., Bolzan, J.F., Cole-Dai, J., Francou, B., 1998. A 25,000-Year Tropical Climate History from Bolivian Ice Cores. Science 282, 1858-1864.

Thompson, L.G., Yao, T., Davis, M.E., Henderson, K.A., Mosley-Thompson, E., Lin, P.-N., Beer, J., Synal, H.-A., Cole-Dai, J., Bolzan, J.F., 1997. Tropical Climate Instability: The Last Glacial Cycle from a Qinghai-Tibetan Ice Core. Science 276, 1821-1825.

Teitler, L.F., Warnke, D.A., Venz, K.A., Hodell, D.A., 2001. Late Pleistocene history of IRD at South Atlantic (Agulhas Ridge) Sites TN057-6-PC4 and ODP 177-1090. Eos, Transactions Am. Geophys. Union. F793.

Thomas, R.H., 1991. Polar research from satellites: A review. Joint Oceanographic Institutions, Washington D.C., 91p.

Tric, E., Valet, J.P., Tucholka, P., Paterne, M., LaBeyrie, L., Guichard, F., 1992. Paleointensity of the geomagnetic field during the last 80 000 years. J. Geophys. Res. 97, 9337-9351.

Veiga-Pires, C.C., Hillaire-Marcel, C., 1999. U and Th isotope constraints on the duration of Heinrich events H0-H4 in the southeastern Labrador Sea. Paleoceanography 14(2), 187-199.

Vaughn, D.G., Doake, C.S.M., 1996. Recent atmospheric warming and retreat of ice-shelves on the Antarctic Peninsula. Nature 379, 328-331.

Venkatesh S., Murphy, D.L., Wright, G.F., 1994. On the deterioration of icebergs in the marginal ice zone. Atmosphere-Ocean 32(2), 469-484.

Vidal, L., Duplessy, J.C., Michel, E., Becque, S., Van Weering, T.C.E., Labeyrie, L., Cortijo, E., Arnold, M., 1997. Evidence for changes in the North Atlantic deep water linked to meltwater surges during the Heinrich events. Earth Planet. Sci. Lett. 146(1-2), 13-27.

Vinje, T.E., 1980. Some satellite tracked iceberg drifts in the Antarctic. Ann. Glaciology 1, 83-87.

Voelker, A., Sarnthein, M., Grootes, P.M., Erlenkeuser, H., Laj, C., Mazaud, A., Nadeau, M.J., Schleicher, M., 1998. Correlation of marine $^{14}C$ ages from the Nordic Sea with GISP2 isotope record: implications for $^{14}C$ calibration beyond 25 ka BP. Radiocarbon 40, 517-534.

Wagner, G., Beer, J., Laj, C., Kissel, C., Mazarik, J., Muscheler, R., Synal, H.-A., 2000. Chlorine-36 evidence for the Mono Lake event in the Summit GRIP ice core. Earth Planet. Sci. Lett. 181, 1-6.

Warnke, D.A., 1970. Glacial erosion, ice rafting, and glacial-marine sediments: Antarctica and the Southern Ocean. Am. J. Sci. 269, 276-294.

Warnke, D.A., Allen, C.P., 1992. "Quartz, SWEAT, and Shears" or "How did that rose quartz get into the Southern Ocean?" EOS, Transactions Am. Geophys. Union. 73, 284.

Watkins, N.D., Ledbetter, M.T., Huang, T.C., 1982. Scotia Arc volcanism recorded in abyssal piston cores downwind from the islands (Antarctica). In: Antarctic Geoscience; 3rd Symposium on Antarctic Geology and Geophysics, Madison, p. 1013-1016.

Webb, R., Rind, D., Lehman, S.J., Healy, R.J., Sigman, D., 1997. Near modern ocean heat transports and enhanced glacial cooling. Nature 385, 695-699.

Weber, M.E., Niessen, F., Kuhn, G., Wiedicke, M., 1997. Calibration and application of marine sedimentary physical properties using a multisensor core logger. Marine Geology 136,151-272.

Weiss, H.,Courty, M.-A., Wetterstrom, W., 1993. The genesis and collapse of third millennium north Mesopotamian civilization. Science 261, 995-1004.

Wendler, G., K. Ahlnas, Lingle, C., 1996. On Mertz and Ninnis glaciers, East Antarctica. J. Glaciol. 42, 447-453.

Westfall, F., Fenner, J., 1991. Pliocene-Holocene polar front zone in the South Atlantic: Changes in its position and sediment-accumulation rates from holes 699A, 701ZC and 701 B. In: Ciesielski, P.F., Kristofferson, Y. (Eds.), Proceedings of the Ocean Drilling Program, Scientific Results Leg 114, Subantarctic South Atlantic. Ocean Drilling Program, College Station, TX, pp. 609-646.

Whitworth, T., III, Nowlin, W.D., Jr., 1987. Water masses and currents of the Southern Ocean at Greenwich meridian. J. Geophys. Res. 92, 6462-6476.

Wilch, T. I., McIntosh, W. C., Dunbar, N.W., 1999. Late Quaternary volcanic activity in Marie Byrd Land: potential 40Ar/39Ar-dated time horizons in West Antarctic ice and marine cores. Geol. Soc. Am. Bull. 111(10), 1563-80.

Yiou, F.G., Raisbeck, M., Baumgartner, S., Beer, J., Hammer, C., Johnsen, S., Jouzel, J., Kubick, P.W., Lestringuez, J., Stievenard, M., Suter, M., Yiou, P., 1997. Beryllium 10 in the Greenland Ice Core Project ice core at Summit, Greenland. J. Geophys. Res. 102, 26-29.

Yokoyama, Y., Esat, T.M., Lambeck, K., 2001. Couple climate and sea level changes deduced from Huon Peninsula coral terraces of the last ice age. Earth Planet. Sci. Lett. 193, 579-587.

Yoon, H.I., 2000. Glaciomarine sedimentation and its paleoceanographic implications along the fjord margins in the South Shetland Islands, Antarctica during the last 6000 years. Palaeogeog., Palaeoclimat., Palaeoecol. 157(3-4), 189-211.

Zwally, H.J., Comiso, J.C., Parkinson, C.L., Campbell, W.J., Carsey, F.D., Gloerson, P., 1983. Antarctic Sea Ice, 1973-1976: Satellite Passive Microwave Observations. NASA, Washington, D.C.

## BIOGRAPHICAL SKETCH

Sharon Kanfoush was born on July 21, 1968 in Utica, New York. She graduated as Valedictorian from Sauquoit Valley Central High School in 1986. She then attended Southampton College of Long Island University where she obtained a Bachelor of Science degree in marine science and geology and completed internships at the Lamont-Doherty Earth Observatory and the Skidaway Institute of Oceanography. After working several years in the environmental consulting field, she pursued graduate work at the State University of New York College at Buffalo. There her research interests focused on paleolimnological reconstruction of the cultural eutrophication of Lake Erie, and she received her Master of Science degree in 1995.

Her research interests changed somewhat upon arrival at the University of Florida. There she focused her efforts on ice-sheet dynamics and paleoceanography and had the opportunity to sail as a shipboard scientist on the JOIDES Resolution for Leg 177 of the Ocean Drilling Program from Capetown, South Africa to Punta Arenas, Chile. Sharon gained much teaching experience while at the University of Florida and won the Ernst Award for Teaching from the Department of Geological Sciences in 1999.

She was employed in 2000-2002 as a Visiting Instructor in Geology and was hired as an Assistant Professor of Geology beginning Fall 2002 at Utica College of Syracuse University in central New York State.

I certify that I have read this study and that in my opinion it conforms to acceptable standards of scholarly presentation and is fully adequate, in scope and quality, as a dissertation for the degree of Doctor of Philosophy.

David A. Hodell, Chairman
Professor of Geological Sciences

I certify that I have read this study and that in my opinion it conforms to acceptable standards of scholarly presentation and is fully adequate, in scope and quality, as a dissertation for the degree of Doctor of Philosophy.

James E.T. Channell
Professor of Geological Sciences

I certify that I have read this study and that in my opinion it conforms to acceptable standards of scholarly presentation and is fully adequate, in scope and quality, as a dissertation for the degree of Doctor of Philosophy.

Paul F. Ciesielski
Associate Professor of Geological Sciences

I certify that I have read this study and that in my opinion it conforms to acceptable standards of scholarly presentation and is fully adequate, in scope and quality, as a dissertation for the degree of Doctor of Philosophy.

Joann Mossa
Associate Professor of Geography

I certify that I have read this study and that in my opinion it conforms to acceptable standards of scholarly presentation and is fully adequate, in scope and quality, as a dissertation for the degree of Doctor of Philosophy.

Claire Schelske
Eminent Scholar Emeritus in Fisheries and Aquatic Sciences

This dissertation was submitted to the Graduate Faculty of the Department of Geological Sciences in the College of Liberal Arts and Sciences and to the Graduate School and was accepted as partial fulfillment of the requirements for the degree of Doctor of Philosophy.

August 2002

Dean, Graduate School